UNIVERSITY OF CALIFORNIA, SAN DIEGO

Energy Deposition in the Body from External Sources to Chemically Trigger Cellular Responses in Desired Localized Regions

A dissertation submitted in partial satisfaction of the requirements for the degree Doctor of Philosophy

in

Bioengineering

by

Stuart Duncan Ibsen

Committee in charge:

Professor Michael Berns, Chair
Professor Sadik Esener, Co-Chair
Professor Michael Heller
Professor Yu-Tsueng Liu
Professor Shyni Varghese
Doctor Wolfgang Wrasidlo

2011

The Dissertation of Stuart Duncan Ibsen is approved, and it is acceptable in quality and form for publication on microfilm and electronically:

_____

_____

_____

_____

_____
Co-Chair

_____
Chair

University of California San Diego

2011

DEDICATION

It takes a village

The PhD is really much more than just the science contributions made to society. It is a personal growth experience unlike any other. By expanding the envelope of human knowledge you are thrown into a situation where you more or less are forced to learn how to learn. The whole process allowed me to run into countless people, including those mentioned here, who touched my life mine in amazingly positive ways. Because of their impact on my life I would like to dedicate this thesis to all of them.

Gene Hsaio's interaction with me is summed up in a memory. At the end of our first year I was leaving San Diego for Hawaii to finish up my work out there and Gene dropped me off at the airport. As I took my tapped boxes and bags out of the back of his truck I told him that he had better not quite the program, otherwise I doubted my own ability to finish. Later that year he moved from masters to PhD and was stuck like me in the stream of the PhD. He and I met at the ice breaking event our first day, and we both had marked on the bingo sheet "Surfing" and I was rather disappointed that someone else had beaten me to it. Turns out Gene and I surfed throughout the entire experience. I watched him push his boundaries in both science and in foreign travel and personal relationships and his enthusiasm and optimism carried me along as well. It was with Gene that I learned how to travel in foreign countries where you don't speak the native language,. It was with Gene I "caught" my first barrel. I can't tell you have excited I was to move into One Miramar right next to Gene. Gene took me on my first ever surf safari, and long distance road trips to Yellowstone and northern California. Gene always had amazing brunches and dinners and movies.

Lucas has been an amazingly patient and level headed sounding board of my ideas for so many years, not just in science, but also in the fine art of personal relationships, technology, photography (he is the most talented photographer I know), media (he introduced me to the Big Bang Theory), and videogames. He never tired of discussing the same problems with me over and over again, which was a great help to me since repetition seems to be the best medicine sometimes. Having him as a roommate all these years has been fantastic and helped make this entire experience not just bearable, but enjoyable. Often times just talking for hours with him about a problem allowed me to solve it in more constructive way than would be able to do on my own. Without Lucas and Gene, I would have finished my PhD much faster, not due to less time spent enjoying life, but because of how dark the whole experience would have been without them.

Carolyn Schutt's impact on my life can not be over stated. She and I had known of each other for several years before Sadik put us together writing a section of the center proposal. Neither of us had any experience writing proposals, but just spending those few hours over that weekend trying to figure out this task together allowed me to instantly see aspects of her true personality (the positivity of which I had always been suspicious). Never before has my brain been re-wired just by being

around a person. Even simple topical electrodes would easily register the difference. She calmed the chaos that came from trying to solve the problems of personal happiness that I once found intractable. I have never met an individual who so understood me as a person, my motivations, my mind, and appreciates the seemingly uncontrollable “Stu Hair”. She redefines concepts in my head and humbles the orderly mathematics I once thought would lead to success and replaced them with the undefinable reality of “it just works”. To her I am eternally grateful.

Danny and Taylor Richter have been a life line to the Scripps world. Danny and I have a background through Outback Adventures and we have had many adventures in the back country and at Scripps socials. They have always included me in activities that I would have no access to otherwise. Our tea times have become an event I always look forward to. Danny’s uncompromising attention to avoiding hypocriticism is a constant reminder to me in my own life and dealings. Danny doesn’t just talk about ideals and lifestyles, he lives them, and that is a rare quality.

The grey whales of San Ignacio need a special tip of the hat as well. They were the draw that allowed me to lead my own expeditions deep into Baja with the help of many people from Scripps. It was the purpose of joining Outback Adventures in the first place. Also to the baby whale, the only one I have ever touched in my life.

Erik Kaestner has also been an Outback friend that stuck. He and I have spent weeks hiking around the backcountry of various places. Level headed and remarkably driven he has become brother like to me as I watch him start his graduate career literally on the day that I finish mine. Driven and insatiable in his love for data, our dinners discussing theories and political ideas have been a highlight of the experience.

Andrew Box for all the support and allowing me to go to the Maldives to surf the best waves of my life. Andrew and I met in Hawaii and still through to this day we have been able to support each other. It didn’t seem to matter whether it was dolphins or drug delivery vehicles he was always there with a sometimes necessarily objective commentary which I have benefited from greatly, at least after I calmed down ☺.

Kristen Taylor, a life long friend, helped me in San Diego in the same way she helped in Hawaii. I remember talking to her on the phone once about the water solubility problems of DOX-PCB. She told me that she’s heard me say these things before about the phantom system, and that she did not believe that my project was dead. “You’ll find a solution, you always have.” It was a very comforting thought in a very difficult time. With some people the interaction is timeless.

Aric Joneja surprised me when he emailed me one day in January of 2010 saying that he had overheard me talking of a trip to Africa I was planning. Because of him I had the chance to experience one of the most amazing things on the planet, a trip to visit the wild Gorillas of Bwindi national reserve in Uganda, and summit Kilimanjaro. I will never forget these experiences.

My friend Elaine, who went with me to Peru and hiked the Inca trail to Machu Pichu. It was the experience of a lifetime and I will never forget just how tough she is as she battled food poisoning to make it to the top. With her, you know you are going to make it safely anywhere.

Songhai Li who lead me through China on one of the grandest adventures I could imagine. He is truly different from any other student I met over there and I am

so glad he came to Hawaii to work more with MMRP. I didn't realize it before but he had never worked with LabView and the speed with which he picked it up was astounding. He is one of those genuinely nice and caring people.

My sister Jennifer who also moved to San Diego a few months before I did. It has been wonderful to live near family for the first time since I left home. It has been wonderful to be a part of her life as she moves along the path of creating a family. Watching my niece Stella grow and develop has been delightful. Thank you Jenn for taking those first steps in our family so that we may all benefit from your experience. Our Chuck dinners have been such a relief in a busy hectic lifestyle.

My brother Steven who has so passionately pursued his dreams of animation and design. From early in his life he had always been an animator and to watch him chase that down with unrelenting energy and determination has been such an inspiration.

My parents Jann and Tom who have still managed to maintain patience as I continue down the road to maturity. I can't even begin to estimate the hours of talking on the phone and in person that have brought so much relief to the problems of my professional and personal life. I have only been able to take the risks of starting these programs and projects and traveling as I have internationally because I know I have a stable support network that will catch me when I fall. It's already been tested more times than I care to remember and I am here today because of it. This achievement is as much their effort as it is mine. I wish them all the happiness they have worked so hard to achieve in their retirement and I can rest easy with the knowledge that they will continue to be there for me as I start the next chapters of this story.

My childhood pets, Kelly, Cricket, KC, Koli, Brittany, Shilo, Kala, Loki, Duncan, and Brody all of who offered unconditional love and support especially through the high school years. I always appreciate Brittany staying with me for hours as I would memorize the history book word for word or work through every math problem of the book for a third time. It never seemed to matter to them how I wasted my time, as long as they were with me while I did it.

I also want to thank my grandparents Earl and Mildred Ibsen and Bill and Dolores Duncan. They supported me so much in the early years of undergrad and grad school. My grandfather Duncan in particular would listen to me for so many hours about the problems of research and classes and then ask "So now for the real question, how about all the girls you've been dating?" He had a good way of keeping it real. They are surely missed.

Tina Wu helped teach me everything I know about cell culture and running the cell toxicity assays. I've been happy to pass on her knowledge because without it I would never have gotten anywhere with the DOX-PCB prodrug. She never made me feel bad, even over the smallest questions and I realty appreciated that.

Stephen Adams's help on the HPLC purification of the DOX-PCB. He has a spirit that simply can not be crushed. I discovered him through his publications on photocleavable compounds and then miraculously, and to my benefit, discovered him again at a poster session for the Nano Tumor Center. As it turned out both our different projects were supported by the same program. No matter what's going on he

manages to make me feel better with his witty comments and observations. Workingwith him is always a pleasure.

Dr. Su has been just a wonderful person to work with. He is truly talented at mass spec and has managed to help me crack the most difficult tissue extraction task I have ever faced. Without his optimism and keeping me motivated to bring him samples early in the morning after a 16 hour protocol I would not have figured out hardly any of chapter 2.

Wolf Wrasidlo's lifetime of experience designing drugs was an invaluable resource as I continued struggling through the DOX-PCB development. He always manages to come up with idea that keeps the project from going under and makes them clinically relevant. His advice and encouragement have been greatly appreciated.

Eran Zahavy and I suffered through 7 months of chemical synthesis development to finally land upon DOX-PCB in its current form. The little drug that could seems to have a life of its own sometimes as it manages to pass every test I put it through. During this time I got a glimpse of a well balanced life in science. Eran manages to raise a family, conduct high level science, and still finds the chance to live for years at a time in different places around the world. I learned a lot about different cultures, different views on work, different views on stress management and different ways to approach and successfully solve a problem. Eran, despite his years of experience, never dismissed my ideas or observations regardless of how naïve my obsession with the meaning behind chemical color changes might have been. He showed me amazing places in Israel and encouraged me to take that scary step forward to see Petra in Jordan. He has a way of making you really wonder "why not?" especially when I told him that something was impossible for me to do. That I will take with me for the rest of my life.

Michael Berns has always been a great supporter of my work, even when it took an unexpected turn outside the scope of his lab. I remember sitting down with Dr. Berns when I had just taken his class and I came to him with the idea of using fiber optics to uncage light sensitive molecules. He told me, I have never done anything like that, but we'll see how we can help you. His advice has been invaluable as I worked through the social and technical challenges of these projects. His love of basic science is inspirational especially in these early stages of development. Sometimes the question itself just has inherent importance.

Sadik Esener has been the best advisor I could ever ask for. He has been endlessly supportive of my ideas and aspirations. He has allowed me to explore on my own and develop the skills necessary to run my own lab some day. From him I have watched how to conduct oneself within the scientific community at a very high level and yet with integrity and decency that is such a rare quality in those so successful. From him I've learned ways to deal with the stress and anxiety of issues like whether or not DOX-PCB will ever reach the clinic. I have been amazed and seen him as a great source of inspiration on how he has handled the challenges of life and still managed to support all us without redirecting any stress. The time I spent with him and his family in Turkey will always be treasured and gave me an insight into a new culture.

I also want to thank my committee whose guidance and advice helped to validate this contribution to the scientific world.

Being surrounded by such wonderful and generous people has made this experience one that changed my life forever. I am so happy, not just with the degree, but how each and everyone has influenced and improved my life. It does apparently take a village. Thank you all so much. I can never adequately repay you for all that you've done.

EPIGRAPH

The person who says it cannot be done should not interrupt the person doing it
–Chinese proverb

The party that's Grad school saw me grow quite a bit
I stayed for the longest that time would permit
Just one more degree
And then I'd have three
But my finances would not recommend it

TABLE OF CONTENTS

LIST OF FIGURES

ACKNOWLEDGMENTS

The following co-authors have contributed immensely to the work presented in each chapter. I very much appreciate their help, support, and contributions

Chapter 1 A Novel Doxorubicin Prodrug with Controllable Photolysis Activation for Cancer Chemotherapy. Co-authors Stuart Ibsen, Eran Zahavy, Wolf Wrasdilo, Michael Berns, Michael Chan, Sadik Esener. This has been published in Pharmaceutical Research.

Chapter 2 Localized Tumor Specific Activation of Photactivatable Doxorubicin Prodrug. Co-authors Stuart Ibsen, Eran Zahavy, Wolf Wrasdilo, Tomoko Hashi, John Norton, Yongxuan Su, Stehpen Adams, Sadik Esener

Chapter 3 A Novel Nested Liposome Drug Delivery Vehicle Capable of Ultrasound Triggered Release of its Payload. Co-authors Stuart Ibsen, Michael Benchimol, Dmitri Simberg, Carolyn Schutt, Jason Steiner, Sadik Esener. This has been published in the Journal of Controlled Release.

Chapter 4 Effect of Microbubble Cavitation on Whole Cell Membranes. Co-authors. Stuart Ibsen, Ruben Mora, Guixin Shi, Carolyn Schutt, Wenjin Cui, Michael Benchimol , Viviana Serra, Sadik Esener.

Chapter 5 Fluorescent Microscope System to Monitor Real-Time Interactions between Focused Ultrasound, Echogenic Drug Delivery Vehicles, and Live Cell Membranes. Co-authors Stuart Ibsen, Michael Benchimol, Sadik Esener

VITA

Doctor of Philosophy, Bioengineering; December 2011
University of California San Diego, La Jolla, CA

Master of Science, Bioengineering; June 2007
University of California San Diego, La Jolla, CA

Bachelor of Science, Biomedical Engineering; May 2002
Johns Hopkins University, Baltimore, MD

PUBLICATIONS

Ibsen, Stuart; Benchimol, Michael; Esener, Sadik. "Instrumentation Design for Fluorescent Visualization of Ultrasound Induced Cavitation." Currently in preparation.

Ibsen, Stuart; Benchimol, Michael; Simberg, Dmitri; Schutt, Carolyn; Steiner, Jason; Esener, Sadik. "A Novel Nested Liposome Drug Delivery Vehicle Capable of Ultrasound Triggered release of its payload." Journal of Controlled Release, accepted and awaiting publication.

Ibsen, Stuart; Zahavy, Eran; Wrasdilo, Wolf; Berns, Michael; Chan, Michael; Esener, Sadik. (2010) "A Novel Doxorubicin Prodrug with Controllable Photolysis Activation for Cancer Chemotherapy" Pharmaceutical Research, 27(9):1848-60.

FIELDS OF STUDY

Major Bioengineering

Studies in Drug Delivery and Drug Discovery
Professors Sadik Esener and Michael Berns

ABSTRACT OF THE DISSERTATION

Energy Deposition in the Body from External Sources to Chemically Trigger Cellular Responses in Desired Localized Regions

by

Stuart Duncan Ibsen

Doctor of Philosophy in Bioengineering

University of California, San Diego, 2010

Professor Michael Berns, Chair

Professor Sadik Esener, Co-Chair

One of the major challenges of modern chemotherapy is to deliver a therapeutic dose of active drug to the tumor tissue without causing systemic exposure. The realization of this goal could considerably reduce the negative side effects experienced by patients. The work conducted in this thesis looks at two different approaches to trigger drug activation with the use of external energy sources. This

avoids the challenges of relying solely on biochemical and environmental differences as triggers. The two triggers used were low intensity focused ultrasound and 365 nm light delivered with a custom designed needle UV LED fiber optic system. Both can be localized within the body to spatially highlight just the tumor tissue creating a stark differentiation between it and the healthy tissue.

The 365nm light based delivery scheme developed here was the first demonstration of a photoactivatable doxorubicin (DOX) prodrug called DOX-PCB. DOX-PCB was shown to be 200 times less toxic than DOX and could be activated to a fully therapeutic form upon exposure to 365nm light. The pharmacokinetics showed a circulation half life comparable to that of DOX and stability against in vivo metabolic degradation. The 365 nm light was shown to adequately irradiate a centimeter of tumor tissue and cause localized activation. In vivo tumors exposed to the light had significantly higher doses of DOX than unexposed control tumors in the same individual.

The second delivery scheme made use of focused ultrasound to activate echogenic drug delivery vehicles. These vehicles were the first demonstration of encapsulating microbubbles within liposomes. Specially designed optical equipment documented that the microbubble was ultrasound responsive. The microbubble was shown to violently cavitate and rupture the outer liposome membrane releasing the payload contents. The three dimensional localization of activation was demonstrated in tissue phantoms.

The strengths of these two delivery schemes could complement each other when used together. The delivery vehicle could achieve high doses of DOX-PCB

within the tumor while the low toxicity prevents harm to the liver and spleen. The 365 nm light could then activate just the DOX-PCB found within the tumor itself causing localized cell death.

Introduction

Background

One of the major challenges of modern day pharmaceutical development is the reduction of side effects particularly in the case of cancer treatment with chemotherapy[1]. Often times the side effects, either transient, such as nausea, or permanent such as cardiotoxicity, limit the dose that can be given to a particular patient[2-4]. These low dose levels do not always completely eliminate the tumor and can lead to the development of drug resistance[5].

These undesirable side effects result from the administered drugs acting on tissues that they are not meant to come in contact with but do as an inventible consequence of the systemic dilution [6]. Preventing the exposure of healthy non-targeted tissue to active chemotherapy agents could reduce side effects and potentially allow larger doses of active drug to interact specifically with the tumor. Many strategies have been developed to reduce healthy tissue exposure but making them truly tumor specific has been difficult.

Strategies involving manipulation of the drug

Early attempts involved injecting the drugs specifically into the tumor. However, the drugs have been shown to have poor penetration to uniformly expose the entire target tissue. The drugs were also quickly drained into the lymph system causing eventual systemic exposure[7].

Drugs have been encapsulated into slow release biodegradable polymers and implanted into the tumor region or lesion site, but again there were problems getting a

uniform dose to the entire tissue[8]. Additional doses of the drug would require additional implantation surgeries. Even with slow release, these drugs are diluted into the rest of the body at low but chronic levels.

Drugs can be chemically modified with targeting ligands to stick preferentially in tumor regions and also facilitate endocytosis[9]. One of the challenges is that tumors can be biochemically different from patient to patient [10] making selection of the correct targeting ligand difficult. There are also a limited number of tumors for which this would be truly effective due to the necessity that the tumor ligand expression be significantly greater than that of the healthy tissue [11].

Another approach has developed into an entire field which pursues the concept of chemically modifying the drug, by covalently attaching blocking groups, to create an inactivated form called a prodrug. This blocking group is designed to reduce the toxicity of the drug to all tissues but will be triggered to release active drug when inside the tumor region. The success of the prodrug heavily depends on the choice of the trigger. The tumor microenvironment of low oxygen levels and low pH has been explored as a potential trigger, but these environments often do not provide enough contrast from healthy tissue to cause truly tumor specific activation[12]. It has been reported that certain tumor tissue types over express enzymes that could be used to cleave the bond between the active drug and its blocking group, however this is not true for all tumors and there is intertumor variation on how much is produced[13]. An additional concern is the wide use of ester bonds as the cleavable link between the drug and the blocking group. Endogenous esterases are a clear choice to activate the prodrug and many tumors over express esterases[14]. However, these efforts are

complicated by the ubiquitous distribution of esterases in vivo especially in the liver, kidneys and plasma[15]. These can overwhelm the tumors enzymatic potential and cause activation of the majority of the prodrug outside the tumor.

Strategies involving drug delivery vehicles

Instead of chemically modifying the drug, the field of drug delivery looks to physically encapsulate the active drug within a carrier. This encapsulated drug is prevented from interacting with healthy tissue during circulation. The goal is to design the vehicle to release drug only inside the tumor. Some examples include Abraxane for delivery of paclitaxel and liposomal Doxil for doxorubicin[16, 17]. These rely on passive accumulation in the tumor tissue and then slow release of the drug. The challenge here is the vehicle's inevitable accumulation and resulting toxicity in healthy tissue[18] especially the liver and the spleen which are designed to remove foreign particles from circulation [19, 20]. Targeting the vehicles to the tumor tissue runs into the same specificity troubles as described above for the drugs[20]. It can help accumulate a higher therapeutic dose in the tumor than would otherwise occur [21] but the vast majority of the delivery vehicles never enter the tumor vasculature before they are eliminated from circulation [20, 21]. Increasing circulation half life by introducing various surface chemistries, such as use polyethylene glycol [22] only prolongs the inevitable liver accumulation [22, 23].

Common Challenges of Prodrugs and Drug Delivery Vehicles

The major difficulty with all the strategies described above is the ability to clearly differentiate the tumor tissue from the healthy tissue in a way that can be universally applied to different patients. This is an inherent problem with cancer. The tumor is derived from healthy tissue which through a series of mutations has changed to have uncontrolled expansion properties. The biochemistry of the tumor is not dramatically different from the original healthy tissue or from the liver. This lack of contrast makes it difficult to target and treat just the tumor cells without affecting the systemic healthy tissue.

Addressing the challenges

To obtain true tissue specificity for drug interactions the tumor must have a property that is truly unique from other tissues in the body. These properties do not necessarily have to be inherent to the tumor itself but can be properties that are externally applied to artificially highlight just the tissue region of interest. If the prodrug or delivery vehicle can be designed to respond to just these artificial triggers then the amount of non-specific activation in non-targeted tissues can be significantly reduced.

Two types of external triggers are considered in this thesis. The first is the use of 365nm light administered to the tissue of choice using LED technology or fiber optics. A photoactivatable prodrug of doxorubicin was developed to be activated by this method. The second is the use of focused ultrasound to activate a drug delivery vehicle. The focal spot of the ultrasound can be quite small and focused to deep

internal tissue from sources outside the body. A novel echogenic nested liposome drug delivery vehicle was developed to explode when exposed to this type of ultrasound. The 365 nm light and the focused ultrasound are two modalities that highlight the tumor tissue in a unique way that is not seen anywhere else in the body to ensure tumor specificity.

The advantages of both approaches can complement each other when used together. The drug delivery vehicle can help accumulate higher doses of the prodrug than could be achieved by systemic injection, and the reduced toxicity of the prodrug helps avoid liver and spleen damage through vehicle clearance. The use of the 365 nm light makes sure that only the prodrug accumulated in the tumor is activated to the toxic form.

Thesis Organization

This thesis is organized into five chapters.

Chapter 1 - Looks at the design, synthesis, and biological effects of a photoactivatible doxorubicin chemotherapy prodrug (DOX-PCB). This has been published in the journal Pharmaceutical Research.

Chapter 2 - Considers the in vivo biodistribution, stability, and the feasibility of activation of the DOX-PCB prodrug in actual biological tissue. A manuscript of this work is currently being prepared for publication.

Chapter 3 - Demonstrates the manufacturing, stability, and ultrasound activatibilty of a liposome drug deliver vehicle which contains an internal microbubble (SHERPA). This has been published in the Journal of Controlled Release

Chapter 4 - Demonstrates the effects of microbubble cavitation over the surface of the cell membrane using a novel method of targeted fluorescent liposome removal. A manuscript of this work is currently being prepared for publication.

Chapter 5 - Documents the custom design of the instrumentation required to observe membrane and cellular interactions of the echogenic drug delivery vehicles when exposed to focused ultrasound. This work is currently being submitted for publication.

Chapter 1

A Novel Doxorubicin Prodrug with Controllable Photolysis Activation for Cancer Chemotherapy

Abstract

Doxorubicin (DOX) is a very effective anticancer agent. However, in its pure form its application is limited by significant cardiotoxic side effects. The purpose of this study was to develop a controllably activatable chemotherapy prodrug of DOX created by blocking its free amine group with a biotinylated photocleavable blocking group (PCB). An n-hydroxy succunamide protecting group on the PCB allowed selective binding at the DOX active amine group. The PCB included an ortho-nitrophenyl group for photo cleavability and a water soluble glycol spacer arm ending in a biotin group for enhanced membrane interaction. This novel DOX-PCB prodrug had a 200 fold decrease in cytotoxicity compared to free DOX and could release active DOX upon exposure to UV light at 350 nm. Unlike DOX, DOX-PCB stayed in the cell cytoplasm, did not enter the nucleus, and did not stain the exposed DNA during mitosis. Human liver microsome incubation with DOX-PCB indicated stability against liver metabolic breakdown. The development of the DOX-PCB prodrug demonstrates the possibility of using light as a method of prodrug activation in deep internal tissues without relying on inherent physical or biochemical differences between the tumor and healthy tissue for use as the trigger.

Introduction

Doxorubicin (DOX) is an effective antitumor antibiotic that is used extensively in the treatment of different human cancers including breast cancer, soft tissue sarcomas, and Hodgkin's and non-Hodgkin's lymphomas [2, 24]. Although it is one of

the more potent chemotherapy agents known, its clinical application is limited by its harmful side effects, the most significant of which is its cardiotoxicity which can lead to cardiomyopathy and congestive heart failure [2-4].

Considerable work has been undertaken to chemically modify DOX and other chemotherapy agents with the goal of reducing their systemic toxicity. One such route is to create prodrugs which exhibit reduced toxicity to healthy tissue and can be transformed into pharmacologically active agents specifically within the tumor region. [4, 25, 26]. Several designs have taken advantage of environmental differences between the tumor tissue and normal tissue, such as hypoxia or low pH, to trigger the prodrug transformation [27, 28]. Some prodrugs have been designed to be activated by enzymes that are secreted by the tumor tissue at higher levels than elsewhere in the body [29-31]. The degree of tumor specificity for prodrug activation in these cases depends upon the degree of difference between the tumor tissue and the healthy tissue with respect to these parameters.

Some prodrug designs focus on tumor specific antigens that are expressed on the surface of the tumor cells. Attaching antibodies to the chemotherapy agents that are specific for those antigens excludes the agent from nontargeted healthy cells. The transformation of the agent is triggered upon antibody/antigen binding and internalization into the cell, usually triggered by the low pH of the intracellular endosome environment[32]. These strategies can achieve higher degrees of tumor specific prodrug activation with increasing amounts of knowledge about the internal environment and the surface antigens specific to a certain tumor. However, tumor cells are not homogenous in their gene expression [33]. This makes targeting every single

cell difficult. They are also not homogenous in their physical location relative to the tumor's hypoxic or low pH zones. Some cells can be difficult to reach, especially with bulky prodrugs, due to poor circulation networks within the tumor tissue. This requires that the prodrug be activated to a very potent drug which can affect cells in the general region of activation.

Instead of relying on inherent differences between the tumor and the healthy tissue to activate prodrugs it is possible to modify the tumor environment and take advantage of those artificial changes to differentiate the tumor region from the rest of the body. One method is to administer therapeutic ionizing radiation and use the small amount of reducing chemical species that can be created through water lysis. These extra reducing species could theoretically fill the role of reducing enzymes in the activation of the prodrug as long as the cleavable linker is sensitive enough to respond to small amounts of the active species produced [34]. Work has also been done to demonstrate the feasibility of covalently attaching photoliable blocking groups to paclitaxel with the capability of releasing paclitaxel upon light exposure [35]. However, the biological consequences of attaching the blocking group and the activity of the released paclitaxel have not been studied.

Another method is to use non-human enzymes to activate the prodrug. This reduces the possibility of any undesired prodrug activation outside the desired region as long as the enzyme itself, or the gene encoding for the enzyme, can be delivered to the tumor tissue specifically [36, 37].

From previous work in this field a few prodrug properties can be identified for use in maximizing the effectiveness of the prodrug. It is desirable that the prodrug be a

modified version of a potent chemotherapy drug and have greatly reduced toxicity compared to the drug itself. The use of a trigger source which is external to the body and localized specifically to the tumor tissue of interest avoids relying on inherent properties of the tumor to differentiate it from normal tissue. The ability of the prodrug to enter cells and maintain its prodrug properties is important to allow time for the circulating prodrug to clear from the system. This ensures only the prodrug that entered the targeted cells is trigged by the external source. Once triggered to activate, the prodrug should release the drug in its intact and pharmacologically active form.

The aim of this study was to design a prodrug that possess these desirable properties. The final design was a caged form of DOX created by blocking its free amine group with a biotinylated photocleavable blocking group (PCB) [38]. This novel DOX-PCB prodrug can be activated upon exposure to UV at 350 nm to release intact DOX. The photocleavable properties come from the incorporation of an o-nitrophenyl group [39]. UV administered to the tissue region of choice, possibly by use of fiber optics or miniature UV light emitting diodes, could trigger active DOX release from the DOX-PCB prodrug specifically in this region.

The introduction of UV radiation to the deep internal tissues through the use of implanted fiber optics or UV light emitting diodes would create a significant and controllable difference between the tumor and the healthy tissue. The only significant source of UV in the deep internal tissues of the body would be the delivered UV, since only 1% of 360 nm UV is transmitted through 1 mm of human skin due to melanin content [40]. The 350 nm light has significant penetration through tissue that does not contain melanin with minimal absorption [41]. The 350 nm light also has minimal

absorption by DNA [42]. The use of UV photocleavable prodrugs, such as DOX-PCB, could allow for activation of the prodrug just in the UV exposed deep tissue region. A higher degree of spatial and temporal control could be achieved this way rather than relying solely on inherent differences between the tumor and the healthy tissue to act as the trigger. The effective spatial range of the UV dose, and subsequent active DOX release, in the tissue can be manipulated by adjusting intensity, duration of exposure, and the placement of the UV diode or fiber optic. The scattering properties of the tissue would help ensure a uniform exposure of the entire region of interest. The timing of the administration of the UV dose can also be controlled to occur when DOX-PCB reaches its most concentrated levels in the tumor region. In this continuing investigation we have demonstrated the feasibility of this approach.

Materials and Methods

Materials

Doxorubicin hydrochloride (DOX) was obtained from Qventas (Branford, CT , USA) and Sigma (St. Louis, MO, USA). Water soluble photocleavable biotin–NHS (PCB) was purchased from Ambergen (Watertown, MA, USA). The components of the synthesis buffer, $NaCHO_3$ and NaOH, were from EMD (San Diego, CA, USA). The NADPH regeneration system was purchased from BD Biosciences (San Jose, CA, USA). The human liver microsomes, and the TOX2 in Vitro Toxicology XTT Assay Kit were both purchased from Sigma (St. Louis, MO, USA). The DMEM cell culture media and the trypsin were purchased from Mediatech Inc (Manassas, VA, USA). The penicillin-streptomycin used in the DMEM medias, the advanced MEM Media, and

the DMEM Media without phenol red were purchased from Gibco (Invitrogen, Grand Island, NY, USA). The fetal bovine serum used in the DMEM media solutions was purchased from Hyclone (Logan, UT, USA). HPLC grade acetonitrile and methanol were purchased from Fisher Scientific (Fairlawn, NJ, USA). The methanol-d_4 and deuterated dimethlyl sulfoxide (DMSO-d_6) were purchased from Cambridge Isotope Laboratories Inc. (Andover, MA, USA). The preparative thin layer silica gel liquid chromatography plates were purchased from Merck. The water used was first filtered with the Milli-Q Plus System (Millipore Corporation, Bedford, USA). The cell line used for the cytotoxicity studies was the human lung cancer cell line A549 purchased from the American Type Culture Collection (ATCC) (Manassas, VA, USA). The PTK2 (*Potorous tridactylus*) kidney epithelial cell line was originally purchased from the ATCC and kindly provided by the Beckman Laser Institute (UC Irvine, CA).

Conjugation of DOX to PCB

DOX was dissolved in water to a 1.2 μM concentration. A 0.1M $NaCHO_3$/NaOH buffer at pH 9.3 was added to the DOX solution to bring the total pH to 9.0. The DOX/buffer solution was then added to 1 mg (1.2 μmoles) of dry water soluble photocleavable biotin (PCB) in a 1:1 molar ratio. The reaction was stirred vigorously with a magnetic Teflon-coated stir bar for 30 min. The DOX-PCB prodrug product precipitated out. The nearly colorless supernatant was removed and the precipitate was dissolved in DMSO. The synthetic scheme is shown in Figure 1.1.

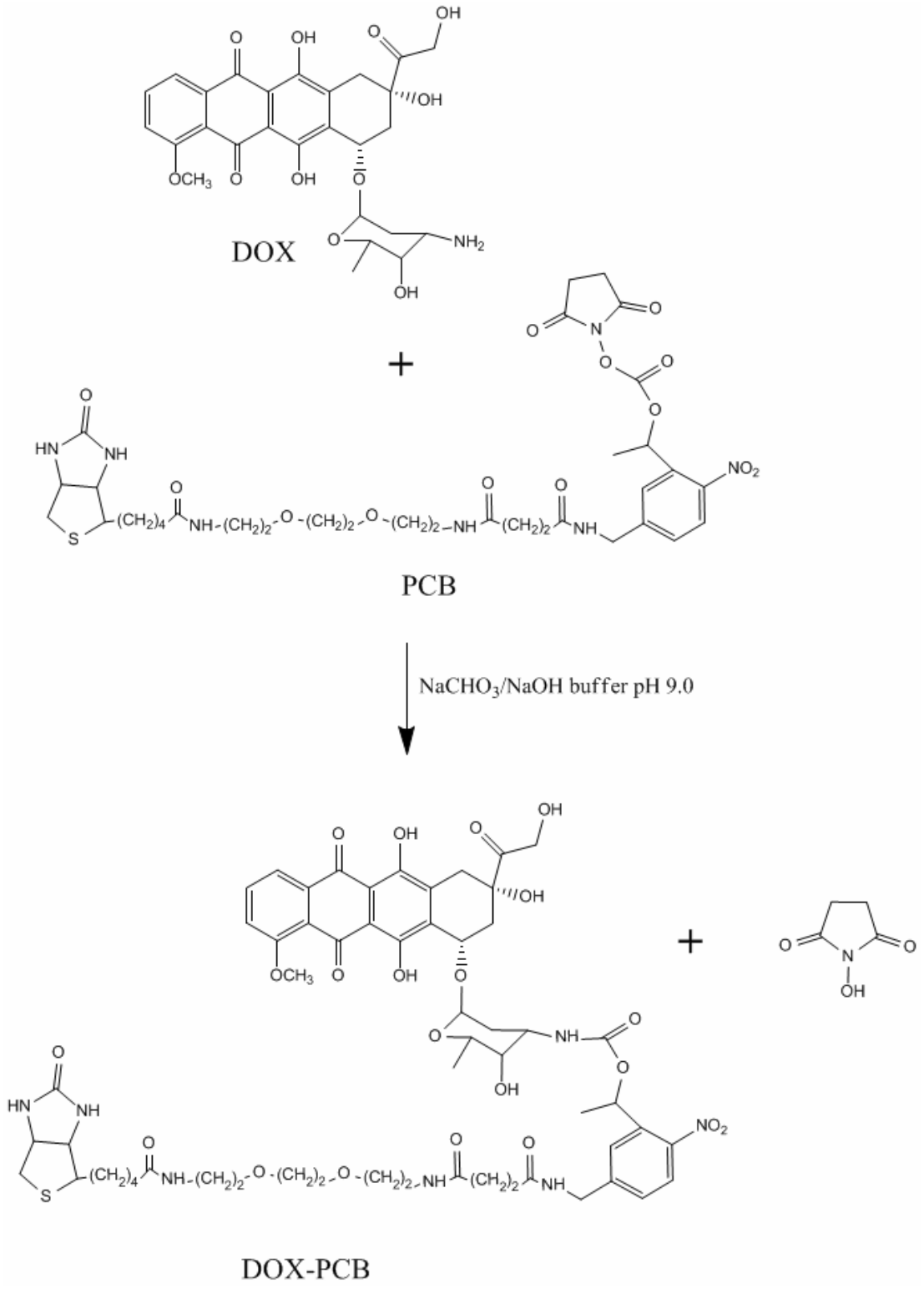

Figure 1.1 – Synthesis scheme for DOX-PCB

Purification of DOX-PCB

Purification was done by preparative thin layer liquid chromatography using a silica gel on a small scale for initial characterization. Later an HPLC semiprep purification was used to obtain larger amounts of DOX-PCB at a higher degree of purity for cell culture work and the DOX-PCB UV stability study. The purification of DOX-PCB in DMSO was done on an Agilent 1200 Series LC (Santa Clara, CA, USA) with a Luna 5u C-18(2) 100A column (250mm x 15 mm, with a 5μm bore size) (Phenomenex, Torrance, CA, USA). Solution A was 100% water and solution B was 100% MeOH. B was increased from 10-100% over 20 min with a flow rate of 50μL/min. Two isomeric forms of DOX-PCB were observed to separate slightly from each other on the column and were collected together in the same sample. The two isomers were also collected separately from one another and no differences in cytotoxicity between the two forms was observed. The overall yield of pure DOX-PCB was 70%.

Characterization

The DOX-PCB compound was characterized by high resolution mass spectrometry, HPLC/ mass spectrometry, and a UV absorption spectral analysis.

High resolution mass spectrometry was preformed on a Thermo Scientific LTQ Orbitrap XL mass spectrometer with electrospray ionization source (Milford, MA, USA). The sample of purified DOX-PCB was dissolved in a mixture of DMSO/water (20/80, v/v).

The HPLC/mass spectrometry analysis was preformed on a Thermo Finnigan LCQdeca mass spectrometer (Milford, MA, USA) using a Magic C-18 column (1.0mm×150mm) (Michrom BioResources, Auburn, CA). Solution A was 2.5% MeOH in water and Solution B was 100% MeOH. B was increased from 10- 95% over 20 min and then held at 95% for 5 min. The flow rate was 50μL/min. The mass spectrometry portion used electrospray ionization (ESI) in positive ion mode. The sample of purified DOX-PCB was dissolved in a mixture of DMSO/water (20/80, v/v).

An absorption spectrum was taken of a purified sample of DOX-PCB in DMSO and of DOX in DMSO using a NanoDrop ND-1000 Spectrophotometer (Wilmington, DE, USA). The measurements of DOX and DOX-PCB (data not shown) reveal that both compounds had an absorption maxima at $\lambda = 485$ nm from the DOX chromophore. DOX-PCB had an absorption at 350 nm due to the nitrophenyl group. This group enabled the photolysis process to occur upon absorption of radiation at 350 nm. The DOX-PCB spectra had the following 6 peaks: UV-visible (abs. DMSO) : 260, 287, 480, 500, 530, 584 nm ($\varepsilon_{cm}^{1\%}$: 25.9, 14.6, 11.0, 11.0, 6.6, 2.0 $\frac{g}{100ml \cdot cm}$).

The theoretical three dimension structure of DOX-PCB in water was determined using ChemDraw Pro.

Release of intact DOX

Two different methods were used to determine that unaltered DOX was released from DOX-PCB.

The first was an HPLC/mass spectrometry analysis where a solution of DOX in DMSO/water (10/90, v/v) and two identical solutions of purified DOX-PCB in DMSO/water (10/90, v/v) were prepared. One of the DOX-PCB samples was exposed to 120 sec of 2.19 mW/cm^2 UV created by a source consisting of a mercury arc lamp with a Mercury Short Arc HBO bulb from OSRAM (München, Germany) with a 330-380 nm bandpass filter. The second sample was not exposed to UV. All three samples were then analyzed using HPLC using the same analysis parameters as described above for the characterization.

The second study was a ^1H NMR analysis to determine if the free amine of DOX was restored after UV exposure. The analysis was preformed with Watergate water suppression on a JOEL ECA-500 device (Peabody, MA, USA) 500 MHz with 1000 scans for DOX-PCB. The sample consisted of purified DOX-PCB in a solution of DMSO-d_6/water (10/90, v/v). An NMR analysis was first run using this sample. The same DOX-PCB sample was then irradiated with 240 sec of UV from the same source as described above. The exposure time was increased to 240 sec to ensure a high percentage of conversion to give a clear signal from the free amine if present. A second NMR analysis using the same parameters as before was taken on this UV irradiated sample. A control sample of pure DOX was also dissolved in DMSO-d_6/water (10/90, v/v). More DOX was used than DOX-PCB because DOX was more readily available and a high signal to noise ratio was desired to give the best indication of the chemical shift from the free amine protons. The same NMR analysis was run on this DOX sample using only 16 scans since this sample had a much higher effective concentration.

Cell uptake and cellular localization

The differences in the intracellular localization between DOX and DOX-PCB were studied using the PTK2 epithelial cell line. This cell line was chosen due to its overall sensitivity to DOX and its natural ability to remain flat during cell division allowing the mitotic spindle and chromosomes to be readily visible. This feature permitted very clear observation of the interaction of DOX and DOX-PCB with the chromosome material when the nuclear membrane was intact and when it was disassembled at different stages of mitosis. The red fluorescence of DOX and DOX-PCB allowed for easy identification of their intracellular localization. The PTK2 cells were obtained already plated in sealed Rose Chambers incubating in advanced MEM Media with 2% fetal bovine serum, nonessential amino acids, 110 mg/L sodium pyruvate, and without penicillin-streptomycin or L-Glutamine from Gibco. A 4 ml solution of 5 μM DOX dissolved in the above media was prepared as well as a 4 ml solution of 50 μM DOX-PCB. DOX-PCB was used at a higher concentration because its toxicity was already known to be significantly lower than that of free DOX and it was of interest to determine its intracellular localization. These solutions were injected into the Rose chamber replacing the 1.8 ml of original media. The cells were allowed to incubate for 2 hours with the drugs before being analyzed using fluorescence microscopy (see subsequent description). After the initial fluorescence analysis, the DOX-PCB incubated cells were then exposed to the UV source for 60 sec. The cells were allowed to incubate in this exposed media for 1 hour before being analyzed again by fluorescence microscopy. To determine if the UV exposure affected the cells and

their behavior with the DOX-PCB, a sample of DOX-PCB solution was exposed to 60 sec of UV by itself and then was injected into the media of a cell culture chamber.

Images of the live PTK2 cells were obtained using a Zeiss Axiovert 200M Microscope (Zeiss, Thornwood, NY) with a 63x phase III, NA 1.4 oil immersion objective. An HCred1 rhodamine filter cube from Chroma (Rockingham, VT, USA) was used for the fluorescent images. All microscope control and imaging utilized the RoboLase system [43].

Cytotoxicity

The cell line used for the IC_{50} studies was the human lung cancer cell line A549 purchased from the American Type Culture Collection (ATCC) (Manassas, VA, USA). The cells were grown on sodium pyruvate free DMEM media containing 4.5 g/L of glucose, L-glutamine, 10% Fetal Bovine Serum, and penicillin-streptomycin. The adherent cells were detached from the expansion flask substrate using Trypsin (.25% T / 2.21mM EDTA) and plated onto a 96 well plate at a density of 10^4 cells per well with 100 μL of media. The cells were allowed to adhere to the bottom of each well overnight.

Experiments were run in two replicates under three different conditions. The first condition was exposure to pure DOX, the second was exposure to DOX-PCB with no UV irradiation, and the third was DOX-PCB with 120 sec of UV irradiation from the same source used in the UV stability experiments. The 20 min and 60 min of UV irradiation conditions were handled in the same manner as the 120 sec. The stock solutions of 15.1 mM DOX and 15.1 mM DOX-PCB in DMSO were diluted to 100

μM in media. A 1/3 serial dilution was then preformed to create media solutions that ranged from 100 μM to 1.7 nM. Pure media was used as the control condition. At the 100 μM concentration there was no observed precipitation of either DOX or DOX-PCB. The IC_{50} of DOX-PCB was not reached at 100 μM concentration so a second experiment was run where the maximum concentration of DOX and DOX-PCB was 1000 μM. The same method of one third serial dilutions as described above was used for the high concentration IC_{50} experiment. No significant precipitation of DOX-PCB occurred although there was precipitation of DOX at the 1000 μM concentration level.

The media of each well with adherent cells was then replaced with the appropriate premixed media/drug solution causing minimal disturbance to the cells themselves. The cells were allowed to incubate at 37ºC for 72 hours. After 72 hours an XTT cell viability assay was performed using the In Vitro Toxicology Assay Kit (TOX2) from Sigma-Aldrich using phenol red free DMEM Media containing 10% Fetal Bovine Serum, and penicillin-streptomycin from Gibco. Absorbance measurements were taken with a Tecan Infinite M200 plate reader (San Jose, CA, USA). The percent viability vs. dose curves were generated using the PRISM 4.0 program from GraphPad Software Inc. (La Jolla, CA, USA) with the sigmoidal dose – response (variable slope) curve fit.

UV Stability Experiments

In order to understand the stability and release characteristics of DOX from the DOX-PCB prodrug upon UV exposure an HPLC/mass spectrometry analysis was preformed using an Agilent 1100 Series LC (Santa Clara CA, USA) connected to an

Agilent MSD G2445D (Santa Clara CA, USA). The column used was a Supelco Discovery HS C18 (5cm X 2.1 mm, with a 3μM bore size) (Bellefonte, PA, USA) and was maintained at a temperature of 20.0°C. The detection wavelengths were λ_1 250 nm and λ_2 400 nm. An 8 μL injection was used with a solvent mixture of acetonitrile (ACN) and water with 0.1%TFA using a gradient of 10-90% ACN.

First a standard curve of total ion count peak values for DOX was created using the above protocol and samples of known DOX concentration from 0.01μM to 100μM in 10X increments in a DMSO/water (20/80, v/v) solution. The peak value of the total ion count for each DOX concentration was collected and the data was fitted to a Boltzman sigmoidal curve using the program PRISM 4.0 from GraphPad Software Inc. (La Jolla, CA, USA) for the concentration range between 0.01 and 100 μM.

Duplicate samples of 100 μM DOX-PCB in DMSO/water (20/80, v/v) in 10 μL amounts where prepared and then exposed to a 1.8 mW/cm^2 UV source for different durations of time as described above. The samples were placed in an Optilux Microtest 96 well assay plate (BD Biosciences, San Jose, CA, USA) with opaque black walls and a clear bottom to prevent reflections of UV in the well ensuring more uniform and repeatable UV exposure to each sample. The cleavage of DOX from DOX-PCB was most sensitive to 350 nm. The peak of the total DOX ion count for each sample was determined using the same HPLC/mass spectrometry protocol as described. These values were then fitted to the standard DOX curve to determine the concentration of the released DOX.

Metabolic Stability using Human Liver Microsomes

To test the metabolic stability of the DOX-PCB molecule a human liver microsome assay was run using the BD Biosciences (San Jose, CA, USA) NADPH regeneration system. The human liver microsomes were purchased from Sigma and had a protein content of 20mg/ml. They were pooled from several different human donors. The following protocol was adapted from the NADPH regeneration system suggested protocol.

One assay was run with pure DOX and the other three assays with DOX-PCB. The pure DOX assay acted as the control by looking for the expected metabolite Doxorubicinol, see Figure 1.7D. All reagents were warmed to 37ºC. The assay solution consisted of 80µL of 0.5M KPO_4, 20 µL of solution A (NADP+ and Glc-6-PO4) from the NADPH regeneration system kit, 4 µL of solution B (G6PDH) from the NADPH regeneration system kit, 278 µL of H_2O, and 8 µL of either an 10mM solution of DOX or DOX-PCB in DMSO. The sample of DOX-PCB used here was not purified because the synthesis reaction went nearly to completion with only a residual amount of DOX present. To this solution was added 10 µL of the microsomes. The samples were then incubated in a shaker at 37 ºC for 30 min.

At the end of 30 min, 400 µL of acetonitrile was added to the reaction. The mixture was vortexed for 2 min to stop the reaction of the microsomes and extract DOX and potential DOX-PCB metabolites from the reaction mixture. The mixture was centrifuged until two layers were obtained. The top acetonitrile layer was removed and centrifuged. An HPLC / mass spectrometry analysis was done on the

filtered supernatant of the acetonitrile layer using the same analysis protocol for the UV stability study with the detection wavelength at 280 nm.

Results

Preparation of the photocleavable prodrug DOX-PCB

We have introduced a photosensitive blocking group to reduce the cytotoxicity and reactivity of the chemotherapy drug Doxorubicin with the option of fully regaining these effects upon UV irradiation. Binding the photocleavable blocking group to the active amine within the DOX structure takes advantage of the high reactivity of this group to ensure that the blocking occurs selectively at this controlled location. Attaching certain groups to the active amine itself has been shown to significantly reduce the toxicity of DOX [44]. Choosing the correct linking molecules attached to the photocleavable group can reduce the drugs toxicity through steric hindrance and also by specific interactions with various intracellular compartments and membranes. For the design of DOX-PCB, a water soluble photocleavable biotinylated compound (PCB) was chosen which included an ortho-nitrophenyl group for its photo cleavability [45], and a water soluble glycol spacer arm ending in a biotin group for enhanced membrane interaction. During synthesis, the photocleavable group was protected with an n-hydroxy succunamide group (NHS) which enabled its covalent attachment to the amine group in the DOX structure. The synthetic scheme is shown in Figure 1.1.

Characterization of DOX-PCB

Characterization was preformed on DOX-PCB to confirm the structure of the compound proposed in Figure 1.1. High resolution mass spectrometry of DOX-PCB found that it had complexed with Na^+. The measured mass of DOX-PCB- Na^+ was 1244.4329 m/z and the theoretical mass was 1244.4316 m/z. These two values are well within the 0.4% calibration error of the analysis and ensures confidence that DOX-PCB had the proposed structure shown in Figure 1.1.

An HPLC/mass spectrometry analysis was preformed on DOX-PCB, and showed a single peak for DOX (peak 1) at 22 minutes of elution as seen in Figure 1.2A. The analysis of DOX-PCB shown in Figure 1.2B showed two peaks at 26 and 27 minutes of elution (peaks 2 and 3). Both peaks had the same characteristic mass of DOX-PCB. These peaks most likely represented two stable diastereoisomeric forms of the compound [46]. The biotin portion of the PCB is chirally homogenous, but the stereo center at the methylene group ortho to the nitro group is a mixture of R and S (Ambergen Inc., personal communication). The interaction of PCB with the hydrophobic portion of the DOX ring structure affects the overall polarity of the two diastereoisomers differently, allowing separation on the C18 column. Both diastereoisomeric forms of DOX-PCB were isolated and no significant difference in cytotoxicity between them was observed. All the studies described here used DOX-PCB samples that combined the two peaks.

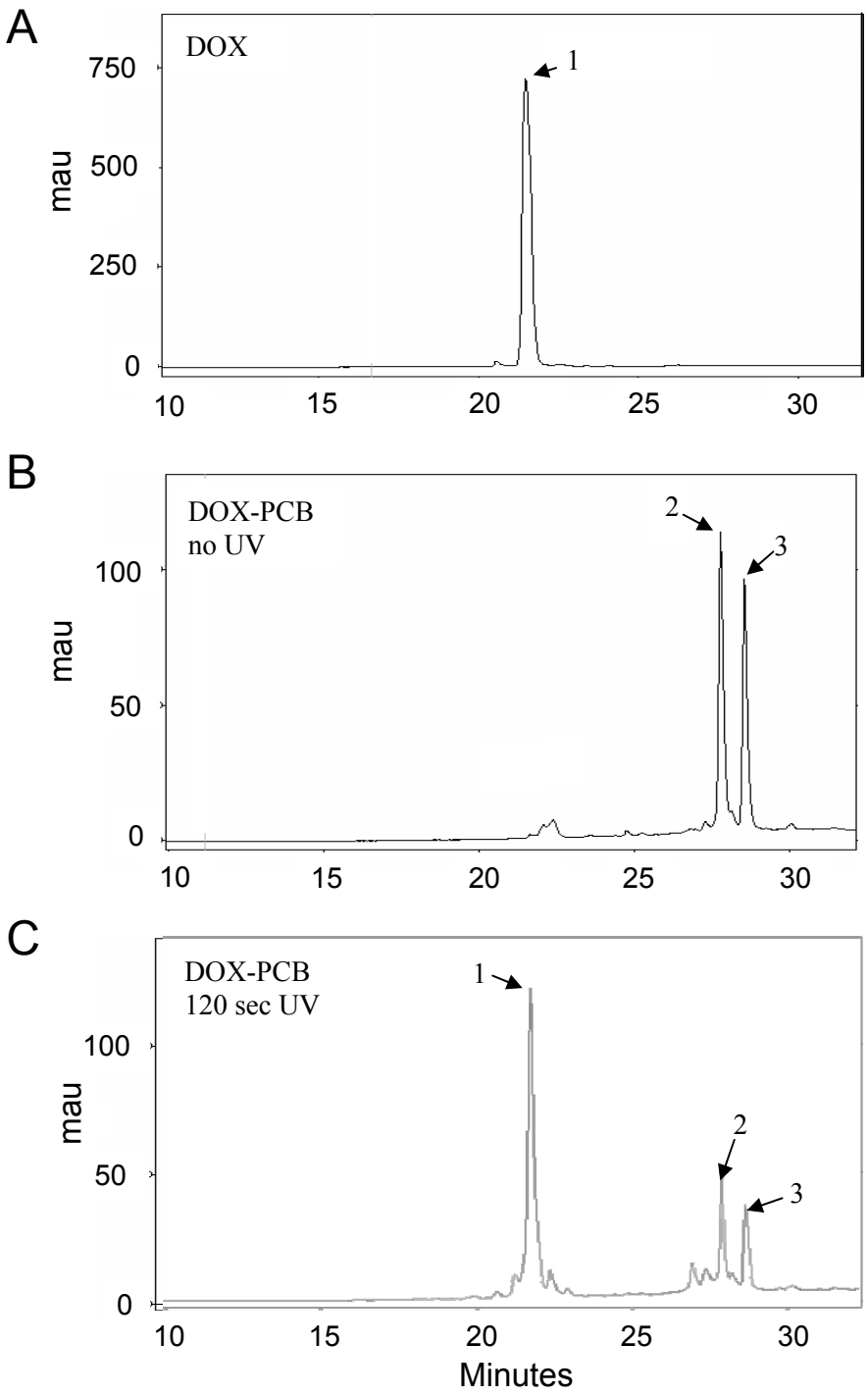

Figure 1.2 – HPLC analysis of DOX-PCB before and after UV exposure.
(A) Peak 1 contains pure DOX.
(B) Peaks 2 and 3 both contain DOX-PCB in two diastereoisomeric forms.
(C) The HPLC of the DOX-PCB sample after exposure to UV. The peak 1 containing DOX appears along with shortened Peaks 2 and 3 containing DOX-PCB.

Release of intact DOX

It is essential that DOX-PCB release active DOX upon UV exposure so as to obtain the maximum therapeutic effect. Substituents left on the DOX could significantly reduce its toxicity and the overall effectiveness of the prodrug. Releasing free DOX from the DOX-PCB conjugate is based upon the photocleavable characteristic of the nitrophenyl group introduced by Patchornik [45]. The mechanism of photolysis has been adapted from established mechanisms and is shown schematically in Figure 1.3 [47]. Light absorption at 350 nm causes the electron configurations in the nitrophenyl group to rearrange inducing the formation of an unstable 5 membered ring with one of the nitro group's oxygen atoms. The destabilization and rearrangement of this ring causes the cleavage, releasing the carbamate group along with DOX. The carbamate undergoes hydrolysis in aqueous conditions producing CO_2 and free DOX.

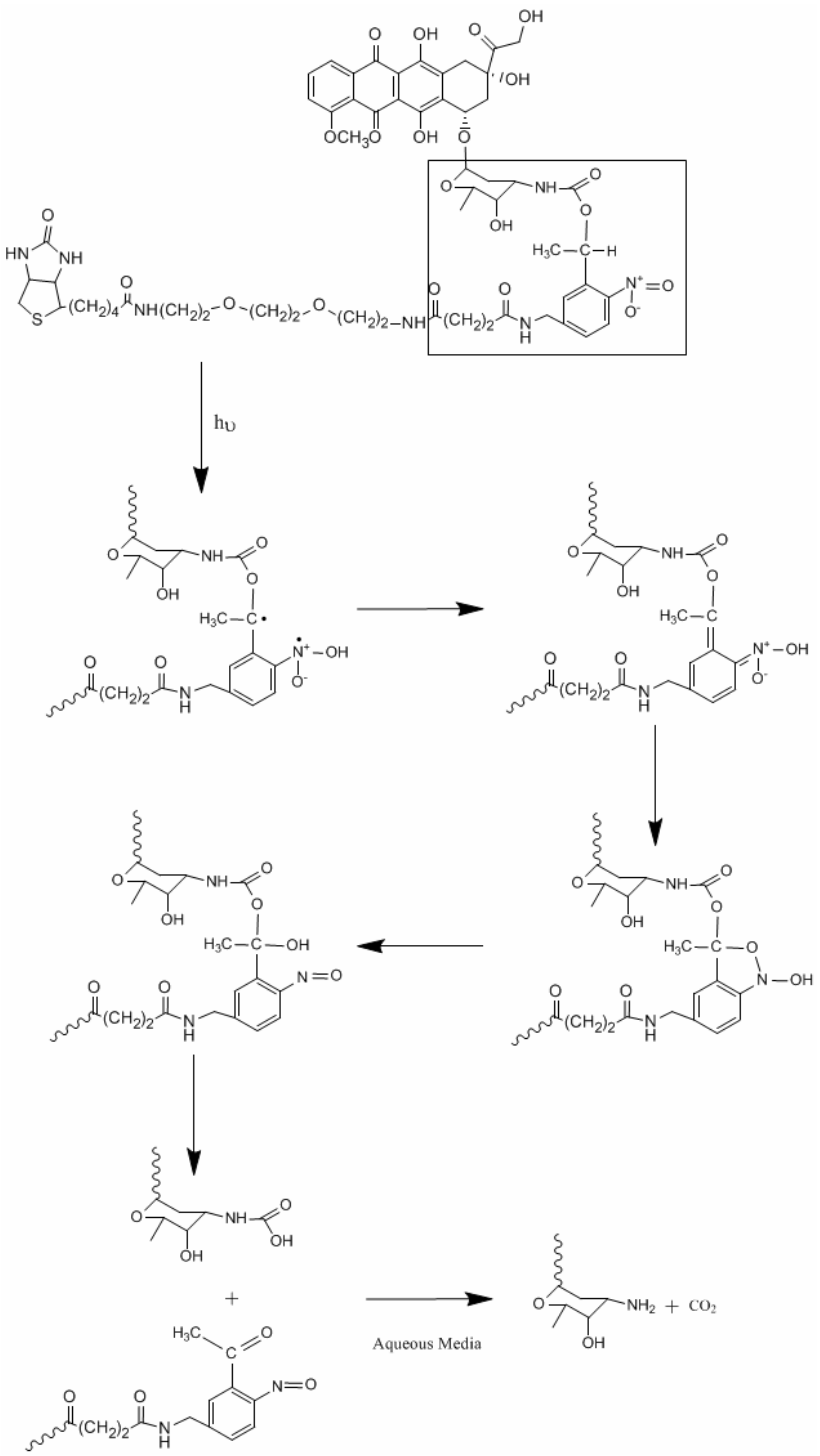

Figure 1.3 – Mechanism of DOX-PCB photolysis and product release with subsequent hydrolysis to produce free DOX and CO_2.

The release of free active DOX from DOX-PCB upon UV exposure was confirmed by an LC Mass Spectrometry analysis. The HPLC for the purified DOX is shown in Figure 1.2A. The mass spectrometry for peak 1 confirms the presence of DOX. The HPLC for purified DOX-PCB with no UV exposure is shown in Figure 1.2B. Mass specs for peaks 2 and 3 confirm the presence of DOX-PCB. The HPLC for the DOX-PCB sample that had been exposed to 120 sec of UV is shown in Figure 1.2C.

The mass spectrometry analysis identified peak 1 as DOX, and peaks 2 and 3 as DOX-PCB.

The release of intact DOX was also confirmed by proton NMR. An NMR of DOX was taken and is shown in Figure 1.4A. It displayed a prominent peak at 5.27 ppm attributed to by the free amine protons under the solvent conditions of DMSO/water (10/90, v/v). An NMR of a purified DOX-PCB sample should not have a chemical shift peak from the two amine protons due to the carbamate linkage. As expected, the NMR of pure DOX-PCB shown in Figure 1.4B demonstrated an absence of the 5.27 ppm peak. This same DOX-PCB sample was then exposed to the UV. The NMR from the sample after the UV exposure is shown in Figure 1.4C. The peak at 5.27 ppm was restored indicating that free DOX was released upon UV exposure.

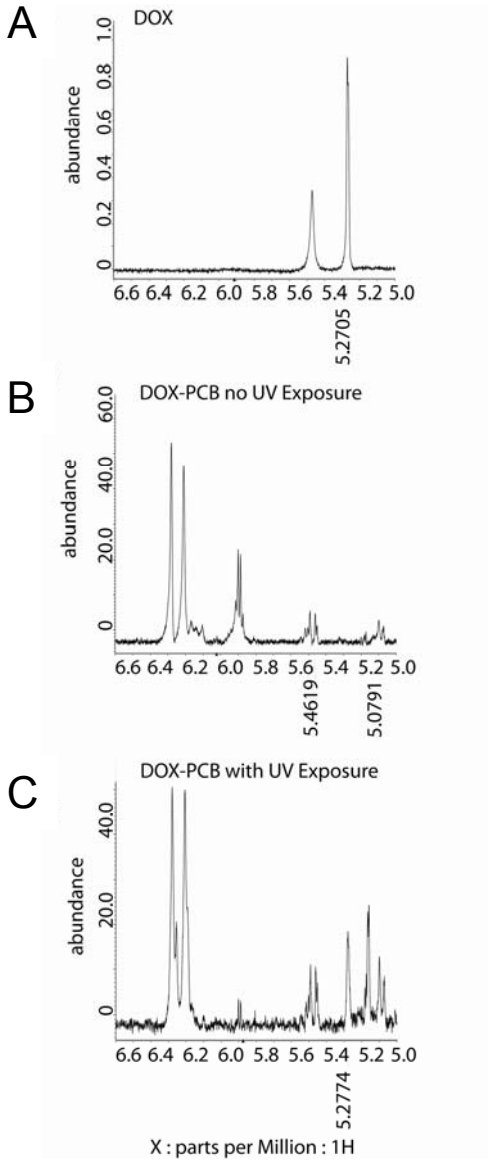

Figure 1.4 – NMR analysis of the chemical shift for free DOX, pure DOX-PCB, and DOX-PCB after UV exposure.
(A) The NMR of DOX showed the chemical shift for the two amine protons to be at 5.27 ppm (DMSO/water, 10/90, v/v).
(B) This peak was absent in a sample of pure DOX-PCB.
(C) After exposure to UV, the DOX-PCB sample had a restoration of the 5.27 ppm peak indicating the release of free DOX.

Theoretical three dimensional structure of DOX-PCB in water

The three dimensional structure of DOX-PCB in water is shown in Figure 1.5. The ball and stick model is shown in Figure 1.5a and indicates that the DOX-PCB molecule folds over on itself in a hairpin structure. This may be caused by hydrophobic interactions between the conjugated ring structure of the DOX with the hydrophobic nitrophenyl compound. Figure 1.5b shows the space filling model to help clarify and proximity of the conjugated ring structure to the rest of the molecule.

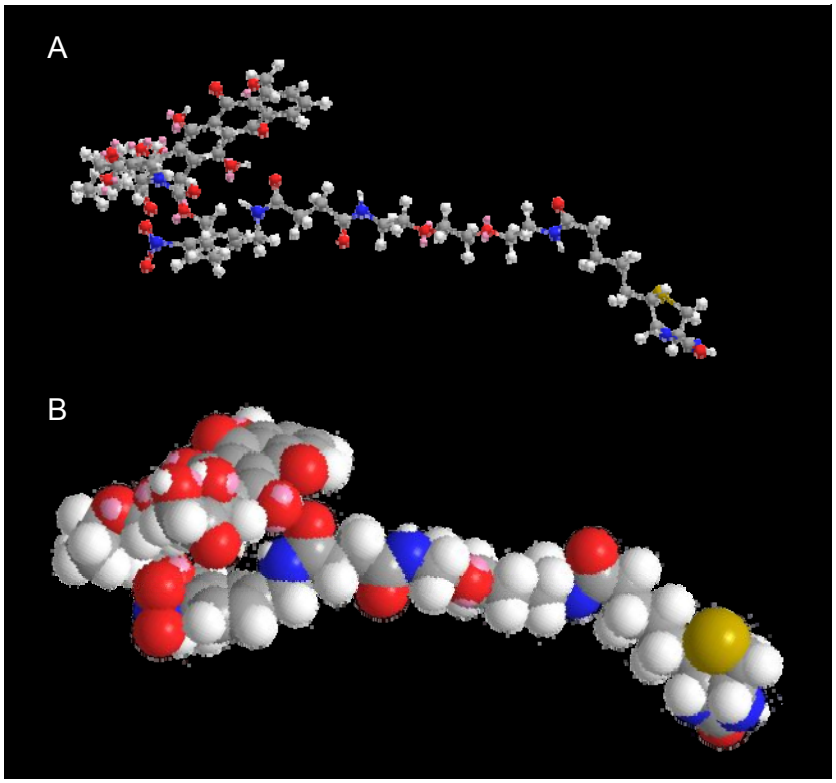

Figure 1.5 - The predicted three dimensional model of the DOX-PCB molecule in water.
(A) The ball and stick model shows the DOX-PCB molecule folds over on itself creating a hairpin structure.
(B) The space filling model helps clarify the proximity of the conjugated ring structure of DOX to the rest of the molecule.

Cell uptake and cellular localization

The free DOX released from DOX-PCB needs to have the same cellular localization properties as normal free DOX for maximum therapeutic effect. DOX and DOX-PCB are naturally fluorescent and their localization can be monitored over time in live PTK2 cells using both phase contrast images (top row in Figure 1.6) and fluorescent images of the same field (bottom row of Figure 1.6). The intracellular localization of DOX was distinct from that of DOX-PCB. Within hours of exposure DOX entered the cells and was concentrated almost exclusively in the nucleus shown by the arrows in Figure 1.6A and Figure 1.6B. The top cell of Figure 1.6A was not undergoing mitosis and DOX penetrated the nuclear membrane and associated with the chromatin most likely through a DNA intercalation mechanism [48]. It can be seen that the cell in the middle of Figure 1.6A was undergoing an abnormal mitosis. The nuclear membrane was degraded and DOX strongly localized to the exposed chromosomes. The abnormal appearing mitosis was most likely caused by the interference of DOX with the DNA replication mechanisms. There were very few observations of cells undergoing mitosis, all of which appeared abnormal.

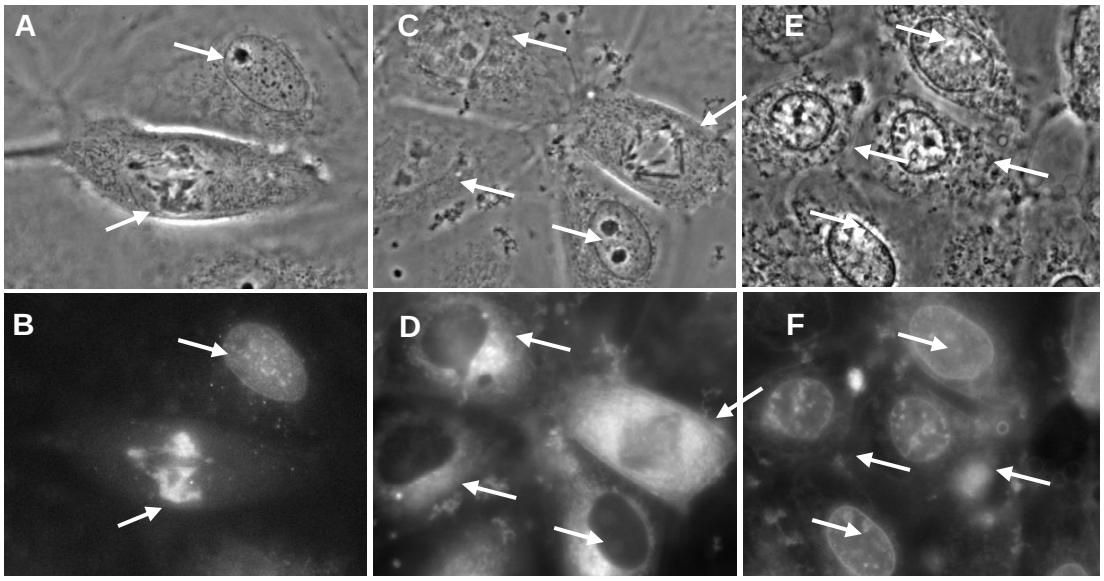

Figure 1.6 – Microscopy images of DOX and DOX-PCB localization within PTK2 kidney epithelial cells.
Panels A, C, and E (top row) are phase contrast images of the cells. Panels B, D, and F (bottom row) are fluorescent images of the same field of view as the images directly above.
(A, B) DOX strongly associated with the chromosomes as pointed out by the arrows.
(C, D) DOX-PCB entered the cells but did not associate with the chromosomes as pointed out by the arrows.
(E, F) When exposed to UV, free DOX was released from DOX-PCB and the chromosomes began to fluoresce as seen pointed out by the arrows.

DOX-PCB also entered the cell quickly. However, it did not concentrate in the nucleus as pointed out by the arrows in Figure 1.6C and Figure 1.6D. DOX-PCB appeared to preferentially accumulate within the cell in regions around the nucleus. Future studies using colocalization staining techniques will help identify which cellular structures DOX-PCB interacts with. The right most cell is shown undergoing a normal appearing mitosis where the nuclear membrane has disassembled. It is clear that DOX-PCB had been excluded from the mitotic spindle and the associated

chromosomes. The DOX-PCB concentration was 10 times higher than DOX and the cells seemed much healthier and appeared to be undergoing normal mitosis.

When the same DOX-PCB chamber of cells from Figure 1.6C and Figure 1.6D was exposed to UV, the red fluorescence accumulated in the nucleus 1 hour after exposure as pointed out in Figure 1.6E and Figure 1.6F. The free DOX that was released from DOX-PCB appeared to be behaving similar to free DOX with its ability to pass through the nuclear membrane and bind to the chromatin. The DOX-PCB that was not photolysed by the UV remained outside the nucleus. These cells appeared to have pyknotic nuclei with a darkened nuclear envelope and also appeared to have highly granulated cytoplasms, both features of cell death. The UV dose received by the cells themselves did not influence the interaction with DOX-PBC. This was evidenced by the fact that control cells which were not exposed to UV, but were incubated with the DOX-PCB sample that was separately irradiated by UV, exhibited the same behavior (data not shown).

The difference in the cellular localization behavior between DOX and DOX-PCB can be partially explained by the three dimensional structure of DOX-PCB as shown in Figure 1.5. The conjugated ring structure of DOX is what intercalated between base pairs of the DNA causing a large portion of the cytotoxicity. The hairpin structure of DOX-PCB sequesters the conjugated ring structure preventing it from having access to the DNA. This may explain the lack of DOX-PCB in the nucleus and in the exposed chromosomes which DOX heavily stains.

Cytotoxicity

For the prodrug effect to be pharmacologically useful, the DOX-PCB needs to show a greatly reduced toxicity compared to that of DOX. The results of the cell proliferation assay on A549 human lung cancer cells are shown in Figure 1.7A. The IC_{50} of the DOX sample was 1.2 μM. The IC_{50} of DOX-PCB was over 200 times higher at 250 μM indicating a significant prodrug effect. The large prodrug effect of DOX-PCB makes it a good candidate to reduce the undesirable systemic side effects of DOX, especially the cardiotoxicity. The observed lack of DOX-PCB interaction with DNA helps to explain the significant reduction in the cytotoxicity of DOX-PCB over that of DOX.

For the prodrug effect to be truly functional, the toxicity of the DOX-PCB sample needs to increase upon UV exposure and release fully active DOX with well characterized potent bioactivity. Figure 1.7B shows a table of IC_{50} values for DOX-PCB samples exposed to the UV for increasing amounts of time. The DOX-PCB samples dissolved in media were exposed to the UV separately and then incubated with the cells, so the cells were never exposed to UV. As exposure time of the media increased, the IC_{50} decreased approaching that of free DOX due to the increasing amounts of free DOX that were released from the DOX-PCB.

A

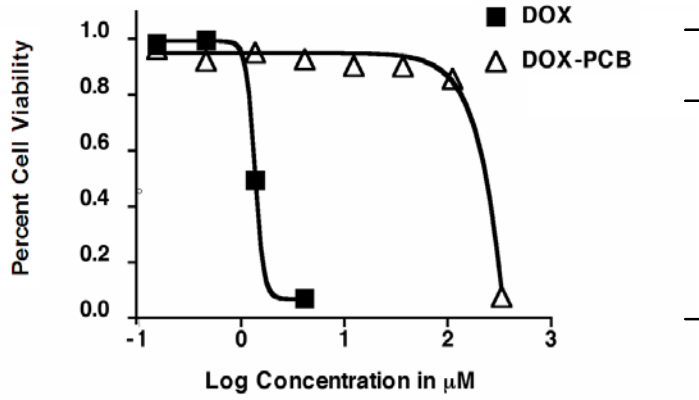

B

UV Exposure time min	IC_{50} Values μM
0	250
2	100
20	5
60	3.5
DOX	1.2

Figure 1.7 – Cell viability results from DOX, DOX-PCB, and DOX-PCB exposed to increasing amounts of UV
(A) Cell viability curve for A549 human lung cancer cells exposed to DOX and DOX-PCB with no UV exposure. The IC_{50} for DOX was 1.2 μM. The IC_{50} of DOX-PCB with no UV exposure was over 200 times higher at 250 μM.
(B) This table shows the IC_{50} values of DOX-PCB samples after different amounts of UV exposure. The DOX-PCB samples were dissolved in media and exposed to the UV and then incubated with the cells, so the cells were not exposed to UV. As UV exposure time increased, the IC_{50} value decreased approaching that of pure DOX due to the higher doses of free DOX released from the DOX-PCB.

UV Stability Experiments

The release characteristics of DOX from the DOX-PCB prodrug had a linear relationship ($R^2 = 0.99$) with the amount of UV exposure (data not shown). After exposure to the 1.8 mW/cm^2 UV source for 10 min, 18% of the total DOX-PCB content in a 100μm sample was converted to DOX. The release rate of intact DOX was 1.8 μM/min.

Metabolic Stability using Human Liver Microsomes

To maintain control over the spatial location of DOX-PCB activation it is important that the only significant pathway of activation be from UV exposure and not

from normal metabolic activity, especially from the liver. Incubation of DOX-PCB with human liver microsomes indicates that the compound is quite resistant to metabolic breakdown. Figure 1.8A shows the HPLC results of the LC Mass analysis of DOX-PCB after incubation with the human liver microsomes. Peak 1 contains DOX-Cl a residue most likely left over from the synthesis. Peak 2 contains DOX-Na which is again most likely a residue from the synthesis. Peak 3 contains DOX-PCB. Peak 4 contains DOX-PCB, most likely the second isomer, as well as a mass spectrometry peak at 579 m/z with the proposed structure shown in Figure 1.8B. This 579 m/z metabolite is not the DOX-Cl complex because it shows up in the 10.2-10.5 min peak on the HPLC whereas DOX-Na and DOX-Cl showed up well before that. The precursor to the 579 m/z metabolite was found in the first of three replicates of this experiment with a mass of 587 m/z with the proposed structure shown in Figure 1.8C. The hydrolyzing enzymes in the liver microsomes most likely cleaved the DOX-PCB molecule producing the unstable 587 m/z fragment which was then fully reduced to the 579 m/z metabolite, much like DOX is reduced to Doxorubicinol shown in Figure 1.8D. The main 579 m/z metabolite was produced in relatively small quantities and has a substituent on the active amine. Although it is unknown what effect this particular substituent will have on the toxicity of this metabolite it has been demonstrated that similar substituents significantly reduce the toxicity of DOX [44].

The product of the microsome incubation of DOX was Doxorubicinol. Doxorubicinol has previously been established as the major metabolite of DOX with the structure shown in Figure 1.8D [49, 50]. This served as a positive control for the microsome protocol.

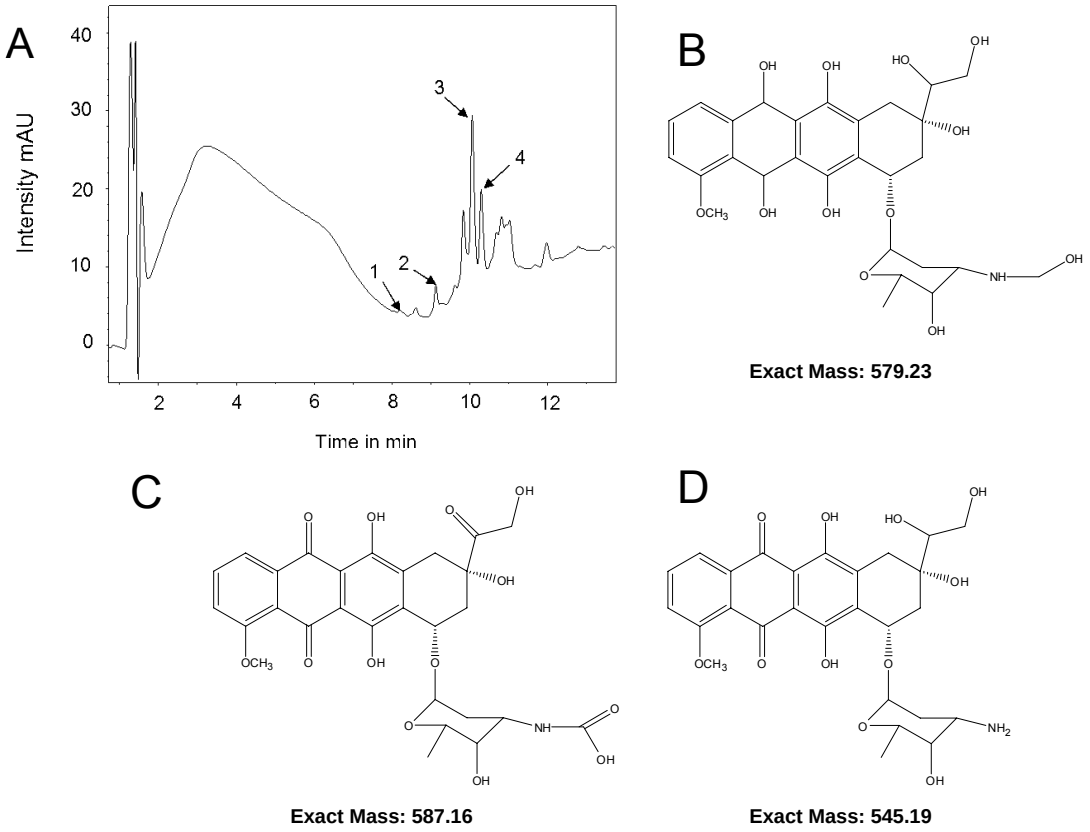

Figure 1.8 – LC mass analysis of DOX-PCB incubated with human liver microsomes and the proposed structures of the resulting metabolites.
(A) HPLC from the LC mass analysis of the human liver microsome experiments.
(B) Proposed structure for the 579 m/z DOX-PCB metabolite.
(C) Proposed structure for the 587 m/z DOX-PCB metabolite that might be the precursor for the 579 m/z metabolite.
(D) Structure of Doxorubicinol

Discussion

In this paper we have developed a new photocleavable prodrug for cancer therapy by incorporating the active chemotherapy agent DOX with the photocleavable protecting group PCB to form the adduct DOX-PCB. It has been shown that DOX-PCB is over 200 times less toxic than DOX and upon irradiation active DOX is

released. With the use of small light emitting diodes or fiber optics to deliver controlled localized doses of 350nm light to desired tissue regions it should be possible to administer a systemic dose of the prodrug and release active DOX only within the tumor region. The prodrug has the potential to enter cells in its caged form without being metabolized to a pharmacologically active form. A systemic administration of the prodrug would allow it to enter cells and remain in the region of interest even after the freely circulating prodrug has been cleared from the system. It is important to note that a control experiment was run where the A549 cells were exposed only to the UV light source used for UV irradiation of DOX-PCB samples. There was no reduction in cell viability compared to control cells after 20 min of exposure. After 60 min of exposure the cell viability was reduced 10%. This reduction may be contributed to by the 334 emission peak from the Mercury Arc lamp leaking through the lower end of the 330-380 nm bandpass filter [51].

The incorporation of the biotin moiety is intended to help increase the clearance rate of the freely circulating DOX-PCB just before UV exposure. Free DOX-PCB in the tumor bloodstream at the time of UV exposure would release free DOX into the circulation. Only DOX-PCB that is present inside the tumor cells should be activated. The biotin on DOX-PCB allows for use of a clearing agent such as modified versions of biotin-galactose-human serum albumin [52] or biotin-LC-NM-$(GalNac)_{16}$ [53] where the biotin would be replaced with streptavidin. These clearing agents very effectively reduce the circulating blood concentration of the target molecule and are designed to use the galactose residue to trigger uptake by galactose receptors in hepatocytes where the entire complex is metabolized. The human

microsome experiments indicate that the DOX-PCB drug will remain intact through that process. The biotin end of the prodrug will also help increase the clearance rate of the PCB fragment created by the UV exposure.

The presence of the biotin on DOX-PCB should not cause undesirable tissue accumulation or protein binding in vivo as has been shown with a compound comprised of biotin bound to a chelated radioisotope [52]. The biotin present on this chelated radioisotope did not cause significant accumulation in any particular tissue, including the liver. The compound was rapidly cleared from the body through the renal system.

The use of photocleavable prodrugs offers an exciting new avenue of investigation in reducing the systemic side effects of chemotherapy drugs and other therapeutic agents while increasing their effectiveness in the desired tissue region. Future work will focus on extensive in vivo characterization including in vivo stability of DOX-PCB as well as its possible therapeutic effectiveness.

Conclusion

One strategy to reduce the toxic side effects of chemotherapy agents is to make prodrugs by chemically modifying the agents in a way to reduce their overall toxicity, but which would also allow them to be activated back to a therapeutic state in the tumor tissue. One of the challenges is to differentiate the tumor from the healthy tissue in order to effectively trigger the prodrug only in the tumor. The triggers of many prodrug designs rely on inherent biochemical differences between the tumor and healthy tissue. These differences can be very subtle and often healthy tissues within

the body will have the same biochemistry as the tumor. To avoid the undesirable activation of the prodrug in these untargeted tissues an artificial difference can be created within the tumor tissue from a source external to the body. The trigger considered here is UV radiation at 350 nm. This is at the very low energy end of the UV spectrum with good tissue penetration and little interaction with DNA and protein. A new prodrug of doxorubicin (DOX-PCB) is described that can be converted to the active drug upon exposure to UV at 350 nm. It was formed by conjugating a photocleavable blocking group to the sugar amine group of DOX. DOX-PCB was shown to have a significant reduction in toxicity over free DOX with a 200 fold lower IC_{50} in cell viability tests. One of the possible reasons for the lower toxicity is that the PCB portion blocks DOX-PCB from intercalating with DNA, which is a main mode of action for DOX. DOX-PCB was shown to be stable in a human microsome experiment indicating that DOX will not be released in a significant amount due to metabolic conversion. DOX-PCB was shown to release biologically active doxorubicin upon exposure to UV at 350 nm increasing the cytotoxicity of the entire sample. It is possible to deliver UV only to the tumor region using UV fiber optics or implantable UV LED's. This could cause the activation of systemically administered DOX-PCB only in the tumor, thereby reducing systemic side effects.

Acknowledgments

The authors are grateful for the support of Anthony Mrse, Norman Baker, Yongxuan Su, Dmitri Simberg, Christina Wu, Dominic Yee, Howard Cottam, and Lianglin Zhang in the collection and interpretation of the data. The authors also wish

to thank Ambergen Inc, for clarification of the structural details of the PCB diastereoisomers. The study was supported by the National Cancer Institute grant # 5 U54 CA119335.

The coauthors of this chapter are as follows: Stuart Ibsen[1], Eran Zahavy[2], Wolf Wrasdilo[3], Michael Berns[4], Michael Chan[3], Sadik Esener[5].

[1]Department of Bioengineering, Moores Cancer Center, University of California San Diego, 3855 Health Sciences Dr. # 0815, La Jolla, CA 92093-0815, Phone (858) 534-9848, Fax: (858) 534-9830, Email: sibsen@ucsd.edu

[2] Department of Physical Chemistry, Israel Institute for Biological Research, P.O. Box 19, Ness-Ziona 74100, Israel.

[3] Moores Cancer Center, University of California at San Diego, La Jolla, CA 92093 USA

[4] Department of Bioengineering, University of California at San Diego, La Jolla, CA 92093 USA

[5]Department of Nanoengineering, University of California at San Diego, La Jolla, CA 92093 USA

Chapter 2

Localized Tumor Specific Activation of a Photactivatable Doxorubicin Prodrug

Abstract

Localized photoactivation of a chemotherapy prodrug specifically in deep internal tumor tissue was demonstrated here for the first time using the doxorubicin/photocleavable biotin prodrug DOX-PCB. In vivo conversion of systemically injected DOX-PCB to active DOX was demonstrated and was localized to tumor tissue exposed to 365 nm light with the use of a customized UV LED delivery system. A control tumor on the other side of the mouse was not exposed to the 365nm light and showed only a trace amount of DOX. The clinical formulation of DOX-PCB for injection required solubilization with the cyclodextrin Captisol system. Pharmacokinetics of DOX-PCB circulation and elimination were also studied in mice not exposed to 365nm light. The DOX-PCB was found to have a circulation half life of 10 min which was comparable to that of DOX itself at 20 min. No DOX-PCB was found in the urine out to 24 hours post injection. No DOX was found in the urine or in the serum indicating that the DOX-PCB was not being activated to DOX by metabolic processes in the mouse. This proof of concept demonstrates the applicability and conversion localization of a light activated prodrug.

Introduction

In chapter 1 a photoactivatible prodrug of Doxorubicin (DOX) was prepared and characterized where the free amine of the sugar moiety was blocked with a nitrophenyl compound conjugated to a short PEG linker and terminated in a biotin as

shown in Figure 1.1. This Doxorubicin/photocleavable biotin (DOX-PCB) molecule was shown to have a 200 times reduction in toxicity to A549 lung cancer cells and could release pharmacologically active DOX upon exposure to 365 nm light. Such a scheme has not been demonstrated in-vivo in the literature before and the study described here looks at the feasibility and localization of this release scheme in-vivo through 3 sets of experiments

The first set of experiments look at UV penetration through ex-vivo tumor tissue and subsequent DOX-PCB activation using the custom designed UV LED delivery system.

The second set of experiments look at the circulation half life and elimination of DOX-PCB in mice.

The third set of experiments look at the in-vivo activation of DOX-PCB within tumor tissue of systemically administered DOX-PCB. Two orthotopic tumors were implanted into mice on either flank. One tumor was exposed to UV using a LED delivery system and the other was used as an internal control.

DOX-PCB required a solubilization agent for in-vivo injection because it displayed poor inherent water solubility. DOX-PCB was observed to be soluble in cell culture media if first dissolved in DMSO and injected straight into the media. This apparent solubility was most likely due to DOX-PCB adsorption to proteins found in the media itself, because the same injection of DMSO/DOX-PCB into water resulted in instant precipitation. For in vivo injection the concentration of DOX-PCB in the injectant needed to be 2mM which made it necessary to use the well characterized and non-toxic cyclodextrin solubilizing agent Captisol. This kept the DOX-PCB soluble in

saline at a high enough concentration without the use of organic solvents to make it safe for injection.

Materials and Methods

Preparation of DOX-PCB

Synthesis of DOX-PCB was preformed as described in chapter 1. The DOX-PCB was then dissolved in 50 µl of DMSO and was then purified on a semiprep HPLC system using a 10-90 ACN:H_2O 0.05%TFA gradient set over 20 min. The resulting fraction containing the two DOX-PCB isomers were collected and pooled into the same sample. The sample was then lyophilized and stored at -20°C wrapped in foil.

UV LED/Fiberoptic Delivery System

A custom designed UV LED/fiber optic delivery system was developed in collaboration with Prizmatix Ltd. that had a fiber optic coupled to a 365 nm LED. The end of the fiber was encased inside a beveled metal tube that was the equivalent of a 22 gauge needle.

Tumor Preparation

A549 cells were expanded in 25 ml flasks. They were trypsinized and washed with cold PBS. They were then resuspended in cold PBS at a concentration of 1 X 10^8 cells/ml. 1.2ml of the cell suspension was added to 1.2 ml of matrigel and kept on ice. 200 µl of the mixture was injected in the left and right flanks of 5 female athymic

nu/nu nude mice. The tumors were allowed to grow for 1 month until they reached the size of $1cm^3$.

Ex-vivo 365nm Light Penetration of Tumor Tissue

A Newport 1830-C Optical Power Meter with a Newport 818-UV detector head and a Newport 883-UV OD3 filter was used to measure the 365 nm light coming from just the UV LED/fiberoptic turned to max power directly in front, from the right side and from above. The system needle was inserted into the middle of a 9x6x5 mm tumor prepared in the manner stated above that was collected from a mouse never injected with DOX-PCB or DOX. The measurements were taken again from a distance of 10 mm. The UV LED was set to maximum power.

DOX-PCB activation in ex-vivo tumor tissue

An ex-vivo experiment was run to establish the activatability of DOX-PCB in an actual tumor sample prepared in the manner stated above that was collected from a mouse never injected with DOX-PCB or DOX, The tumor was cut into 3 sections of 30 mg each. The first sample was injected with 10 µl DMSO containing 224 ng of DOX-PCB and 20 ng of DOX. The other two samples were injected with 10 µl DMSO containing just 224 ng of DOX-PCB. One of these samples was exposed to 30 min of UV using the UV fiber optic system described above. The entire 10 µl injection of DMSO did not enter the tissues because it was very stiff and the DMSO came back through the needle track. However, the tissue was incubated in the excess DMSO fluid for 15 min giving the DMSO enough time to penetrate deep into the sample carrying

the dissolved compounds with it. The tissue integrity was not compromised by the DMSO.

DOX-PCB Solubilization with Captisol Cyclodextrin

It was found that the DOX-PCB was solubilized in the cyclodextrin better when first treated in the following manner to create a solvent complex and possible salt. 1 mg of the lyophilized DOX-PCB powder was dissolved in 500 µL of methanol and dried in a speedvac. The dried DOX-PCB was then dissolved in 50 µL of DMSO. This was also dried down in a speedvac but only until it was in an almost dry tacky state. 10 µL of a $NaHCO_3$/NaOH buffer at pH 9 was added. The entire mixture was then dissolved in 500 µL of methanol and put in a small agate mortar. The motor was placed under low vacuum for at least 5 hours to evaporate the methanol. The 10 µL of a $NaHCO_3$/NaOH buffer helped to change the pH as the methanol evaporated ionizing the DOX-PCB to assist in the formation of the Captisol complex.

After the methanol was evaporated from the mortar, 40 mg of Captisol brand cyclodextrin dry powder was added and mechanically ground with the dried DOX-PCB with the small pestle until a fine purple colored powder was formed. 200 µL of sterile saline was added and then solution bath sonicated for 10min. The maximum concentration achieved of the DOX-PCB in the Captisol solution was 2 mM. The samples were centrifuged at 18,000 rcf for 5 min to eliminate any precipitated DOX-PCB. The concentration of DOX-PCB in the supernatant was then measured using absorbance on a NanoDrop ND-1000 spectrophotometer.

DOX-PCB blood circulation half-life and urine elimination.

Two female nude mice were injected with 200 µl of the DOX-PCB/Captisol solution. Blood samples were collected at 5, 15, 30, 60 min and at 24 hours. The blood was centrifuged and 15 µl of serum was collected. Urine was collected when naturally possible from the mouse out to 24 hours.

Serum Extraction Method

30 µl of acetonitrile was added to the 15 µl blood serum samples from each time point. The samples were bath sonicated for 10 min. The sample was centrifuged at 18,000 rcf for 10 min and the supernatant collected. 30 µl of the supernatant was used for LC/mass analysis.

Urine Extraction Method

ACN was added to the urine sample (1:1)(v:v). The sample was then bath sonicated for 10 min. The sample was centrifuged at 18,000 rcf for 10 min. The supernatant was taken and dried in a speed vac. The precipitant was redissolved in 50 µl of ACN and sonicated. The sample was centrifuged again and the supernatant removed for analysis.

DOX-PCB Activation In Vivo

The 200 µl of DOX-PCB Captisol were injected slowly into the tail vein of the mouse. The mice were anesthetized with 120 µl of ketamine 4 min later which was enough to keep the mouse anesthetized for the 30 min duration of the UV

administration. 10 min after the DOX-PCB injection the UV LED was inserted into the middle of the tumor and turned to full power delivering 240 μW/cm^2. Only the tumor of the right side of the mouse was exposed. The UV was administered for a total of 30 min. Blood was drawn at 30 min after injection to obtain the circulating concentration. The mouse was then sacrificed and the tumors and other internal organs collected for analysis. Blood was also collected for serum analysis as described above.

DOX In-Vivo Control

A control mouse was injected with an identical dose of DOX dissolved in saline with 80 mg of Captisol to compare with DOX-PCB. The DOX mouse was treated the same as the DOX-PCB mice being given 120 μl of ketamine 4 min after tail vein injection. However, no UV was administered to the mouse. Blood was drawn at 30 min after injection to obtain the circulating concentration. The mouse was then sacrificed and the tumors and other internal organs collected for analysis. Blood was also collected for serum analysis as described above.

Tissue Extraction Method

30 mg of tumor tissue was frozen in liquid nitrogen and freeze fractured using a metal mortar and pestle. 400 μl of a 50 mM ascorbic acid buffer with 2mM D-L Saccharic acid raised to a pH of 4.5 by titration with 1 M NaOH was added o the tissue powder. This buffer solution stoped any enzymatic degradation of DOX or DOX-PCB within the tissue although studies showed that a 15 min incubation with the tissue powder in PBS did not cause any measurable degradation of DOX. The tissue

was aspirated 20 times in the buffer to break up the compacted powder chunks into a fine suspension. The sample was spiked with 20 ng of Epirubicin (EPI) from a (1:100)(v:v) ethanol mixture which was used as an internal standard. EPI is an isomeric form of DOX and can be separated from DOX on HPLC. It should display the same DNA intercalation properties as DOX. The spiked sample was allowed to incubate with the tissue suspension for 15 min to allow for tissue integration. The DNA was denatured from its double helix form to single stranded form to cause the release of any intercalated DOX by addition of 50µl of 3M $AgNO_3$ which caused the suspension to turn dark black. The samples were asperated 20 times and vortexed for 5 min. The excess Ag^+ ions were precipitated by the addition of 50 µl of 3M NaCl upon which the solution turned light grey. The sample was aspirated 20 times and vortexed for 5 min. To precipitate out proteins and other water soluble compounds 1.25 mL of acetonitrile/methanol (2:1)(v:v) was added. The sample was aspirated 20 times, vortexed for 10 min and then bath sonicated for 10 min. The sample was then centrifuged for 5 min at 3724 rcf. The supernatant was transferred to 2ml eppendorf tubes and centrifuged again at 18,000 rcf for 5 min to remove any possible debris. The sample was then speedvaced for approximately 1 hour to a volume of 500 µl to remove most of the acetonitrile and methanol. This helped to concentrate the sample 3 times and also helped sharpen the peaks of the different compounds on HPLC/MS/MS. A small amount of precipitation occurred but it was shown that this did not measurably reduce the DOX or DOX-PCB content of the supernatant. If the concentration was continued and the water volume reduced to 100 µl then significant

precipitation of the DOX-PCB and DOX did occur. This method was shown to have a DOX extraction efficiency of 80%.

Results

Ex-vivo 365nm Light Penetration of Tumor Tissue

The intensity of the 365 nm light coming from the UV LED/fiberoptic turned to max power was 240 $\mu W/cm^2$ as measured from 10mm directly in front. The UV light was undetectable from 10 mm to the right side of the fiber optic end and 10 mm from directly above.

The 365 nm light was heavily scattered in the tissue causing it to isotropically exit the tumor tissue. The measured intensity was 2 $\mu W/cm^2$ from 10 mm directly in front was, 2.9 $\mu W/cm^2$ from 10mm directly from the right side and 1.4 $\mu W/cm^2$ from10 mm from directly above.

DOX-PCB activation in ex-vivo tumor tissue

The results of the ex-vivo tumor exposure experiment are show in Figure 2.1. Fig 2.1a shows the LC/MS/MS trace for the extraction from tumor tissue spiked with DOX, EPI, and DOX-PCB. Peaks for all three compounds are present. Figure 2.1b shows the trace for the tumor sample injected with just DOX-PCB and EPI. No DOX is present. Figure 2.1c shows the trace for the tumor sample spiked with just DOX-PCB and EPI and then subsequently exposed to 30 min of UV. As can be seen the DOX peak is restored and the DOX-PCB peaks have been dramatically reduced in

magnitude due to the nearly complete conversion to DOX. This demonstrates that DOX-PCB can be converted to actual DOX within tissue using the 365 nm light.

Figure 2.1 - Ex-vivo tumor tissue activation of DOX-PCB.
(A) This shows the LC/MS/MS trace of the tissue extraction preformed on a tumor sample injected with DOX, EPI and DOX-PCB. The EPI serves as an internal standard.
(B) This shows the trace of a tumor sample injected only with EPI and DOX-PCB. As can be seen no DOX is present.
(C) This shows the trace from a tumor sample injected only with EPI and DOX-PCB and then exposed to 30 min of 365 nm light from the UV LED system. As can be seen the DOX peak is restored while the DOX-PCB isomer peaks are greatly reduced in intensity.

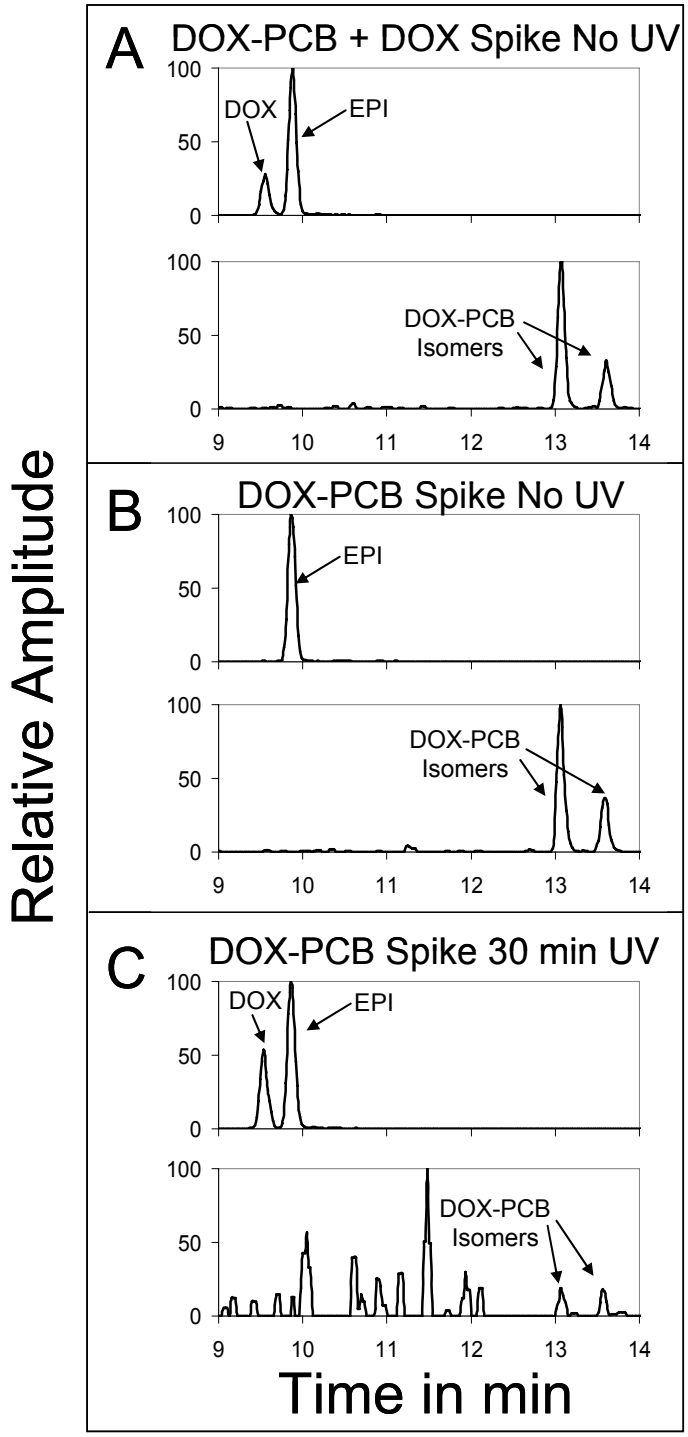
A
DOX-PCB + DOX Spike No UV
DOX
EPI
DOX-PCB
Isomers
B
DOX-PCB Spike No UV
EPI
DOX-PCB
Isomers
C
DOX-PCB Spike 30 min UV
DOX
EPI
DOX-PCB
Isomers
100
50
0
9
10
11
12
13
14
Relative Amplitude
Time in min

DOX-PCB Solubilization with Captisol Cyclodextrin

The encapsulation of DOX-PCB within the Captisol cyclodextrin was successful and resulted in the desired concentration of 1.2 mg of DOX-PCB in 200 µl of saline. The three dimensional structure of the β-cyclodextrin molecule [54] has a hydrophobic internal barrel. Captisol is a slightly modified version of β-cyclodextrin where there is a sulfobutylether used to separate a sodium sulfonate salt from the hydrophobic cavity to improve water solubility. The structure of DOX interacting with the hydrophobic barrel through the conjugated ring structure has been proposed [54] and should be similar to how DOX-PCB interacts with the cyclodextrin. The predicted structure of DOX-PCB in water is shown in Figure 1.5 and forms a folded hairpin. Interaction with the hydrophobic barrel of the cyclodextrin prevents interaction of the hydrophobic conjugated ring structure of DOX with the hydrophobic nitrophenyl compound preventing aggregation in saline solution.

DOX-PCB Circulation Half Life

DOX-PCB was found to have an in-vivo mouse alpha phase circulation half life of 10 min, which is comparable to that of DOX which around 20 min[55]. The serum concentration over time is shown in Figure 2.2 No DOX was found in the blood at any time point.

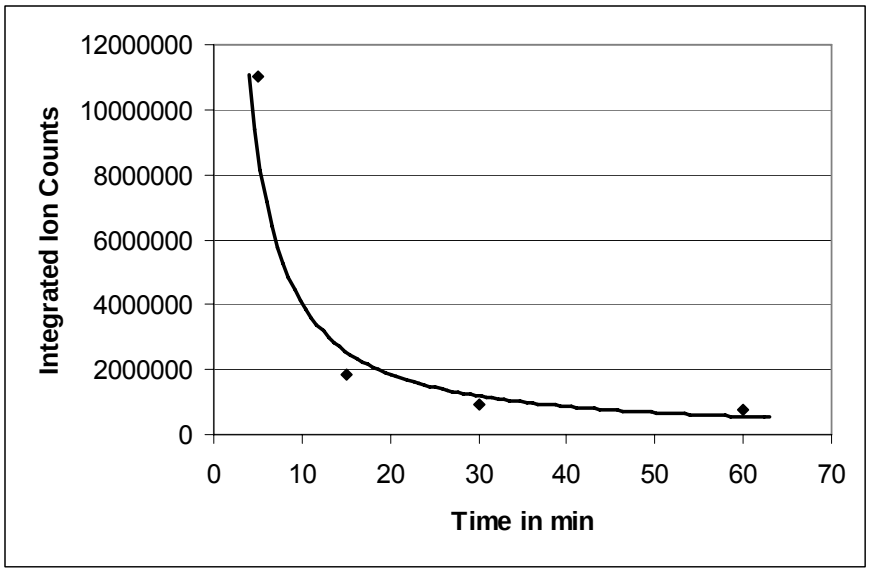

Figure 2.2 - The serum concentration of DOX-PCB as a function of time. No DOX was detected at any time point.

Urine Extraction

No DOX-PCB was found in the urine at any of the collected time points out to 24 hours. No DOX was found in the urine out to 24 hours.

DOX-PCB activation in vivo

The tumors collected from the mice were sectioned into 6 pieces as shown in Figure 2.4 a and b. The tumor was not spherical but rather oblong in shape and is shown schematically edge on in Figure 2.4a. The line down the center shows where the tumor was cut in half. The two halves were subsequently cut into 6 pieces as shown in Figure 2.4b. The mass of the different pieces is shown in Figure 2.3.

Tumor Section	No UV Mass in g	30 min UV Mass in g
1	0.0255	0.0496
2	0.0405	0.0825
3	0.0267	0.0426
4	0.0334	0.0382
5	0.0534	0.0833
6	0.0258	0.0547

Figure 2.3 – Mass of the different tumor sections for both the UV and non-UV exposed tumors

Pieces 1 and 4 were combined together and pieces 3 and 6 were combined together to increase the mass to increase the chances of finding DOX.

DOX-PCB was found in the tumor tissue in both the UV exposed and unexposed tumors as shown in Figure 2.4c-f and Figure 2.5c-f. However, only the tumor exposed to the UV contained a significant amount of DOX as shown in Figure 2.4c-f. The DOX appeared in all 4 sections of the tumor tissue in roughly equal amounts. There was only a trace amount of DOX found in two sections of the non-UV tumor as shown in Figure 2.5 c and f.

No DOX was found in the serum of the mouse after the 30 min of UV exposure in the tumor as shown in Figure 2.6.

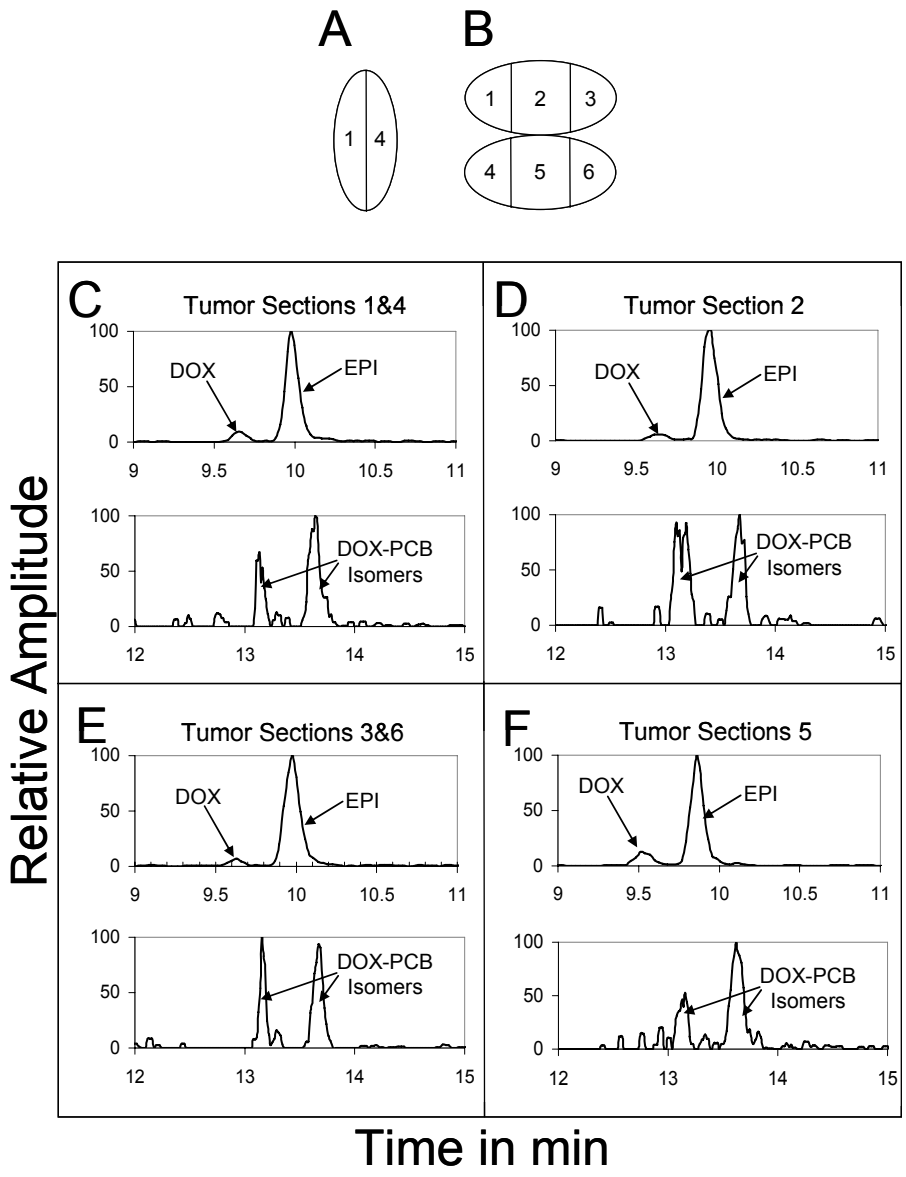

Figure 2.4 – LC/MS/MS data showing the presence of DOX-PCB and DOX in the in-vivo tumor tissue exposed to 30 min of 365nm light.
(A) Edge on view of the tumor in schematic representation showing how the tumor was sectioned in half.
(B) Open view of the halved tumor showing the numbered sections.
(C) LC/MS/MS traces of the tumor tissue extraction for pieces 1 and 4 combined together showing both DOX and DOX-PCB presence.
(D) LC/MS/MS traces for piece 2 showing both DOX and DOX-PCB presence.
(E) LC/MS/MS traces of the tumor tissue extraction for pieces 3 and 6 combined together showing both DOX and DOX-PCB presence.
(F) LC/MS/MS traces for piece 5 showing both DOX and DOX-PCB presence.

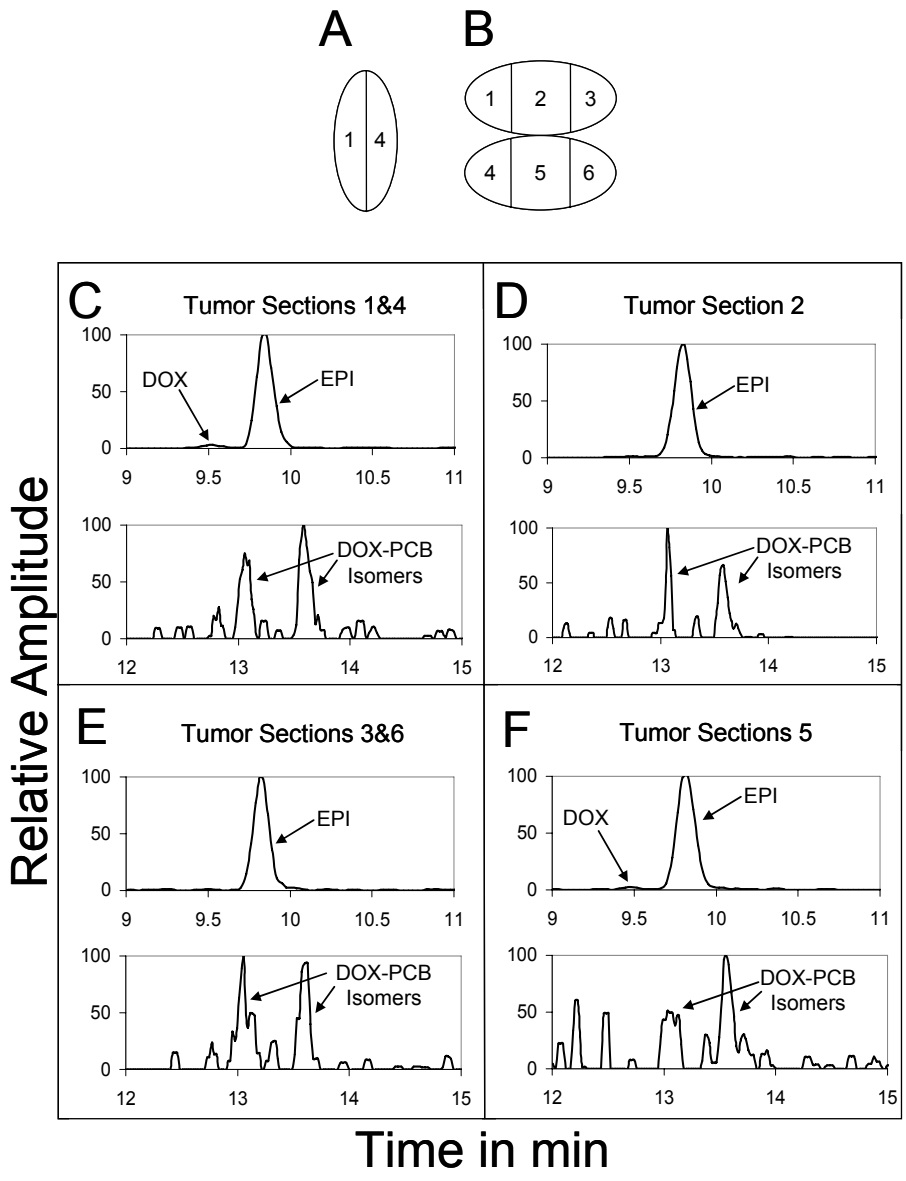

Figure 2.5 – LC/MS/MS data showing the presence of DOX-PCB and DOX in the in-vivo tumor tissue exposed to 30 min of 365nm light.
(A) Edge on view of the tumor in schematic representation showing how the tumor was sectioned in half.
(B) Open view of the halved tumor showing the numbered sections.
(C) LC/MS/MS traces of the tumor tissue extraction for pieces 1 and 4 combined together showing DOX-PCB presence and a trace amount of DOX.
(D) LC/MS/MS traces for piece 2 showing only DOX-PCB presence.
(E) LC/MS/MS traces of the tumor tissue extraction for pieces 3 and 6 combined together showing only DOX and DOX-PCB presence.
(F) LC/MS/MS traces for piece 5 showing DOX-PCB presence and a trace amount of DOX.

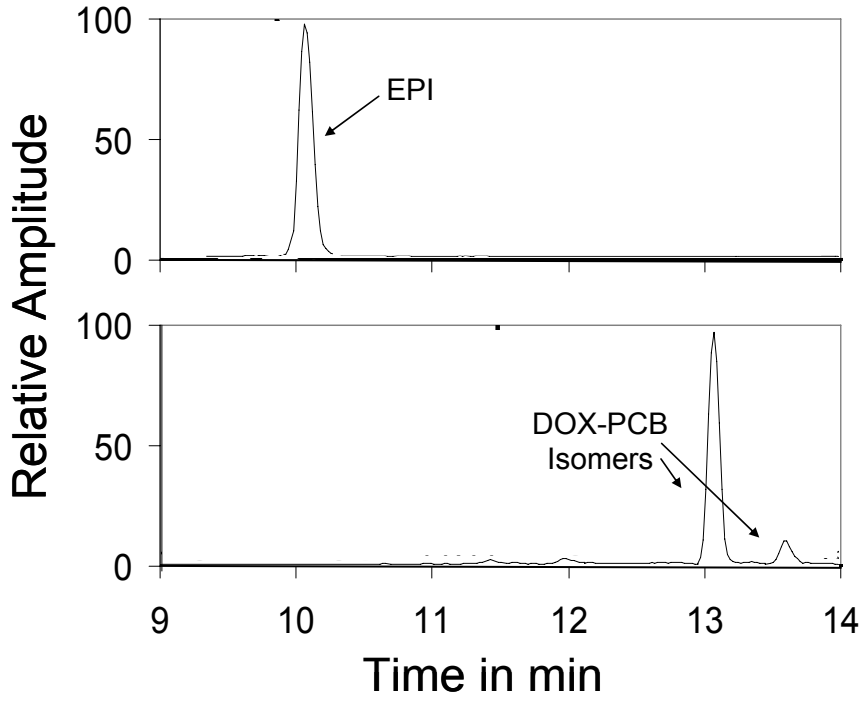

Figure 2.6 – LC/MS/MS trace of the serum extraction preformed on the serum collected after the 30 min UV exposure in the tumor.
No DOX was found indicating that the activated DOX is not immediately swept into circulation in measurable quantities but primarily stays within the tissue where it was activated.

DOX In-Vivo Control

The tumor extraction from the DOX control mouse showed that DOX was present in the tumor when injected systemically confirming that the orthotopic tumor model was allowing drug accumulation within the tumor.

Discussion

The ex-vivo tissue penetration of the 365 nm light was significant over the nearly 1 cm distance of tumor tissue. Even though the power measured directly in front of the tumor was 100 times less than that measured from just the fiber optic itself without the tumor tissue, that energy was distributed over the entire tumor tissue surface. There was sufficient 365nm light exiting the tumor tissue to cause significant conversion of DOX-PCB when exposed for a 30 min time period. This conversion of DOX-PCB to DOX was demonstrated to occur within tumor tissue itself showing that there is nothing inherent about the tissue that would prevent conversion.

The 10 min alpha phase circulation half life of DOX-PCB was comparable to that of the 20 min half-life for DOX itself showing that DOX-PCB was not immediately removed from circulation and thus it made it several passes through the liver. The lack of DOX in the serum or the urine shows that DOX-PCB was stable to normal metabolic processes. This also indicates that any DOX that is produced in the body would most likely be a result of the light activation pathway. DOX-PCB activation within the ex vivo tumor tissue showed that the conversion of DOX-PCB was not inhibited inside tissue and that the 365 nm light had significant penetration depth even through several millimeters of tissue.

The preliminary in vivo activation data shows that DOX-PCB makes it to the tumor tissue itself and that it can be converted to DOX in measurable quantities. This is significant because the tumor tissue itself was very poorly vascularized reducing the efficiency of any compound to accumulate. The localization of the DOX release due to the 365nm light exposure comes from the significantly smaller trace amount of DOX

detectable in the tumor tissue not exposed to UV from the other side of the mouse. This shows that the DOX generated by the UV light did not get immediately swept into circulation but was able to penetrate into the local tumor tissue. This is also confirmed by the observation that no DOX was found in the serum after the 30 min of UV exposure. If DOX was being swept into the circulation it was being done so in extremely small quantities.

The pharmacokinetics, lack of metabolic activation as shown in chapter 1, and localized light activation of DOX-PCB as described here demonstrate the desirable qualities of this compound. The 200 times reduction in toxicity of DOX-PCB coupled with the circulation time should allow larger doses to be administered than possible with pure DOX. This increases the amount that could reach even poorly vascularized tumors. The release of fully toxic DOX from DOX-PCB allows inefficiencies in the tumor delivery and activation to still yield therapeutic amounts of DOX.

Efficiency of photo activation needs to be considered here as well. Compounds that have high efficiency of activation with wavelengths of light that have greater tissue penetration (such as red or infrared) open the possibility of massive uncontrolled drug activation due to environmental light sources in the clinical situation. It is important that the compound has low activation efficiency to wavelengths that penetrate tissue. 365 nm of light is a special wavelength that has very low penetration through skin but reasonable penetration through tumor tissue which reduces the possibility of environmental 365 nm light from reaching and activating the compound. The extremely small amount of 365 nm light that does make it into deep vascularized skin would have little activation effect on DOX-PCB since its activation

is relatively inefficient at this wavelength. Compounds that have greater efficiency at 365nm would increase the danger of uncontrolled release near the skin surface where small amounts of 365nm can penetrate, causing detrimental effects to the patient. DOX-PCB activation is more efficient at shorter wavelengths of UV below 365 nm but tissue penetration at these wavelengths is negligible, especially through the skin, preventing uncontrolled release from occurring. The tissue penetration of 365 nm light and the lower activation efficiency of DOX-PCB help to truly localize the release of DOX to just the region exposed through use of the UV LED fiber optic system. The low efficiency of activation can be overcome by simply increasing the exposure time of the 365 nm light in the tumor region. As demonstrated here, 30 min is sufficient to activate measurable amounts of DOX in a 350 mg sized tumor. This most likely occurred at the periphery of the tumor where the vascularization was much higher, meaning the 365 nm light penetrated the whole tumor mass from the center. It did this isotropically as the amount of DOX in each section of the tumor was roughly equivalent.

Conclusions

The DOX-PCB prodrug solubilized with Captisol cyclodextrin and used in combination with 365 nm light administered from the UV/LED fiberoptic source has demonstrated highly localized activation and tissue retention of DOX. DOX-PCB was found to have a circulation half life of 10 min which is sufficient circulation time to reach even a poorly vascularized tumor tissue in activatable amounts. The 365nm light was shown to penetrate the tumor tissue to sufficiently release measurable amounts of

pure DOX from DOX-PCB within the tumor tissue. No DOX was found in the serum sample collected after the 30 min of light exposure indicating that activated DOX was not immediately swept into systemic circulation but rather stayed within the tissue where it was activated. The DOX delivery efficiency was high enough to be considered a proof of concept for the approach of using photoactivation as a prodrug activation scheme.

Acknowledgments

I am very grateful for the contributions from the following co-authors of this chapter: Stuart Ibsen[1], Eran Zahavy[2], Wolf Wrasdilo[3], Tomoko Hayashi, John Norton[3], Yongxuan Su[4], Stephen Adams[5], Sadik Esener[6]

[1]Department of Bioengineering, Moores Cancer Center, University of California San Diego, 3855 Health Sciences Dr. # 0815, La Jolla, CA 92093-0815, Phone (858) 534-9848, Fax: (858) 534-9830, Email: sibsen@ucsd.edu

[2] Department of Physical Chemistry, Israel Institute for Biological Research, P.O. Box 19, Ness-Ziona 74100, Israel.

[3] Moores Cancer Center, University of California at San Diego, La Jolla, CA 92093 USA

[4] Department of Chemistry and Biochemistry, University of California at San Diego, La Jolla, CA 92093 USA

[5] Department of Pharmacology, University of California at San Diego, La Jolla, CA 92093 USA

[6]Department of Nanoengineering, University of California at San Diego, La Jolla, CA 92093 USA

Chapter 3

A Novel Nested Liposome Drug Delivery Vehicle Capable of Ultrasound Triggered Release of its Payload

Abstract

The use of focused ultrasound can be an effective method to locally highlight tumor tissue and specifically trigger the activation of echogenic drug delivery vehicles in an effort to reduce systemic chemotherapy side effects. Here we demonstrate a unique ultrasound triggered vehicle design and fabrication method where the payload and a perfluorocarbon gas microbubble are both encapsulated within the internal aqueous space of a liposome. This nested lipid shell geometry both stabilized the microbubble and ensured it was spatially close enough to interact with the liposome membrane at all times. The internal microbubble was shown to fragment the outer liposome membrane upon exposure to ultrasound at intensities of 1 - 1.5 MPa. The focused ultrasound allowed the release of the internal payload to localized regions within tissue phantoms. The vehicles showed high payload loading efficiency of 16%, stability in blood of several hours, and low level macrophage recognition in vitro. High speed fluorescent videos present the first optical images of such vehicles interacting with ultrasound. This ability to open the outer membrane in small regions of deep tissue could provide a second level of spatial and temporal control beyond biochemical targeting, making these particles promising for in vivo animal studies.

Introduction

Indiscriminate exposure of all cells in the body to a systemically administered chemotherapy drug is the main cause of harmful toxic side effects[6]. Certain drug

delivery vehicles such as Abraxane for delivery of paclitaxel and liposomal Doxil for doxorubicin[16, 17] reduce exposure of non-targeted cells to the drug while accumulating a therapeutic dose within the tumor. Passive accumulation in the tumor tissue due to the enhanced permeation and retention of the vasculature[16] coupled with slow drug release limits the bioavailability to non-tumor organs[56]. However, this slow release also limits the maximum levels of drug in the tumor[57], and nonspecific accumulation in healthy tissue remains a major hurdle[16].

The use of tumor targeting ligands has the potential to improve the preferential accumulation of these delivery vehicles in tumor tissue [58, 59]. The delivery requires endocytosis of the targeted vehicle with subsequent endosomal escape[60, 61]. However, saturation of the targetable receptors limits the targeting efficiency. Also, tumor "receptors" are rarely unique to the tumor [62] and the targeted particles accumulate in other healthy tissues, especially in the liver and spleen, causing local toxicity [19].

To address the difficulties of pure biochemical targeting, an independent non-biochemical trigger is required to cause instantaneous drug release only from the particles that have accumulated in the tumor tissue. Ultrasound is an attractive trigger candidate due to its low cost, wide availability, its generation external to the body, and its independence from biochemical or physical properties of the tumor. It can be focused to small volumes of deep tissue on the order of several cubic millimeters[63] to avoid healthy tissue. It is non-ionizing, and does not damage tissue as long as the exposure is kept below 720 mW/cm^2 [64, 65].

The best particles to respond to ultrasound at safe exposure levels are gas-filled microbubbles[66] already approved for human use as ultrasound contrast agents [67, 68]. Ultrasound causes large size fluctuations in microbubbles due to the large density difference between the compressible gas and the surrounding water, which induces microstreaming of fluid around the microbubble and disrupts nearby membranes [69]. Microbubbles can also adiabatically implode (cavitate) producing a shockwave and water jets which can penetrate nearby membranes. This causes sonoporation and can facilitate delivery of DNA or drugs into cells[68, 70-72]. Significant work has been done to employ microbubbles as delivery vehicles in vivo [70, 72] without much success [73]. This is likely attributed to extremely short circulation times of microbubbles in vivo (3-15 min half-life [73]) and to limited payload capacity.

Surface loading of a hydrophilic payload, such as DNA, is limited by the surface area of the microbubble[74-77] and leaves it exposed to degradation and potential immune system recognition. Hydrophobic payloads are carried in limited volumes of thickened lipid, polymer, or oil surrounding the microbubble [76, 78] but when fragmented the hydrophobic drug will be contained in relatively large lipid particles reducing diffusion rates.

Drug loaded liposomes have been attached to the surface of microbubbles[79], however the points of attachment can concentrate shear stress during transport through the microvasculature and destabilize the entire particle. Separate drug-loaded liposomes and microbubbles can be targeted to the same tissue, but successful delivery of the drug depends on very close co-localization of both particles because the cavitation shockwave is only effective at disrupting membranes within a few tens of

microns. It is unlikely that both particles would be present in sufficient proximity and concentration to deliver a therapeutic dose.

To protect the microbubble and address the challenges described above, the microbubble and the payload can be encapsulated together within a protective outer liposome membrane shell. Previous efforts to incorporate gas bubbles into liposomes have used freeze drying techniques[80] or chemical reactions that create CO_2 microbubbles[81], but have very low yields. They also lack sufficient control over gas and payload entrapment, stability, and internal geometry, resulting in a large distribution of properties. Such distributions reduce the effectiveness of ultrasound to activate the entire population. Premade microbubbles stabilized with a lipid monolayer can be made independently using standard probe sonication techniques which increases bubble half-life in storage and *in vivo*. Microbubbles of desired size ranges can be collected and subsequently encapsulated in liposomes.

The most common methods of liposome encapsulation involve exposure to vacuum, sonication, heating, and/or extrusion, all of which destroy microbubbles. Ethanol injection is gentle enough to allow the microbubbles to survive the encapsulation process but produces liposomes too small to encapsulate a microbubble[82]. Detergent dialysis methods[83] can make liposomes large enough to encapsulate microbubbles and are gentle enough to not destroy them in the process.

Here we demonstrate a new manufacturing method to reproducibly encapsulate and protect premade microbubbles in a liposome as shown schematically in Figure. 3.1a. This method is similar to detergent dialysis but uses organic solvents to dissolve the lipids. A slow diffusive introduction of water allows the lipid membranes to seal

and encapsulate the large microbubbles. We refer to these malleable nested structures as SHockwavE-Ruptured nanoPayload cArriers (SHERPAs).

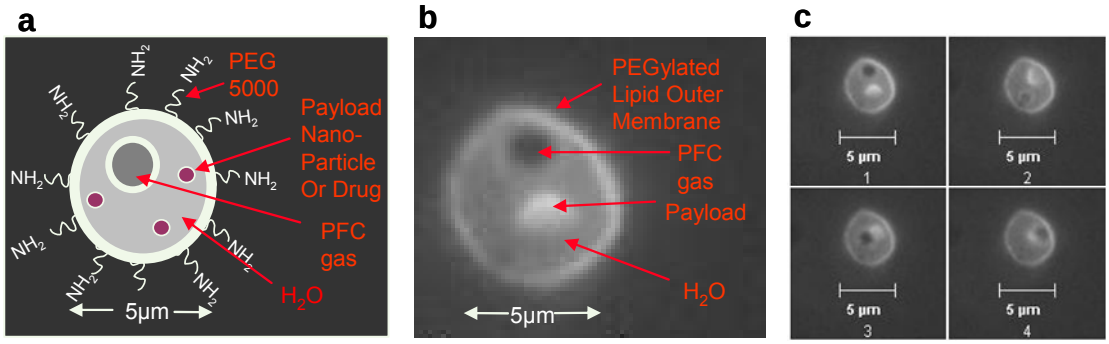

Figure 3.1 – SHERPA nested structural design
(a) A schematic of the nested liposome SHERPA design.
(b) Fluorescent image of a SHERPA resulting from the described manufacturing process. The payload is a small fluorescently labeled lipid membrane.
(c) A series of sequential pictures taken of the SHERPA showing the microbubble and fluorescent lipid payload moving around inside due to Brownian motion. This confirms that the microbubble and payload were internal to the outer membrane and not just attached to the outside.

Material and Methods

Materials

L-α-phosphatidylcholine (EPC) from chicken eggs, distearoyl phosphatidylcholine (DSPC), distearoyl phosphatidylethanolamine-methyl poly(ethylene glycol) MW5000 (mPEG-DSPE), and cholesterol were purchased from Avanti Polar Lipids, Inc. (Alabaster, AL). 1,2-propanediol, glycerol, ethanol, and perfluorohexane were purchased from Sigma-Aldrich. All water was purified using the Milli-Q Plus System (Millipore Corporation, Bedford, USA). DiO was purchased

from Biotium, Inc. CA. The PBS was purchased from Hyclone Laboratories Inc. (Logan, UT).

SHERPA production

1. Lipid Preparation

The SHERPAs were manufactured in a two step procedure with the microbubbles being formed through a probe sonication process and subsequently encapsulated in the outer liposome. The desired payload of nanoparticles or water soluble drug can be introduced in Solution 1, Solution 2, or in the PBS used for the final encapsulation step.

Solution 1: Outer Liposome Lipid Solution-

A 1.5 mL eppendorf tube was filled with 76 µL of EPC in chloroform (26 mM)(20 mg mL^{-1}) and 10 µl of cholesterol in chloroform (100 mM)(387 mg mL^{-1}). The chloroform was removed by evaporation while vortexing under an argon stream. 125 µL of ethanol was then added and the solution was vortexed at 3200 rpm for 30 sec. To visualize lipid membranes, 5 µL of 1 mM DiO (Biotium, Hayward, CA) in ethanol was added.

Solution 2: Microbubble Solution-

A 1.5 mL eppendorf tube was filled with 25 µL of DSPC in chloroform (51 mM) (40 mg mL^{-1}) and 20 µL mPEG5000-DSPE in chloroform (8.6 mM) (50 mg mL^{-1}). The chloroform was removed by evaporation while vortexing under an argon

stream. Then 450 µL of 1,2-propanediol was added. The solution was vortexed at 3200 rpm for 30 sec, and then placed in a heating block at 60 °C.

After 10 minutes, the solution was vortexed at 3200 rpm for 10 sec, and 150 µL glycerol was added. The solution was gently vortexed for 30 sec, and then placed back into the 60 °C heating block. The heating, vortexing cycle was repeated until the glycerol was fully mixed in and the solution was homogeneous. This solution was then transferred to a 4 ml glass vial with a narrow neck. The neck of the glass vial was covered with parafilm to create a barrier and prevent loss of PFH gas during the violent sonication process.

The headspace of the container was filled with perfluorohexane gas using the method shown in Figure 3.2 at 25 °C. 0.5 ml of the PFH liquid was first drawn into a 5 ml syringe. The plunger was then pulled all the way to the back of the syringe leaving 4.5 ml of air space. The syringe was rotated to coat all the walls of the syringe with the PFH several times to encourage fast vaporization of the PFH into the air. The metal needle of the syringe was bent at 130° from vertical and the syringe held upright as shown in Figure 3.2A. The needle of the syringe was then inserted through the parafilm barrier and 4 ml of PFH/air mixture inside the syringe was injected into the air space as seen in Figure 3.2B. Care was taken to not inject any liquid PFH into the vial. The air that was originally in the vial head space was forced out of the vial through the needle track hole made in the parafilm.

As shown in Figure 3.2C the tip of the probe sonicator (Fisher Scientific Model 100 Sonic Membrane Disruptor) was then inserted through the parafilm and positioned 1 mm below the surface of the lipid solution. The sonication power used

was 25 W for 20 seconds. The temperature of the solution began at 25 °C but increased to approximately 40 °C at the end of the sonication. This bubble solution was put immediately on ice to help preserve the microbubbles and facilitate the formation of lipid sheets.

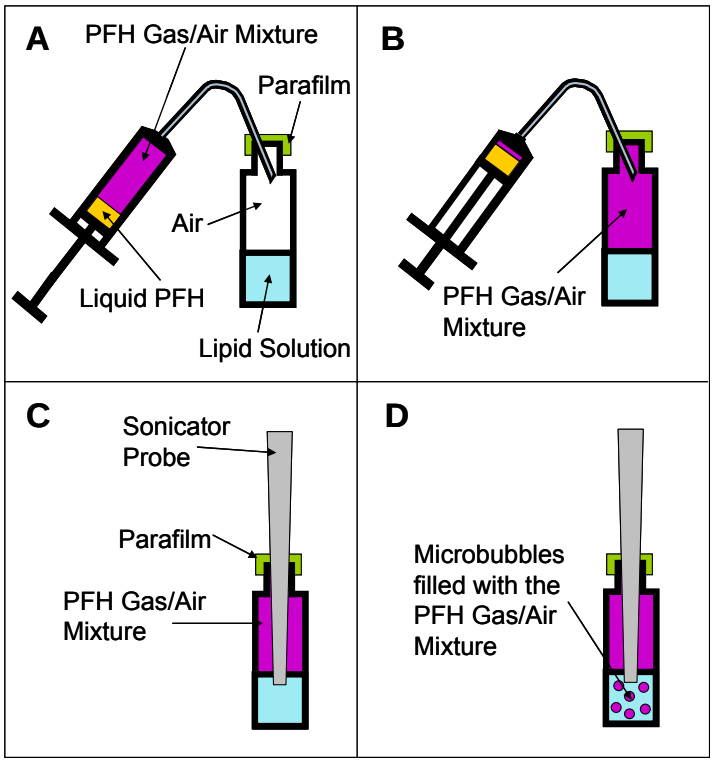

Figure 3.2 – Schematic representation of the manufacturing process for the PFH/air mixture filled microbubbles.
(a) A 5 ml syringe is filled with 0.5 ml of liquid PFH. The PFH is allowed to evaporate and mix with the air in the syringe until it reaches equilibrium. The top of the glass vial containing the lipid solution is covered with parafilm to reduce gas exchange from within the vial to the atmosphere
(b) The PFH/air mixture is injected into the head space of the vial containing the lipid solution. Care is taken to prevent injection of any liquid PFH. The original air that was in the vial is displaced through the needle track hole made in the parafilm
(c) The probe sonicator tip is inserted through the parafilm into the vial and the tip is positioned 1 mm below the surface of the lipid solution.
(d) The probe sonicator is turned on and creates microbubbles which incorporate the PFH/air gas mixture in the headspace. These microbubbles are coated with the lipids from the solution.

2. Microbubble Encapsulation and SHERPA Formation

After allowing Solution 2 to cool to room temperature, Solution 1 was added drop wise to Solution 2 under vortex at 3200 rpm. This new solution was Solution 3. 1.5 mL Eppendorf tubes were each filled with 200 µL of Solution 3. 100 µL of PBS was gently added to the bottom of each tube to initiate the closing of the lipid sheets and formation of the SHERPA. After 10 min, the tubes were rotated gently at an angle until the bubbles mixed thoroughly throughout the solution.

3. Microbubble Stability

Figure 3.2D shows that once the sonication process began the only gas that could have been incorporated into the forming microbubbles was the PFH/air mixture. Control experiments showed greater long term stability for microbubbles made with the PFH gas and air mixture over those made with just pure air.

Allowing the PFH liquid to evaporate into the airspace of the syringe allowed the PFH gas to naturally come to equilibrium with the liquid PFH and the atmospheric gasses at atmospheric pressure. This process ensured that the PFH gas was present in a concentration that provided stability to the microbubble at atmospheric pressure and gas composition. Microbubbles made with no PFH would simply dissolve away and collapse. If the PFH gas concentration was too high then the PFH would recondense into a liquid droplet collapsing the microbubble. If the PFH gas concentration was too low then there would be a driving force for nitrogen to leave the microbubble and shrink its size to the collapse radius [84, 85].

For the purpose of these observational experiments the SHERPA were not stabilized with a PFH gas concentration against arterial pressure like the microbubbles used for ultrasound contrast imaging. The microbubbles described here were stabilized for atmospheric pressure and gas composition because these were the conditions they were exposed to while being tested in the ultrasound microscope setup. The microbubbles needed to be stabilized only against atmospheric pressure because the Laplace pressures on the microbubbles were greatly reduced due to the reduction of interfacial tension caused by the lipid coating [86]. For in vivo experiments the microbubble manufacturing process described here could be easily modified to have the same PFH mixture already developed to stabilize for in vivo pressure conditions [84].

4. Purification

The desired microbubble-containing liposomes were separated from the empty liposomes by gentle centrifugation. The positive buoyancy of the entrapped microbubbles caused the actual SHERPAs to rise to the top of the reaction solution allowing them to concentrate. A Beckman Coulter Allegra X-15R Centrifuge was used at 524 g. The purification was done in an inverted syringe inside a 50 ml tube oriented so the SHERPA would rise against the plunger. The subnatant, containing mostly empty liposomes, could be expressed and replaced with fresh solution to purify the SHERPAs as well as wash them from any unreacted materials or unencapsulated payloads.

Retention Time of Doxorubicin

A sample of doxorubicin-loaded SHERPAs (.37 mg/mL DOX) was prepared, by dissolving 0.4 mg of doxorubicin hydrochloride (Jinan Wedo Industrial Co., Ltd. Shandong Province, China) in the bubble solution. The sample was diluted 1:20 by volume in PBS to improve dialysis performance. One sample of SHERPAs without DOX was prepared to determine the background fluorescence, and one solution of just the equivalent solvents and DOX was used to determine the dialysis rate of DOX.

Each sample (250 μL) was dialyzed against 1 L PBS using Spectra/Por cellulose ester membrane tubing with a molecular weight cutoff of 1MDa. The 1 MDa pore size was chosen because it was much larger than the DOX molecule, allowing unrestricted diffusion across the membrane. The smallest liposomes manufactured were too large to pass through these membrane pores so all of the liposomes were retained. When measuring drug retention time it was crucial that the dialysis rate was much faster than the SHERPA leakage rate, so the DOX would not build up in the fluid surrounding the liposomes inside the dialysis tubing. For each measurement, the relative concentration of doxorubicin within the dialysis tubing was determined by measuring the fluorescence with the TECAN Infinite 200 plate reader (Männedorf, Switzerland). The excitation and emission wavelengths were 475 and 595 nm respectively. The DOX-loaded SHERPA were analyzed at times 0, 0.5 hrs, 2 hrs, 6 hrs, and 24 hrs. For each time point, a separate sample was dialyzed.

Encapsulation Efficiency of IgG

To load the SHERPAs, mouse IgG was dissolved into the microbubble solution (solution 2) before the addition of water caused outer membrane sealing. A sandwich ELISA was used to assay the amount of free IgG. A detailed protocol is included in the supplementary material. The background signal was determined by an identical sample with no IgG. For a positive control, IgG was added to the outside of this sample. Alternate liposomes were prepared by hydrating a lipid film with a solution containing IgG.

The difference between the sample and the positive control was taken to be the amount encapsulated. The percent encapsulation was calculated by dividing the difference by the background-adjusted positive control.

SHERPA characterization

1. Phagocyte uptake experiments

1.1. Macrophage Culture

J774A.1 mouse macrophages were purchased from American Type Culture Collection (ATCC) Manassas, VA, USA. Cells were cultured in a 75 cm^2 flask with DMEM containing 10% Fetal Bovine Serum, glutamate and penicillin-streptomycin antibiotics (all purchased from Gibco, Invitrogen, Carlsbad, CA). SHERPAs and fluorescent beads (FluoSpheres, Invitrogen, Carlsbad, CA) were incubated with the macrophages for 1 hr.

1.2 Dendritic Cell Culture

Peripheral Blood Mononuclear Cells (PBMCs) were isolated from the blood of normal volunteers (San Diego Blood Bank) over a Ficoll-Hypaque (Amersham Biosciences, Uppsala, Sweden) density gradient. To generate dendritic cells (DCs), PBMCs were allowed to adhere to culture plates for 1h. The non-adherent cells were washed off and the adherent cells were cultured in RPMI 1640 medium supplemented with 2 mM L-glutamine (GIBCO-BRL Life Technologies; Grand Island, NY, USA), 50 mM 2-mercaptoethanol (Sigma, St. Louis, MO, USA), 10 mM HEPES (GIBCO-BRL), penicillin (100 U/mL),streptomycin (100mg/mL) (GIBCO-BRL) and 5% human AB serum (Gemini Bio Products West Sacramento, CA, USA), supplemented with 1000 U GM-CSF/mL (Cardinal Health, Dublin, OH, USA) and 200U IL-4/mL (R&D Systems, Minneapolis, MN) at days 0, 2, and 4. Immature DCs were harvested on days 5-7. These N178 human dendritic cells were incubated with SHERPAs for 1 hr, and FITC-dextran (IVGND1845, Invitrogen, Carlsbad, CA) was used as a positive control. Results were analyzed with FACS using the FACSCalibur system (BD Biosciences, San Jose, CA) and fluorescence microscopy.

RESULTS

SHERPA Structure

The dialysis-based manufacturing process described above produced the desired SHERPA structure consisting of a nested 5 μm liposome containing a 1 μm microbubble as shown schematically in Figure 3.1a and with fluorescence microscopy in Figure 3.1b. The Brownian motion of the microbubble and payload of the SHERPA

was contained entirely within the outer membrane as shown in a series of sequential pictures in Figure 3.1c. These structures were observed to be stable for several days.

SHERPA Production

1. Microbubble Formation

The probe sonication of the heated glycerol and 1,2-propanediol mixture containing dissolved DSPC and mPEG5000-DSPE successfully created microbubbles coated with a stabilizing lipid monolayer. This increased their resistance to the subsequent introduction of ethanol. DSPC was chosen because its long saturated tails result in a high T_c of 55 ºC. The brush layer created by the mPEG5000-DSPE helped increase SHERPA stability by preventing microbubbles from merging with each other and the outer liposome membrane. Perfluorohexane was chosen as the gas due to its established biocompatibility and low water solubility which increased the microbubble stability[77]. The high viscosity environment of the glycerol and 1,2-propanediol increased the concentration of microbubbles (~10^8/mL) by reducing their direct physical contact until they reached a more stable state.

2. Microbubble Encapsulation

The addition of the ethanol solution containing the egg PC lipid, cholesterol, and the lipophilic dye DiO to the microbubble solution drop wise under high vortex created lipid structures that intermixed with the microbubbles as shown in Figure 3.3a. These structures appear to be unclosed lipid sheets whose free ends were stable under these solvent conditions. The viscosity of the solvent was important because it slowed

the diffusion of added water into the region of these lipid sheets, making their free ends slowly unstable over several minutes. The increasing instability of the free ends caused the sheets to seal with themselves and neighboring sheets encapsulating the intervening microbubbles to form SHERPAs as shown in Figure 3.3b. Figure 3.3c shows a magnified view with several SHERPAs present. Egg PC was chosen because its very low transition temperature (T_c) of -15 ºC increased the flexibility and fluidity of the outer membrane, allowing the lipid sheets to seal. The flexibility could also help increase particle circulation time by allowing easier passage through the microvasculature. The cholesterol amount was optimized to increase stability of the outer liposome and improve drug retention time. Some of the mPEG5000-DSPE from the microbubble solution was also incorporated into the outer membrane. This was demonstrated by preventing charge interactions between SHERPAs doped with positively charged DOTAP lipid and cell surfaces. SHERPAs that were doped with DOTAP but did not have mPEG5000-DSPE attached readily to the surface of HUVEC cells. This indicates that the external surface of the SHERPAs were PEGylated and able to maintain a steric separation from the cells. This property is crucial to prolonging in vivo circulation time.

The large microbubbles shown in Figure 3.3a disapeared in Figure 3.3b and 3.3c because the added water made the solution less viscous. The larger bubbles floated quickly to the top, where they aggregated and destabilized. The 1-2 μm diameter microbubbles of choice rose more slowly and were much more stable when exposed to increasing concentrations of water in the formation process.

Encapsulation and Retention Time of Doxorubicin

One fundamental property of a drug delivery vehicle is its ability to contain its payload while in transit. The outer lipid membrane sheets of the SHERPA which close around the microbubble must seal to encapsulate a drug such as doxorubicin (DOX). DOX is currently dose limited by its cardiotoxic side effects, especially when administered systemically in free form [3, 87, 88]. DOX can be incorporated into the SHERPAs by its addition to the bubble solution, or to the water during the final formation step. The concentration of the DOX inside the SHERPA is the same as the concentration of the drug in these preparation solutions because this solution is encapsulated within the SHERPA along with the microbubbles. The SHERPA can be loaded with higher concentrations of DOX by using higher concentrations in the preparation solutions.

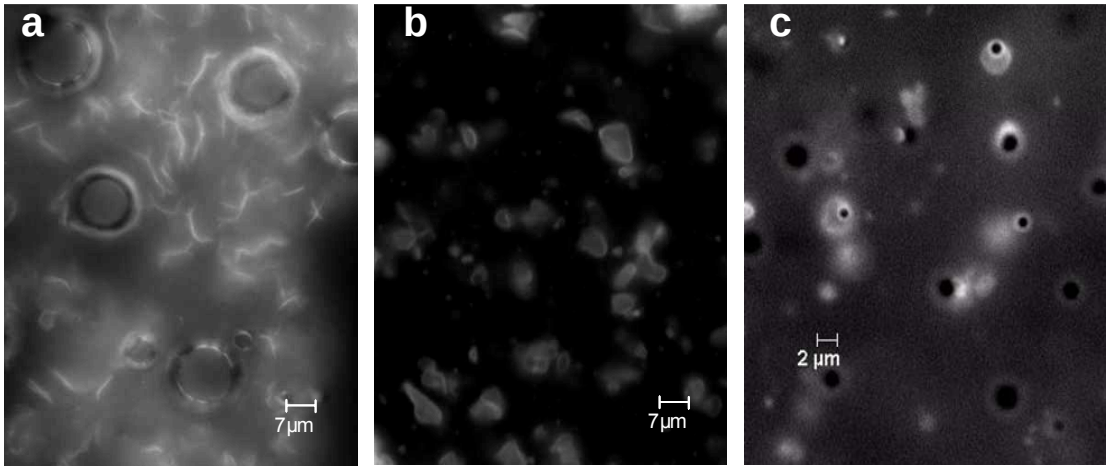

Figure 3.3 – SHERPA formation.
(a) The fluorescently labeled lipid structures mixed with the microbubbles shown before the final water addition step during SHERPA formation. The lipid structures appear to be open sheets whose free ends are stable under these mixed solvent conditions of glycerol, 1,2-propanediol, and ethanol.
(b) After addition of water to the microbubble and ethanol mixture shown in Figure 3.3a, the open free ends of the lipid sheets become energetically unstable and they seal with themselves and with the free ends of surrounding sheets encapsulating the intervening microbubbles. This magnification level is the same as in Figure 3.3a.
(c) This shows a close up of the SHERPAs just after formation.

The encapsulation of DOX is shown in Figure 3.4a. The retention time of free DOX was determined by dialyzing DOX-loaded SHERPAs against PBS, and measuring the DOX concentration over time from the fluid within the dialysis tubing. For passively loaded DOX, the release followed an exponential decay with tight correlation. The retention half-life was 4.74 hours, and is in good agreement with the literature for other liposomes loaded with free DOX [89]. In the future, the retention time of DOX can be increased 10 times or more from this value by inducing the DOX to form crystals inside the liposomes by using proper pH gradients [89].

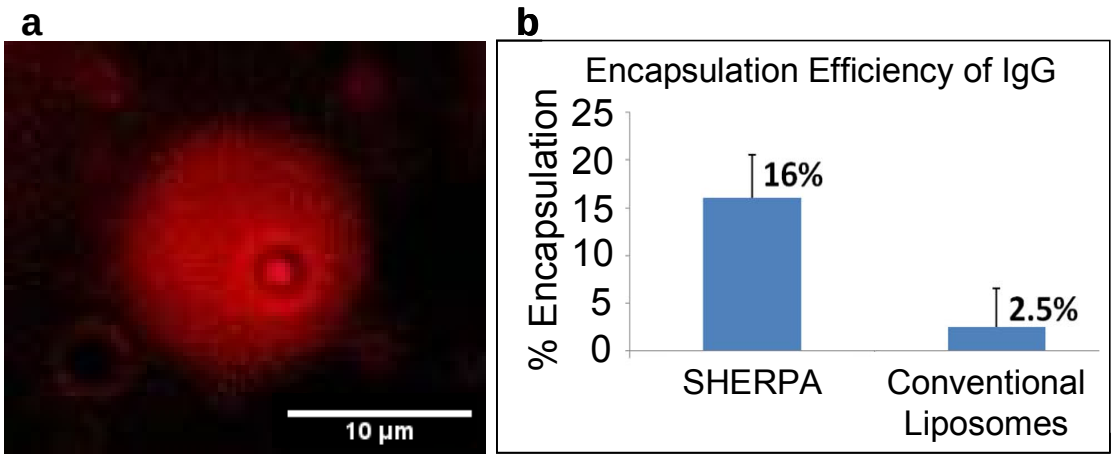

Figure 3.4 – SHERPA payload loading.
(a) Demonstration of doxorubicin loading. Red fluorescence from entrapped doxorubicin can be seen as a diffuse sphere. This liposome also contains a microbubble shown by the dark inner circle.
(b) Efficient loading of a macromolecule, IgG, was demonstrated and quantified using ELISA. Other liposomes were prepared by standard methods for comparison.

Encapsulation Efficiency of Microbubbles and Biomolecules

To evaluate the encapsulation efficiency of the SHERPA, mouse IgG was used as a model large biomolecule payload. An ELISA was performed to calculate the percent loading of IgG (150 kD, ~5 nm) into the SHERPAs. The samples were added directly to capture antibodies after formation, to minimize experimental error. Only free IgG was accessible to bind capture antibodies and contributed to the ELISA signal. The mean percentage of the entire volume of the preparation solution that was encapsulated within the SHERPA outer liposome was 16%. This was high for passive entrapment and much higher than the 2.5% measured for the liposomes prepared by thin film hydration [90] as shown in Figure 3.4b. This is likely due to the larger size of

the SHERPA liposomes and the fact that the lipids sheets are well suspended with the payload before sealing.

The encapsulation efficiency of the microbubbles into the SHERPA outer liposomes was lower (1-5%) because the IgG was small enough to fit into any sized SHERPA but the microbubbles were on the micron size and could only fit into the larger liposomes. However, these microbubble-containing SHERPAs were easily separated from the empty liposomes by buoyancy driven methods, since the microbubble inside reduces the overall density of the SHERPA compared to empty liposomes and bulk solution.

SHERPA Interaction with Ultrasound

1. Ultrasound Intensity Level of 1.5 MPa

The custom built high speed ultrasound microscope setup described in the methods section was used to observe the interaction of the fluorescently labeled SHERPA with ultrasound. Cavitation of the internal microbubble was observed at ultrasound intensity levels of 1.5 MPa as shown in Figure 3.5a. Here the microbubble underwent a violent implosion producing a shockwave that fragmented the fluorescent lipid outer membrane into a cloud of fine debris. It is important to note that an empty liposome was present right next to the SHERPA as shown in Figure 3.5a frame 1. This empty liposome contained no microbubble and was exposed to the same ultrasound pulse that cavitated the SHERPA, but had no visible reaction or disruption of the membrane. This shows that the ultrasound exposures required to cavitate the microbubbles would not harm the membranes of cells even in the focal zone. This

localized effect of the cavitation on surrounding membranes illustrates the importance of the co-localization of the liposome and microbubble. A jet of debris material was also ejected from the site of cavitation as seen in frame 3 of the sequence. Fluid ejection is a well documented mode of microbubble cavitation[91].

2. Ultrasound Intensity Levels Below 1 MPa

A second mode of interaction between SHERPAs and ultrasound at levels below 1 MPa was observed in which the microbubble did not undergo cavitation, but instead had a less violent response. The size modulation of the bubble initiated an opening and unfolding of the SHERPA outer membrane as shown in Figure 3.5b, probably due in part to microstreaming[91]. These free ends made the open membrane an unstable high energy structure.

3. Localized SHERPA Activation

The localized activation of SHERPA only near the focal region of the ultrasound was demonstrated in an agar tissue phantom using a biotin/avidin binding scheme. An agar gel was prepared with a 1 mm diameter channel molded through the center to simulate a blood vessel which was coated with avidin. SHERPAs were made with DSPE-PEG2000-Biotin so the biotin was present on both the inner and outer surface of the SHERPA outer membrane. Biotins on the outside of the SHERPA were blocked by incubation with an excess of free avidin. The outer membrane was stained with DiO for visualization and the SHERPAs were introduced into the channel. The agar blocks were then insonified with focused ultrasound of various intensities. The

control agar block showed very little nonspecific binding of the SHERPA to the walls of the channel after being washed with water as shown in Figure 3.5c. Low intensity ultrasound ruptured the SHERPA only in the focal region, creating fluorescent membrane fragments with exposed free biotin that was originally on the inner leaflet of the SHERPA membrane. These fragments were then able to bind to the avidin coated walls of the channel allowing them to remain on the channel surface after it was flushed with water. Higher intensity ultrasound ruptured a larger number of SHERPA resulting in a higher fluorescent signal as well as creating a larger region of activation.

SHERPA Stability in Biological Fluids

SHERPA stability was evaluated by dilution into a blood sample followed by fluorescent microscopy. Intact SHERPAs were observed for up to two hours. Brownian motion caused the SHERPAs to interact with the surrounding red blood cells (RBCs), demonstrating their membrane flexibility. Much like the cells, they appeared to change their shape to pack closely with neighboring groups of RBCs a shown in Figure 3.6a. The flexibility can potentially help reduce uptake from the spleen by mimicking the ability of RBCs to squeeze through the filtration system. No attachment or clotting induction of the SHERPAs on the RBCs was observed.

Figure 3.5 – Interaction of SHERPA with Ultrasound.
(a) Sequence of images showing a cavitation mode of ultrasound interaction with a SHERPA. Frame 1 shows the SHERPA before ultrasound exposure. Frame 2 shows the very onset of ultrasound exposure. Frame 3 shows the results just after the microbubble cavitation event creating a cloud of fluorescent debris. A jet of material has shot out from the main debris cloud. Frame 4 shows the diffusion of the membrane fragments 1.2 seconds after the cavitation event.
(b) Sequence of images showing a popping type mode of SHERPA interaction with ultrasound. Frame 1 shows the SHERPA with its fluorescent outer membrane before exposure to ultrasound. Frame 2 shows the very onset of ultrasound exposure. Frame 3 shows the SHERPA membrane popping open on the lower right hand side and beginning to open up. Frame 4 shows the SHERPA fully opened up.
(c) Images of ultrasound activation of SHERPA in simulated blood vessel channel within an agar block. The channel was coated with avidin and the SHERPA were functionalized with biotin. The biotin on the outside of the SHERPA was blocked with free avidin The control showed very little nonspecific binding of the fluorescently labeled SHERPA to the surface of the channel. Insonification with focused ultrasound ruptured SHERPA in the focal region allowing the biotin on the inside to bind to the surface of the channel. Higher intensity focused ultrasound created more activation and widened the range of SHERPA rupture causing larger deposition.

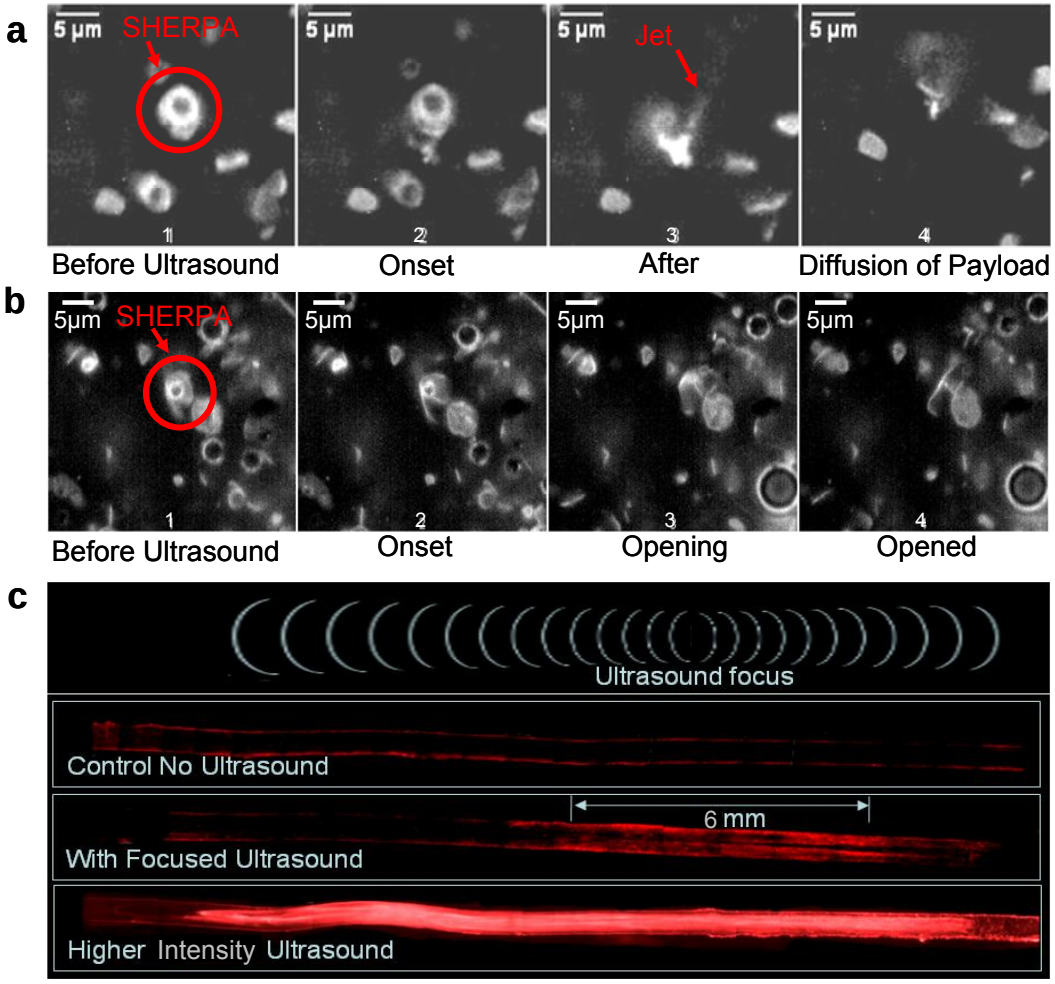
a
5 µm
SHERPA
Jet
1
2
3
4
Before Ultrasound
Onset
After
Diffusion of Payload
b
5µm
SHERPA
Before Ultrasound
Onset
Opening
Opened
c
Ultrasound focus
Control No Ultrasound
6 mm
With Focused Ultrasound
Higher Intensity Ultrasound

Macrophage Uptake of SHERPA

An effective drug carrier must be able avoid clearance by phagocytes for a sufficient period of time to reach its target. This nested design has a smooth PEG coated outer surface which presents less of a target for the immune system. J774 mouse macrophages were used to model the uptake of particles and liposomes fabricated by our method. SHERPA membranes were labeled green, and red Fluosphere beads were used as a positive control to show that the incubation solution did not inhibit the function of the macrophage. After 1 hr of incubation, macrophages were inspected by fluorescence microscopy. Figure 3.6b shows strong macrophage uptake of red Fluospheres with no visible phagocytosis of SHERPAs.

SHERPAs were also incubated with N178 human dendritic cells and analyzed by FACS and fluorescence microscopy. The FITC-dextran control was contained within 96.9% of cells, whereas only 3.49% of cells contained fluorescently labeled SHERPAs. Scatter data showed no evidence of cell death. This indicates the possibility that the SHERPAs will have a low clearance rate from the immune system.

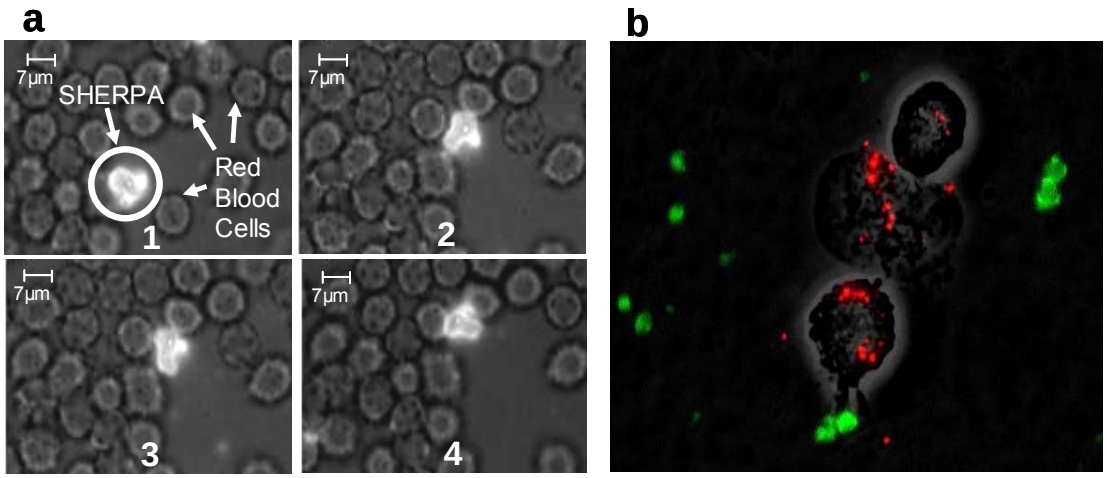

Figure 3.6 – SHERPA in vitro behavior.
(a) SHERPA interaction with red blood cells. The outer membrane of the SHERPA is very flexible and allows it to change shape so as to achieve close packing with surrounding red blood cells as shown through this sequence of pictures. The only driving force for this is Brownian motion.
(b) Three J774 macrophages have engulfed nearly all the fluospheres (red). No liposomes (green) can be seen inside the macrophages.

Discussion

The SHERPA nested geometry has several attractive features as a drug delivery vehicle. The smooth continuous outer liposome with its PEG coating protects the internal microbubble and payload from degradation, reduces immune system recognition, and creates far greater loading capacity than microbubbles alone. The surface-to-volume ratio is far less than that of nanoliposomes which allows higher surface densities of targeting ligands to be used to increase targeting efficiency without the risk of receptor saturation. The materials used in the construction of SHERPAs are bioresorbable and the perfluorocarbon gas can be cleared through exhalation.

The SHERPA are intended for intravenous injection which allows the SHERPA and the payload to penetrate every region of the tumor where the vasculature reaches, as opposed to an intratumoral injection where the SHERPA would be limited in their mobility from the injection site. The flexibility of the outer membrane can mimic the flexibility of red blood cell membranes and could help to increase circulation time of the SHERPA by allowing easier passage through the microvasculature. The SHERPA drug delivery vehicles themselves are not meant to extravasate from circulation into the tumor tissue. The main role of the SHERPA is to bring a highly concentrated payload into the tumor region through the vasculature. The payloads consisting of therapeutic nanoparticles or drug molecules are capable of extravasation once released from the SHERPA, especially inside the tumor region due to the "leaky" vasculature. The release of payload from the SHERPA located in the vasculature of the tumor will expose both the endothelial cells and the tumor tissue itself to the payload. Future work will explore the circulation time of these particles and the effect of focused ultrasound on payload delivery from the circulating particles to selected tissue regions.

The nested SHERPA structure always keeps the microbubble, large payload, and cell membrane in close proximity, increasing the chance for sonoporation[92] which is initiated by the cavitation event. Simultaneous pore formation in the cell membrane and release of high concentrations of payload in the same region could allow payload to travel down its concentration gradient into the cells, bypassing the need for endocytosis, and endosomal escape. With the resolution of focused ultrasound on the order of several cubic millimeters, SHERPAs residing in

surrounding healthy tissue will be unaffected. They will break down gradually, diluting their payloads into the blood stream, making cellular delivery much less effective, and preventing accumulation of the drug[92]. This sonoporation effect may also occur during non-cavitation microbubble interactions from the microstreaming of fluid around the microbubble[91]. Transient holes formed in the cell surface can be on the order of 100 nm in diameter and allow for payload uptake to occur over several minutes[93].

Conclusions

Here we have demonstrated a process for consistent production of liposomes containing stabilized microbubbles. Though the overall structure is new, the outer liposome is amenable to standard functionalization and modifications well documented in the literature. These can increase their preferential accumulation in tumor sites to achieve maximum SHERPA concentration at the moment when the region is selectively insonified with ultrasound. This allows for both spatial and temporal control over activation with a burst release of a highly concentrated payload making these particles promising for in vivo studies.

Acknowledgements

The authors are grateful for the insightful discussions with Ahmet Erten while conducting these experiments. The study was supported by the NCI Grant No.

5U54CA119335-05, and by the UCSD Cancer Center Specialized Support Grant P30 CA23100.

The co-authors of this chapter are as follows: Stuart Ibsen[1*+], Michael Benchimol[2+], Dmitri Simberg[3], Carolyn Schutt[1], Jason Steiner[4], Sadik Esener[5]

[1]Department of Bioengineering, Moores Cancer Center, University of California San Diego, 3855 Health Sciences Dr. # 0815, La Jolla, CA 92093-0815, Phone (858) 534-9848, Fax: (858) 534-9830, Email: sibsen@ucsd.edu

[2]Department of Electrical & Computer Engineering, Moores Cancer Center, University of California San Diego, La Jolla, CA 92093 USA

[3]Moores Cancer Center, University of California San Diego, La Jolla, CA 92093 USA

[4]Department of Material Science, Moores Cancer Center, University of California San Diego, La Jolla, CA 92093 USA

[5]Department of Nanoengineering, Moores Cancer Center, University of California at San Diego, La Jolla, CA 92093 USA

[*]Corresponding Author

[+]These authors contributed equally to this work

Chapter 4

Effect of Microbubble Cavitation on Whole Cell Membranes

Abstract

Sonoporation is a widely used technique which uses microbubbles and ultrasound to increase the efficiency of DNA transfection into cells and is being considered to facilitate drug delivery in vivo. The microbubble cavitation events produce a shockwave that creates 100 nm sized holes in the cell membrane which allows diffusion of outside DNA and particles into the cell. Here we demonstrate that the effect of the shockwave on the cell membrane goes far beyond just the poration hole formation and can extend out 24-26 μm cell membrane away from the bubble itself across the. This was determined by monitoring the removal of fluorescent non-echogenic liposomes from the surface of single cells after nearby microbubble cavitation events. The extended shear stress experienced across the cell membrane has implication for microbubble design both in vitro DNA transfection and in vivo drug delivery applications especially when dealing with shear sensitive cells such as endothelial cells.

Introduction

Transfection of DNA into mammalian cells to change genetic expression has become a major tool for biological and pharmaceutical research and in industry. DNA itself is rarely taken up by mammalian cells due to the large size of the DNA and the various membranes and barriers created by the cell[94]. Several methods have been developed to facilitate the transfer of DNA across the cell membrane with successful

expression of that DNA including the use of viral vectors[95], cationic liposome fusion[94], microinjection directly into the cells[96], optoporation[97], and electroporation[98]. Concerns exist about the efficiency of using these techniques to transfect large populations of cells and about the extra DNA information that is necessarily delivered when using viral vectors[99].

Another technique known as sonoporation uses ultrasound to physically create small ruptures in cell membranes[99, 100]. These holes allow the DNA, or other agents of interest, to passively flow down their concentration gradient into the cell. The transfection efficiency of sonoporation can be increased significantly when microbubbles are incubated with the cells during the ultrasound exposure[100]. This allows large populations of cells to be efficiently transfected as well as avoid the introduction of unnecessary DNA.

The microbubbles interact with the cells under various mechanisms when exposed to ultrasound. The first major class of interaction is the induction of size changes in the microbubble diameter as it compresses and expands with the compression and rarefaction of the ultrasound pulse[101]. This oscillation can cause micro-streaming to occur around the microbubble edges[102] and can disrupt cell membranes[102, 103].

When the microbubble shell stiffness and size allow resonate interaction with the ultrasound to occur the microbubble can undergo a violent implosion event, known as cavitation, which sends out a shockwave intense enough to open transient holes in cell membranes[104]. These holes can be on the order of 100nm in diameter and remain effectively open for up to 20 seconds[105]. This allows large molecules to

enter the cells following passive diffusion[105, 106]. The cavitation event has been shown to cause the formation of chemically reactive species including free radicals, and light which can extend into the UV and soft X-ray spectrum[107] all of which could affect living cells.

Although much work has been done to show the size and lifetime of the holes generated in the membranes, little is known about how the rest of the cell membrane is affected. Scanning electron microscopy has been conducted on the surface of cells after cavitation exposures showing indentations and ruptures in cell membranes[108] but the preparation process needed for the microscopy techniques alters the membrane and makes it difficult to understand the full extent of cavitation shockwave effects on the whole cell. It is also not possible to know how many cavitation events were near the cell at the time of exposure.

Information about how much of the cell surface is affected can be used in the transfection application to tailor microbubble properties to have less affect on cells while still efficiently causing sonoporation. The extent of cellular effect and damage is also important to understand from the drug delivery standpoint. The use of microbubbles as facilitators of sonoporation for drug delivery applications is currently being explored for in vivo applications[109]. Understanding the extent of influence the microbubble cavitation has on the entire cell membrane is important to design the delivery system to produce the desired level of damage and effect on the cells. This is of particular interest for endothelial cells which are the mostly likely to interact with the delivery vehicle.

The focus of this study was to determine the extent of the disruption to whole cell membranes from nearby microbubble cavitation events. To do this, non-echogenic liposomes were targeted to the surface of adherent endothelial cells to act as cell membrane surface markers. Human Umbilical Vein Endothelial Cells (HUVEC) were chosen because of their ability to express the αvβ3 integrin on their surface[110] which can be targeted with cyclic RGD[111] and because endothelial cells are the most applicable cell type for drug delivery applications. The removal of targeted liposomes from the surface of the cell due to nearby microbubble cavitation was monitored using fluorescence microscopy allowing the extent of the blast region to be measured.

Materials and Methods

Materials

L-α-phosphatidylcholine (EPC) from chicken eggs, distearoyl phosphatidylcholine (DSPC), distearoyl phosphatidylethanolamine-methyl poly(ethylene glycol) MW5000 (mPEG-DSPE), and cholesterol were purchased from Avanti Polar Lipids, Inc. (Alabaster, AL). 1,2-propanediol, glycerol, ethanol, and perfluorohexane were purchased from Sigma-Aldrich. All water was purified using the Milli-Q Plus System (Millipore Corporation, Bedford, USA). DiO was purchased from Biotium, Inc. CA. The PBS was purchased from Hyclone Laboratories Inc. (Logan, UT). Human Umbilical Vein Endothelial Cells (HUVEC) were purchased from the American Type Culture Collection (ATCC) (Manassas, VA, USA). EBM-2 was purchased from Lonza Inc. The trypsin (.25% T / 2.21 mM EDTA) was purchased

from Mediatech Inc. (Manassas,VA, USA). The penicillin-streptomycin used in the EBM-2 media was purchased from Gibco (Invitrogen, Grand Island, NY, USA). The fetal bovine serum used in the EBM-2 media solution was purchased from Hyclone (Logan, UT, USA).

cRGD Lipid Conjugation

The cRGD lipid construct was created by first adding 0.805µl of 10x PBS to 7.244µl of 25mg/ml cRGD stock. Then 20.55µl of 2mg/ml Traut's Reagent was added and incubated for 20 min on a shaker to activate the cysteine residue. Separately, an 88.24µl aliquot of 3.4 mM DSPE-peg10k-malimide (in chloroform) was dried under an argon stream and then resuspended in 88.24µl of PBS. The activated cRGD was then added to this solution and incubated for 1.5 h on shaker.

A 30kD microcon filter was used to purify and concentrate the lipid conjugate product beginning with 3 washes of 200µl PBS with a centrifuge rate of 12,000 rcf for 5 min. The final lipid concentration was 3-5mM by concentrating the product to 60-100ul.

HUVEC Culture

The HVEC cells were cultured with EBM-2 media with pen/strep from Hyclone and 10% FBS From Invitrogen. At around 80% confluency the adherent cells were detached from the expansion flask using Trypsin (.25% T / 2.21 mM EDTA). The cells were them plated out onto Lab-Tek II Chamber Slide 8 well chamber slides from Thermo Scientific at a density of 3000 cells per well in 300 µl of EBM-2 media.

These low densities were used to make sure the cells would be continuously expanding and not reaching near confluence to avoid any suppression of αvβ3 integrin expression by the cells. It also ensured that the cells would be spatially isolated from one another so the microbubble cavitation events would affect only single cells.

Liposome preparation with Microbubbles

Liposomes were prepared along with the microbubbles using an encapsulation method fully described in chapter 3. This method was chosen because large payloads can be encapsulated within these liposomes making them of interest for drug delivery. The liposomes used for these experiments were empty making them non-echogenic so when isolated by themselves they would not be influenced by the ultrasound. The manufacturing process consisted of a two step procedure with the microbubbles being formed through a probe sonication process and subsequently mixed with lipid sheets which closed to form empty liposomes.

Microbubble Solution-

A 1.5 mL Eppendorf tube was filled with 25 µL of DSPC in chloroform (51 mM) (40 mg mL^{-1}) and 20 µL mPEG5000-DSPE in chloroform (8.6 mM) (50 mg mL^{-1}). The chloroform was removed by evaporation while vortexing under an argon stream. Then 450 µL of 1,2-propanediol was added. The solution was vortexed at 3200 rpm for 30 sec, and then placed in a heating block at 60 °C.

After 10 minutes, the solution was vortexed at 3200 rpm for 10 sec, and 150 µL glycerol was added. The solution was gently vortexed for 30 sec, and then placed

back into the 60 °C heating block. The heating, vortexing cycle was repeated until the glycerol was fully mixed in and the solution was homogeneous.

The headspace of the container was filled with perfluorohexane gas. A probe sonicator (Fisher Scientific Model 100 Sonic Membrane Disruptor) was operated at the liquid/gas interface in short pulses to produce microbubbles. The sonication power used was 25 W. The bubble solution was put immediately on ice. Perfluorohexane was chosen as the gas to fill the microbubbles due to its low water solubility which increased the incubation half life of the microbubbles with the cells themselves

Liposome Lipid Solution-

A 1.5 mL Eppendorf tube was filled with 76 µL of EPC in chloroform (26 mM)(20 mg mL^{-1}) and 10 µl of cholesterol in chloroform (100 mM)(387 mg mL^{-1}). The chloroform was removed by evaporation while vortexing under an argon stream. 125 µL of ethanol was then added and the solution was vortexed at 3200 rpm for 30 sec. To visualize lipid membranes, 5 µL of 1 mM DiO (Biotium, Hayward, CA) in ethanol was added. To allow targeting to the αvβ3 integrin 16 µl of the 4mM cRGD lipid construct described above was added to constitute 40% of the final pegylated lipid content in the liposome.

Liposome and Microbubble Formation

After allowing the microbubble solution to cool to room temperature, the liposome solution was added drop wise to the microbubbles under vortex at 3200 rpm.

1.5 mL Eppendorf tubes were each filled with 200 μL of this mixed solution. 100 μL of PBS was gently added to the bottom of each tube to initiate the closing of the lipid sheets and formation of the liposomes. After 10 min, the tubes were rotated gently at an angle until the bubbles mixed thoroughly throughout the solution.

This produced both microbubbles and liposomes which had cRGD on their surfaces.

Liposome and Microbubble targeting to cells

The EBM-2 media was removed from the adherent HUVECs in the chamber slides and replaced with the microbubble/liposome solution described above for 2 min. This gave the cRGD targeted liposomes and microbubbles enough time to adhere to the surface of the live cells. Non-adhered liposomes and microbubbles were washed away with PBS and the chambers and rubber sealing gasket were removed from the chamber slide to allow a glass coverslip to be placed on top for imaging.

Imaging and Ultrasound Notification

The slide and coverslip were imaged and insonified using a custom built system described in chapter 5. Briefly, the system used a water tank to couple the ultrasound to the cell samples. Ultrasound was generated with a submersible Panametrics 2.25 MHz transducer (V305-Su, 1" spherical-focus) using a Panametrics BCU -58 - 6W waterproof connector cable. A needle hydrophone from Onda Corporation (HNP-0400 Broadband Needle Hydrophone AH - 2020-100 with hydrophone pre amp, 50kHz - 100 MHz, 0 +20 db.) was used to measure the sound

field, and a Photron FASTCAM 1024 PCI acquired the image sequences. The National Instruments PCI 5412 arbitrary waveform generator was used to create different waveforms and was controlled using a custom designed LabVIEW 8.2 program. A 300 W amplifier from Vox Technologies (model number VTC2057574) was used to create acoustic intensities at the focal region of up to 1.6 MPa.

The glass slide containing the cells was placed at the air water interface so that a Nikon 100X oil immersion objective could be used for fluorescent imaging. The ultrasound was pointed to focus at the bottom of the glass slide. The glass attenuated the ultrasound intensity but transmitted enough energy to cause cavitation of the microbubbles without causing visible disturbance to non-echogenic liposome membranes or cell membranes (see chapter 3).

Results

Cavitation Effect From a Single Microbubble on a Single Cell

The effect of a single microbubble on a single cell has been documented as shown in Figure 4.1a-d. Figure 4.1a shows the bright field image of an adherent HUVEC cell and attached microbubble before exposure to ultrasound. The microbubble is pointed out by the arrow and was identified by its unique lensing effect which caused different distortions in various focal planes and also the creation of bright spots of focused light when illuminated with white light. The outline of the cell is visible as the dark outline. Figure 4.1b shows the fluorescent image of the HUVEC cell before exposure to ultrasound. The fluorescent cRGD targeted non-echogenic liposomes have adhered to the surface of the cell and show its exact outline. Figure

4.1c shows the cell after exposure to the focused ultrasound. The microbubble is gone and fluorescent liposomes have been removed from almost half the surface of the cell. The cell has not been blasted apart because the left-hand side of the cell is still intact and there is still a faint visible outline of the right-hand side of the cell indicating that the right side is still largely intact. The cavitation event created by the collapsing microbubble was powerful enough to partially detach this cell from the substrate casing a rotational translation. The image has been reregistered to align the cell with its original orientation. Figure 4.1d shows which liposomes have been removed by the cavitation shockwave as the red colored regions. This figure was generated by taking the difference between Figure 4.1b and 4.1c, increasing the contrast of this difference image until it was just white or black pixels, color mapping the white pixels to red, and then overlaying the red image on top of the original pre-ultrasound image shown in Figure 4.1b. The blast region, as defined by the region of removed liposomes, can be estimated by drawing the blue circle around the red region as shown. In this case the blast region measures at 49 μm in diameter.

The effect of a single microbubble cavitation event on a smaller sized HUVEC cell is shown in Figure 4.1g-j. Here the microbubble is pointed out by the arrow in Figure 4.1g. The before and after images show that just the top section of the cell was affected by the cavitation event. The blast radius measured here was smaller than the other cells at 12 μm. This may be due to the thin narrow geometry of the cell where the microbubble was out on the periphery and the rest of the cell was shielded by the large bright lipid cluster. This demonstrates that the effect is still localized, even on small cells.

Cavitation Effect from Multiple Microbubbles of Different Sizes on a Single Cell

The effect of multiple microbubbles on the surface of a cell has been documented as shown in Figure 4.1e-f. Figure 4.1e shows the pre-ultrasound bright field image of an adherent HUVEC cell along with 3 large microbubbles and a fourth smaller microbubble at the top of the cell as pointed out by the arrows. Figure 4.1f shows the fluorescent image of the cell showing the adherence of the fluorescent non-echogenic liposomes around the edge of the cell. The microbubbles are still visible due to a small amount of white light that is allowed through the objective. Figure 4.1g shows the cell after exposure to ultrasound. The cell remained adherent to the substrate and did not undergo any translations. The fluorescent liposomes have been removed from the upper third of the cell. Figure 4.1h shows the liposomes that were removed as the red regions. This figure was generated in the same manner as Figure 4.1d. The blast region on the cell itself can be estimated by the blue circle and has a diameter of 46 μm.

Figure 4.1 – a-d Single microbubble interaction with a single cell, e-f Multiple microbubbles of different sizes interacting with a single cell.

a. Bright field image of an adherent HUVEC cell before ultrasound exposure showing the single adhered microbubble pointed out by the arrow. This microbubble had a diameter of 3 μm.
b. Fluorescent image of the same cell as above showing the fluorescent liposomes outlining the edge of adhered HUVEC cell before ultrasound exposure. These liposomes have been targeted to the surface of the cell using cRGD to attach to the αvβ3 integrin expressed on the cell surface
c. Fluorescent image of the same cell as above after ultrasound exposure. The microbubble has cavitated and the resulting shockwave removed fluorescent liposomes from half the surface of the cell
d. The red regions of this image show the liposomes that were removed from the original pre-ultrasound picture shown in Figure 4.1b. The blue circle shows the blast region as defined by the removal of the liposomes. In this case the blast region measures at 49 μm in diameter
e. Bright field image of another adhered HUVEC cell with the attached microbubbles of different sizes pointed out by the arrows before ultrasound exposure. The top most microbubble had a diameter of 4 μm and the other three microbubbles had diameters ranging from 6-9 μm.
f. Fluorescent image of the same HUVEC cell as above before ultrasound exposure showing the fluorescent adhered liposomes around the edge.
g. Fluorescent image of the same HUVEC cell as above after ultrasound exposure showing fluorescent liposomes being removed from the upper third of the cell.
h. The red regions of this image show the liposomes that were removed from the original pre-ultrasound picture shown in Figure 4.1f. The blue circle shows the blast region and measures at 46 μm in diameter
i. Brightfield image of a much smaller HUVEC cell attached to just one microbubbles as pointed out by the arrow.
j. Fluorescent image of the same HUVEC cell as above before ultrasound exposure showing the fluorescent adhered liposomes all across the surface of the cell
k. Fluorescent image of the same HUVEC cell as above after ultrasound exposure showing fluorescent liposomes being removed from the upper portion of the cell.
l. The red regions of this image show the liposomes that were removed from the original pre-ultrasound picture shown in Figure 4.1j. The blue circle shows the blast region and measures at 12 μm in diameter.

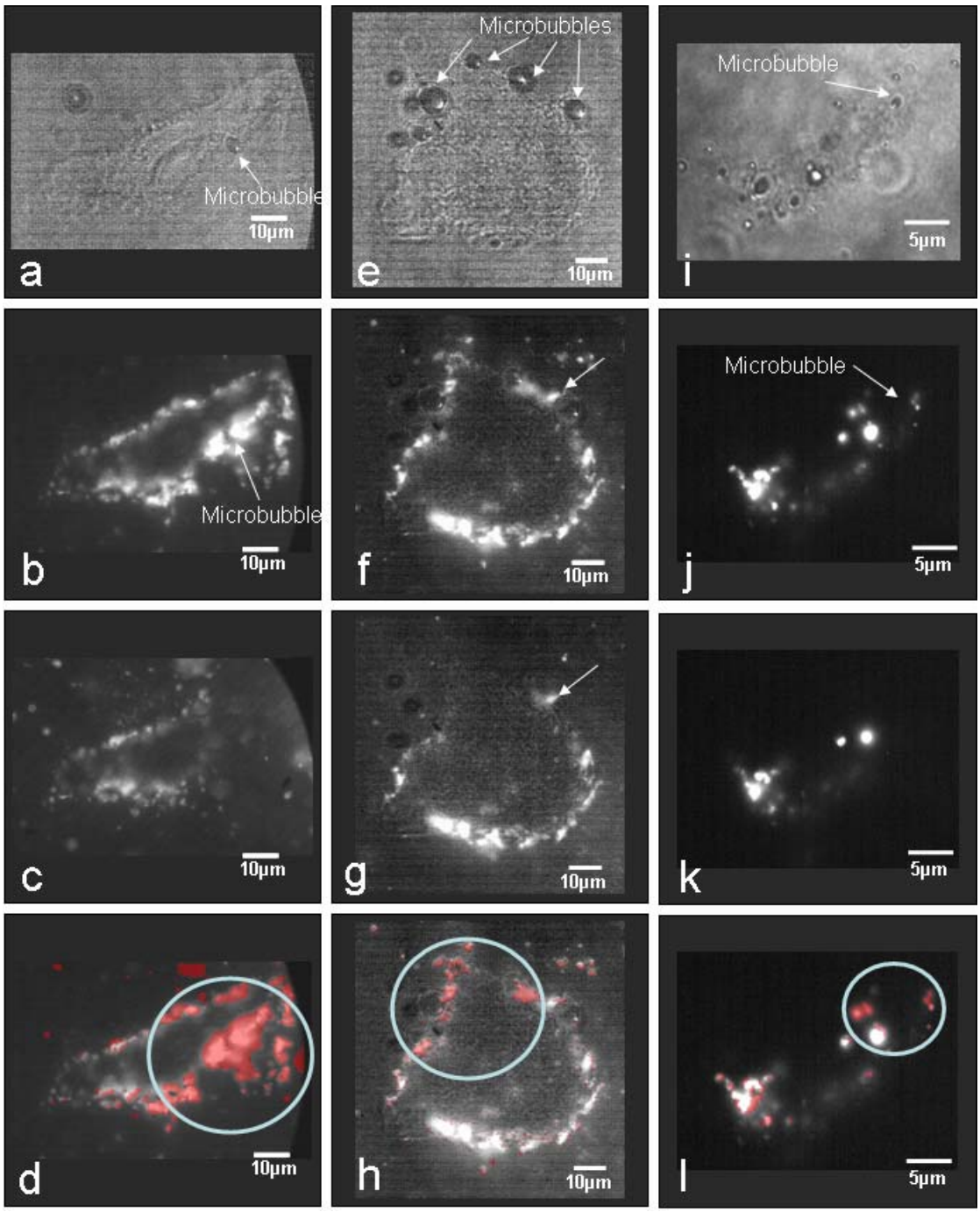
Microbubble
10μm
a
Microbubbles
10μm
e
Microbubble
5μm
i
Microbubble
10μm
b
10μm
f
Microbubble
5μm
j
10μm
c
10μm
g
5μm
k
10μm
d
10μm
h
5μm
l

Discussion

The effect of a single microbubble on a single cell is shown in Figure 4.1d indicating that a large portion of the cell surface was affected by the cavitation shockwave beyond just punching small holes in the membrane. The removal of attached liposomes shows that the shockwave reaches out at least 24 μm from the microbubble itself across the cell surface. This surface disruption is important to consider when dealing with cells which are sensitive to surface shear stress, such as these HUVECs, which can alter their gene expression upon exposure to shear stress[112]. The changing gene expression could change the affect of potentially delivered payload on the cells.

The effect of multiple microbubbles of different sizes on the cell shown in Figure 4.1h and appears to be quite similar to the cell with the single microbubble shown in Figure 4.1d interims of overall blast radius despite the fact that there were more microbubbles. This may be due to a resonance effect that the 2.25 MHz ultrasound had on the microbubbles. The top most microbubble had a diameter of 4 μm and the other three microbubbles had diameters ranging from 6-9 μm. The single microbubble attached to the cell in Figure 4.1d had a 3 μm diameter. It is probable that the 2.25 MHz ultrasound frequency really only resonated with the smaller microbubbles in each case. Free microbubbles on the 6-9 μm diameter range were observed to aggregate when exposed to the focused ultrasound due to secondary Bjerknes forces[113] rather than cavitate[114]. The free microbubbles with smaller diameters were observed to cavitate rather than aggregate due resonance oscillations that were created by interacting with the 2.25 MHz frequency. It is unlikely that the

three larger microbubbles in Figure 4.1h cavitated when exposed to the ultrasound and may have instead been destroyed by the cavitation shockwave produced by the smaller microbubble at the top of the cell. Further evidence that the larger microbubbles did not cavitate comes from the continued adherence of a fluorescent liposomes pointed out by the arrow in Figure 4.1f and 4.1g. If that right most microbubble had cavitated then this liposome should have been removed, as well as the fainter ones located to the right. Instead those liposomes remained intact indicating that microbubble did not cavitate. What is shown in Figure 4.1h is really the blast radius from the smaller microbubble without significant contribution from the three larger microbubbles. The blue circle defining the blast region was not centered at the smaller microbubble because only the effect on the cell itself is measurable, but presumably the shockwaves radiates out in a nearly spherical manner on a radial distance scale of at least 100 μm [115]. If the circle is centered at the top most smaller microbubble the effective blast radius of the smaller microbubble at he top of the cell increases to 55 μm.

Conclusions

The extent of the disruption of the cell membranes as defined by the removal of adhered liposomes to the cell surface has been documented here for the first time. The case of a single microbubble attached to a single cell and the case of multiple microbubbles of different sizes on a single cell have been documented. The cell with multiple microbubbles most likely had cavitation influence from just the smaller microbubble at the top due to resonance effects between the 2.25 MHZ driving

ultrasound. The larger sized microbubbles were shown to aggregate under these conditions rather than cavitate. This means that in both cases the main affect on the cells was from cavitation of a single microbubble, the extent of which was about 24-26 μm away from the microbubble itself. This can mean that up to half of an average HUVEC cell surface would be affected by a single cavitation event, not just small regions of the membranes where the sonoporation holes are generated. This has implications for both the delivery of genes in the field of transfection and for the effect on endothelia cells in vivo for drug delivery applications. Ideally the effect on the entire membrane would be kept to a minimum so the cells can maintain normal function.

Acknowledgments

I am grateful for the contributions to this chapter by the following co-authors: Stuart Ibsen[1], Ruben Mora[2], Guixin Shi[3], Carolyn Schutt[1], Wenjin Cui[3], Michael Benchimol[4] , Viviana Serra[1], Sadik Esener[5]

[1]Department of Bioengineering, Moores Cancer Center, University of California San Diego, 3855 Health Sciences Dr. # 0815, La Jolla, CA 92093-0815, Phone (858) 534-9848, Fax: (858) 534-9830, Email: sibsen@ucsd.edu

[2]Department of Biology, University of California San Diego, La Jolla, CA 92093 USA

[3]Moores Cancer Center, University of California San Diego, La Jolla, CA 92093 USA

[4]Department of Electrical & Computer Engineering, Moores Cancer Center, University of California San Diego, La Jolla, CA 92093 USA

[5]Department of Nanoengineering, Moores Cancer Center, University of California at San Diego, La Jolla, CA 92093 USA

Chapter 5

Fluorescent Microscope System to Monitor Real-Time Interactions between Focused Ultrasound, Echogenic Drug Delivery Vehicles, and Live Cell Membranes

Abstract

The recent rapid development in the field of ultrasound triggered drug delivery makes it essential to study the real-time interaction between live cells and delivery vehicles when exposed to focused ultrasound. This information has not previously been obtainable due to limitations in the optical systems used to perform basic physics on microbubble interaction with ultrasound and systems used to document basic interaction between microbubbles and cells. Here an instrument is described which for the first time combines fluorescent imagining, high speed videography, and focused ultrasound with designable pulse sequences in a manner that allows for real time observations of live adherent cells. This information allows the chemical and physical properties of the drug delivery vehicle to be tailor designed along with the ultrasound pulse sequences to interact with specific cell types to cause the most efficient drug delivery.

Introduction

Ultrasound triggered drug delivery promises to specifically deliver drugs to desired locations at desired times in the body. Ultrasound focused to the targeted tissue region interacts directly with systemically circulating echogenic drug delivery vehicles designed to release payload only in the ultrasound focal region. This can avoid unnecessary and potentially dangerous payload release in healthy tissue. Unfortunately, the development of new prototype echogenic delivery vehicles has been hampered because the real time cellular level impact of individual delivery

vehicles during insonation has been difficult to image and study. Ultimately the success of a delivery vehicle design will depend on its interaction with live cells when exposed to focused ultrasound, especially its interaction with the membranes of vascular endothelial cells, which are the first to receive exposure.

The new instrumentation described here was developed to study the cellular interaction of the echogenic drug delivery vehicles with individual live cells allowing real time evaluation as well as long term monitoring. This makes it possible to rapidly evaluate many types of vehicle designs and materials.

The need for rapid evaluation of different delivery vehicle designs comes from a recent expansion in the field of ultrasound triggered drug delivery[116, 117] with the development of delivery vehicles based on new nested liposome designs as shown in chapter 3. These vehicles incorporate internal payloads consisting of echogenic particles and gas microbubbles along with the therapeutic drugs. These vehicles are injected into the circulation system of the body where they pass through healthy tissue without allowing drug exposure. At the diseased region, the vehicles can be triggered to open and release their payloads upon insonation with focused the ultrasound. Only the small region of desired tissue located within the focal volume of the ultrasound would receive a high enough intensity to trigger drug release as shown in chapter 3. These ultrasound focal volumes can be on the order of a few cubic millimeters in size[63] allowing for exquisite spatial resolution. The vehicles which are not within the focal volume of the ultrasound are left unaffected and will be eliminated from circulation through normal clearance mechanisms without exposing the healthy tissue to the drug payload. Reducing the exposure of healthy tissue to the active drug will

reduce the systemic side effects experienced by many modern medications, especially those from chemotherapy. To achieve these delivery properties new vehicle designs using different materials need to be rapidly tested and evaluated. This requires a specialized imaging system to quickly evaluate the interaction of these vehicles with the membranes of live endothelial cells.

Previous imaging systems have been designed to understand the basic physics of microbubble interactions with ultrasound. These instruments have documented ultrasound driven microbubble oscillation at extremely high frame rates[101], acoustic induced lateral translations of the microbubble[118], changes to the internal structure of the microbubble during oscillation against a solid surface[119], and diameter changes of free floating microbubbles[120, 121].

Typically, the cellular effects of ultrasound triggered drug delivery vehicles have been documented by imaging a cell population before and after insonation. Though fluorescent tags can aid in tracking the destruction and delivery, researchers are often left to infer the exact occurrences during the application of ultrasound. Acquiring real-time information about ultrasound-particle interactions is necessary to provide a complete story.

Instruments have been designed to document the interaction of microbubbles adjacent to cells using white light illumination[122] and the interaction of microbubbles internalized by free floating cells with ultrasound[120], but detailed studies of membrane interaction were not possible due to difficulty visualizing the edges of the membranes. Fluorescent systems have been designed to monitor the influx of cell membrane impermeant dyes into cell interiors after nearby microbubbles

were insonated with ultrasound [106,123]. However, only white light was used to visualize the cell membrane itself so the extent of the interaction and effect from the microbubble was not measurable. Microbubble interactions with empty liposomes has been documented using fluorescence[124], but live cells were not monitored. Electron microscopy and flow cytometry have also been used to study the effect of microbubbles on cell membranes[108], but these studies were conducted post ultrasound exposure and are not capable of giving real-time information.

Although useful for understanding basic microbubble physics and basic cellular interactions, the specialized instruments described above are not designed to study the larger scale interactions of the delivery vehicles with the external membranes of large adherent endothelial cells. These adherent cells are most like the endothelial cells found lining the blood vessels that these drug delivery vehicles will first interact with. These interactions ultimately determine if the vehicle being tested will have useful drug delivery properties.

One of the problems of optically imaging cell membranes and the liposome membranes of the delivery vehicles is that they are difficult to observe with white light microscopy. Phase contrast can be used to better resolve the membranes, but the microscope setups require special lighting from a condenser which must be only a few inches away and directly in line with the microscope objective. This creates a geometric problem because the ultrasound requires the sample to be submersed in a tank of water to couple the ultrasound from the generating transducer to the experimental sample. The tank must be large enough to prevent reflections from the sides that can interfere with the desired ultrasound waveform.

Even if phase contrast imaging was possible with these large water tanks, the exact boundaries of cell membranes are difficult to determine and empty liposome membranes are especially difficult to image. It is also difficult to obtain information on how the lipids might be rearranging along the surface when exposed to a disturbance. The exact edges of cell and liposome membranes can be more effectively monitored using fluorescent dyes that attach or incorporate into the membranes themselves. The fluorescence microscopy also allows for excitation light and subsequent fluorescent light to be focused and collected through the same objective, eliminating the need for a condenser and allowing for the use of a large water bath.

The instrument described here has been designed to take advantage of fluorescent imaging and allows live adherent endothelial cells to be monitored while using a sensitive high speed camera to collect fluorescent images of membrane interactions. This allows the fragmentation of the membranes to be studied and allows the fluid motion that is created by microstreaming around oscillating microbubbels and cavitation shockwave events to be monitored. It also allows the extent of microbubble influence on the surface of cells to be monitored.

Instrument design

Water Tank

A 10 gallon water tank was used to allow coupling between the ultrasound transducer and the submerged sample. The large size of the tank helped attenuate reflections of ultrasound from the sides of the tank and from the air/water interface. To further reduce reflections a 1-cm thick block of acoustically absorbent rubber (Aptflex

F28, Precision Acoustics Ltd., Dorchester, UK) was installed at the opposite end of the tank directly in line with the longitudinal axis of the transducer as shown in Figure 5.1.

Focused Ultrasound Generation

The ultrasound pulse sequence used to insonify the sample was generated using a National Instruments PCI 5412 arbitrary waveform generator board run by a custom designed automation program using LabVIEW 8.2. The arbitrary waveform generator allowed custom ultrasound pulse sequences to be designed to create different interactions between the microbubbles and the membranes. The ultrasound pulse sequence was sent to a Panametrics 2.25 MHz transducer (V305-SU) with a 2.54 cm spherical-focus. The focal zone of the ultrasound was 1 mm^3. A Panametrics BCU -58 - 6W waterproof connector cable was used to fully submerge the transducer under water. A 300 W radio frequency amplifier from Vox Technologies (VTC2057574) was used to amplify the signals sent to the transducer, creating acoustic intensities in the focal region of up to 1.6 MPa.

Sound Field Quantification

The sound field of the transducer within the tank was mapped using a submersible broadband needle hydrophone (HNP-0400) from Onda Corporation in connection with their AH - 2020-100 hydrophone pre amp (50kHz - 100 MHz, 0 +20 db). The high level of directionality and small spatial volume allowed the needle hydrophone to easily find the actual 1 mm^3 focal zone of the transducer so the samples could be directly aligned in that volume.

Optical System

The microscope system was designed with two types of objectives. The first was the Nikon MRF07620 CFI W Flour 60X water dipping objective. This could be submerged 5 cm under the surface of the water to observe ultrasound interactions in the bulk fluid. This objective had a 2 mm working distance which was large enough to allow the lens to stay out of the ultrasound focal region while imaging the sample. A Nikon 100X oil immersion objective was also used because the oil immersion allowed for a greater numerical aperture to collect the light from the fluorescence more efficiently. This allowed high magnification videos to be collected while maintaining the desired high frame rates. The use of oil prevented the total submersion of the oil objective in water so the sample had to be located at the air/water interface. The ultrasound transducer orientation was changed to aim the focal zone directly at the sample in the vertical orientation as shown in Figure 5.1. This potentially could create interference patterns in the region of the sample due to reflections from the air/water interface, but acoustic energy was deposited in that region which had significant interaction with the samples. Placing the samples at the air/water interface is also a model for monitoring interaction with ultrasound and the delivery particles near the internal surface of the lungs.

White Light Illumination

The sample could be illuminated with white light using a Ram Optical Instrumentation 150 Illuminator fiberoptic light source which generated the light from

outside the tank and directed it through the tank wall to a mirror submerged in the water. The mirror was adjusted to reflect the light up into the objective. The white light allowed the cells to be observed without the need for fluorescence and was very useful to find microbubbles which were not visible when using just the fluorescence. Independent control over the two light sources was important for viewing cell and liposome interactions with ultrasound simultaneously.

Experimental Sample Retention

Three different sample holders were designed to analyze ultrasound interaction under different conditions. Blocks of agar tissue phantoms were added to these sample holders to either encase them, or sit between them and the ultrasound transducer to better simulate acoustic conditions that would be experienced in vivo.

The first sample holder was a custom fabricated 15 μm-deep microwell chamber molded in a 0.5 cm thick slab of polydimethylsiloxane (PDMS) and covered on top by a glass coverslip. The PDMS is an optically clear, flexible, rubber like material that attenuates ultrasound but allowed a significant amount of energy through a 0.5 cm thickness to reach the sample contained within the well. The microwell was used both at the air/water interface for use with the oil immersion objective and completely submerged underwater for use with the water immersion objective. When used at the air/water interface the coverslip was positioned above the water surface with the PDMS slab halfway submerged in the water so as to conduct the ultrasound from the underwater transducer into the sample well.

The second sample holder design consisted of two pieces of thin clear plastic sheet placed on top of each other and held taught within a circular hoop support structure. The plastic sheets were optically clear and did not significantly attenuate the ultrasound energy. Holding the sheets tightly together allowed a 15 μL of sample fluid to spread out between the sheets thin enough to reduce background fluorescence from out of focus liposomes. This holder was used completely submerged underwater with the water dipping objective.

The third sample holder was a 200 μm diameter micro-cellulose dialysis hollow fiber manufactured by Spectrum. These thin tubes were nearly both optically and acoustically transparent and were used completely submerged with the water immersion objective. The cellulose tubes were connected to syringes to inject fluid containing the delivery vehicles allowing them to flow through the tubes to study ultrasound interaction in a simulated blood vessel environment and under conditions of flow. The samples needed to be diluted in these situations because the background fluorescence from the out of focus liposomes in the tube created unfavorable signal to noise ratios under dense vehicle concentrations.

These different sample holders were designed to be embedded in agar tissue phantoms to help better simulate the distortions and scattering that focused ultrasound would experience in vivo. This allowed the robustness of these ultrasound activations to be studied for better understanding of how these particles would interact in the vivo ultrasound sound field.

Alignment

The sample holder, the transducer, and the needle hydrophone were mounted to manual XYZ directional microstages so their alignment could be precisely controlled. The sample holder, transducer focal volume, and focal zone of the microscope objective were all precisely aligned to make sure sufficient ultrasound energy was deposited into the observable region of the sample holder.

Fluorescent Imaging

Florescence imaging was essential to detect the fluorescently labeled liposome membranes. This was achieved by incorporating a Nikon J-FL EPI-Fluorescence attachment with the use of a Nikon GFP-3035B-NTE GFP Brightline filter cube. A Nikon 100W Hg arc lamp with a CHIU Technical Corp M-100T power supply provided the excitation light. A Nikon trinocular body tube was mounted to the top of the EPI-Fluorescence attachment which allowed the bionocular eye pieces to be installed for visual observation, as well as a Nikon 0.9x to 2.25x zoom CCTV/microscope adapter which allowed the field to be scanned at low power and then zoom in on important details.

High Speed Videography

A Photron FASTCAM 1024 PCI high speed video camera acquired the image sequences. The camera was fitted with a C mount adapter to interface with the top of the zoom CCTV/microscope adapter on the trinocular body tube. Movies of the fluorescent imaging could be captured at speeds of 60 – 18,000 frames per second.

The use of quantum dots created much brighter fluorescence than the traditional fluorescent dyes allowing the higher frame rates to be achieved.

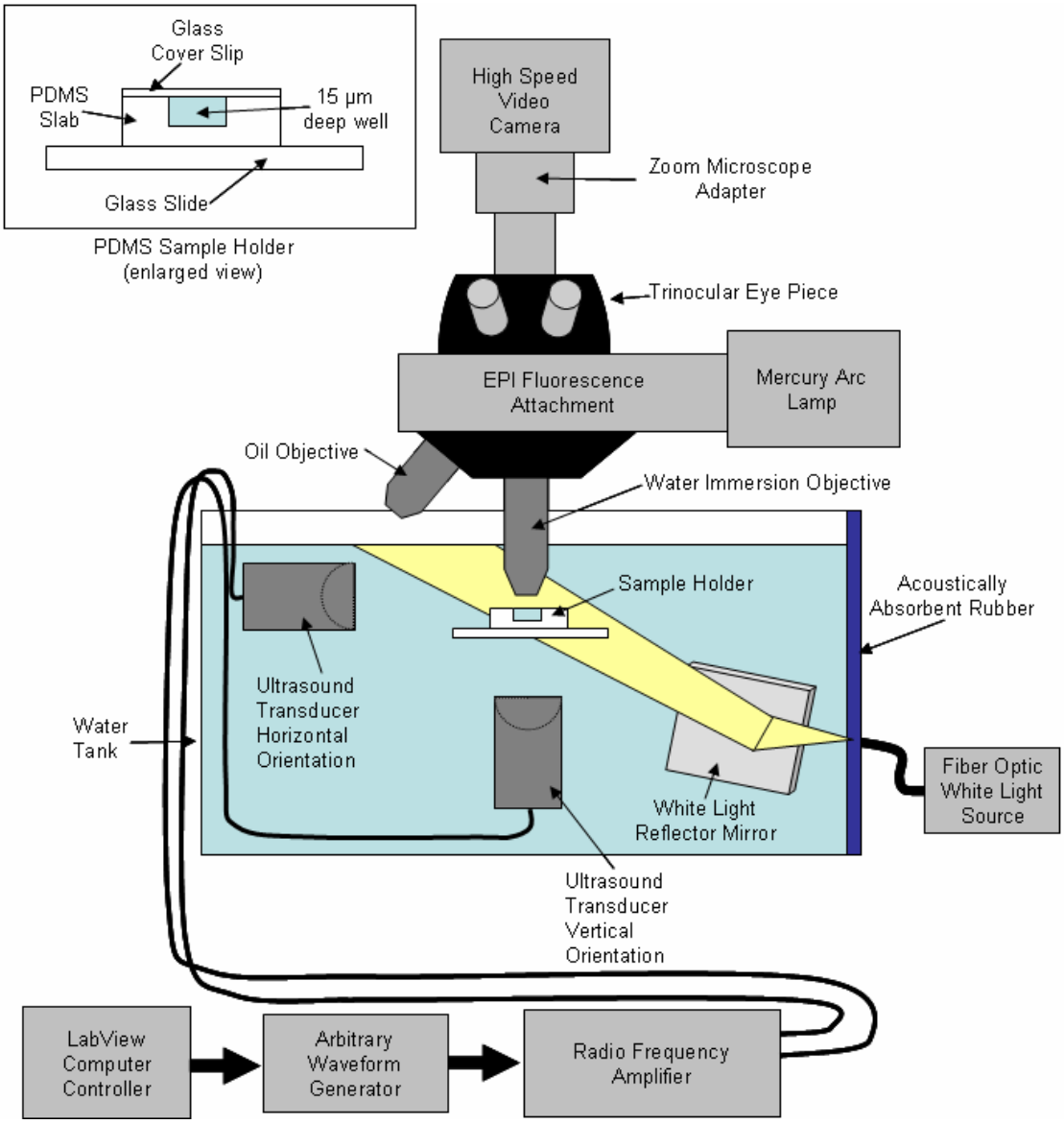

Figure 5.1 – Schematic of the optical, electrical and acoustic components of the system.

Documentation of Microbubble Interaction with Fluorescent Liposome Membrane

With the fluorescent imaging it was possible to visualize the interaction of just the echogenic drug delivery vehicles themselves with the focused ultrasound as shown in Figure 5.2. The vehicle shown by the arrow consisted of a microbubble on the inside surrounded by a water space and a fluorescently labeled outer membrane. Here the ultrasound pulse sequence was designed using the arbitrary waveform generator to cause cavitation of the encapsulated microbubble as seen in frame 2. Frame 3 shows the fragmentation of that fluorescent membrane leaving the lipid debris cloud seen in frame 4.

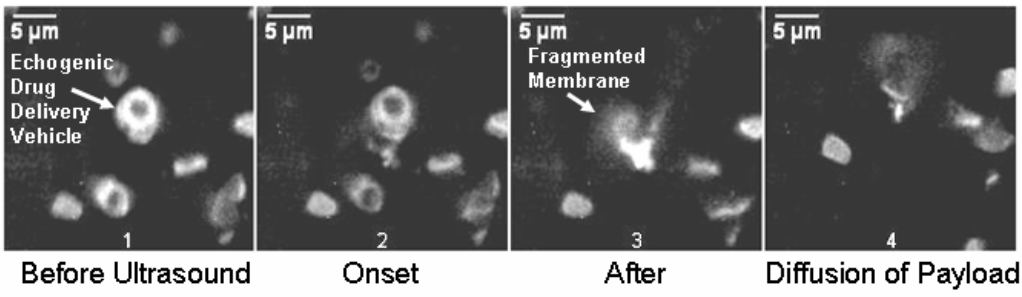

Figure 5.2 – Fluorescent image sequence showing the interaction of focused ultrasound with the microbubble inside the echogenic drug delivery vehicle and subsequent rupture of the outer membrane leaving a debris field of fluorescent lipid particles.

Documentation of Echogenic Drug Delivery Vehicle Interaction with Nearby Artificial Cell Membranes

Artificial cell membranes were created to test membrane interactions under less violent conditions. A different ultrasound pulse sequence was designed to pop the microbubble rather than cavitate it. This was conducted while the echogenic vehicle was near the membrane surface of an artificial cell as seem in frame 1 of Figure 5.3. These artificial cells were also labeled with fluorescent dye to determine their exact edges. In frames 2-4 the outer membrane of the vehicle was popped open and slowly unfolded near the artificial cell causing no visible damage to its outer membrane.

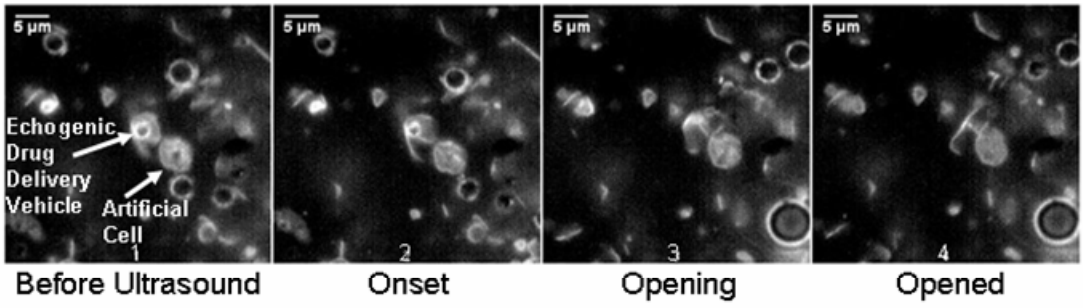

Figure 5.3 – Fluorescent image sequence of the interaction between an echogenic drug delivery vehicle and an artificial cell membrane.
The ultrasound pulse sequence was designed to induce a low level rupture and unfolding of the vehicle's outer membrane.

Documentation of Echogenic Delivery Vehicle Interaction with Cell Membranes

The interaction of the echogenic drug delivery vehicles with cell membranes of adherent endothelial cells was also documented as shown in Figure 5.4. Here the surface of the cell is covered in fluorescent liposomes which are non-echogenic and do

not respond to ultrasound. Only three are pointed out in the figure but the rest of the surface is covered with them as shown. These liposomes are biochemically targeted to integrins expressed on the cell surface and mark the exact edges of the cell membrane. When exposed to the focused ultrasound the three microbubbles cavitated sending out a shockwave which affected the surface of the cell by removing the attached liposomes. The attachment of the liposomes to the surface of the cell is particularly important to understand the extent of the affect from the microbubble. This allows the entire surface of the cell to be monitored to understand more than just whether the membrane has been permeabilized. This image sequence shows disturbance to the cell membrane only in the upper third of the cell.

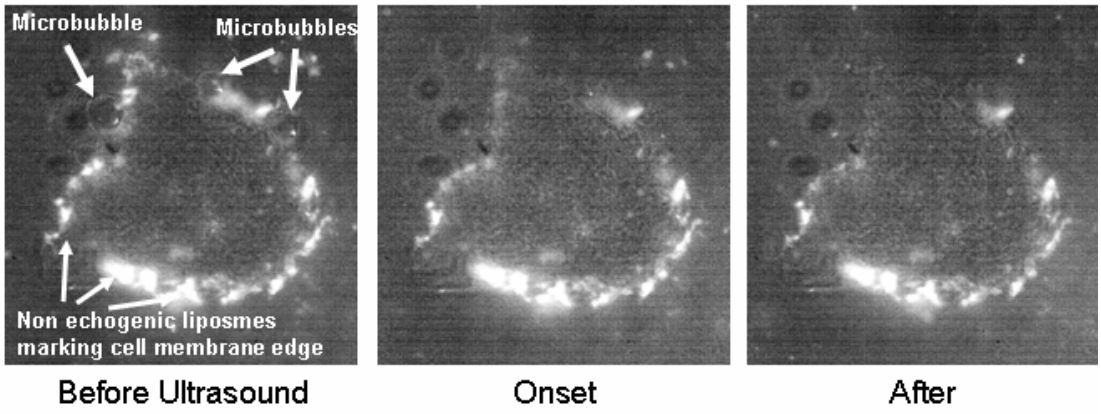

Figure 5.4 – Fluorescent and white light image sequence showing the interaction of microbubbles with the labeled surface of an adherent endothelial cell.
Non-echogenic liposomes have been biochemically targeted to attach to the surface of the cell outlining the exact edges of the cell in fluorescence in the "Before Ultrasound" frame. In the "Onset" frame the ultrasound interaction shows the cavitation of the microbubbles and subsequent removal of adherent fluorescent liposomes from the cell surface due to interaction caused by the cavitation shockwave. In the "After" frame the fluorescent liposomes are torn from the cell membrane only in the upper third portion of the cell.

The effect of a single microbubble on the surface of an adherent cell is shown in Figure 5.5. Here the surface of the cell is covered with targeted non-echogenic liposomes which show the outline of the cell. A single microbubble is pointed out toward the right. The cavitation event created upon insonation with ultrasound was so violent that the cell was partially broken from the substrate causing a rotational translation of the cell. The cavitation also affected the surface of the cell membrane removing the non-echogenic liposomes from nearly half of the cell surface.

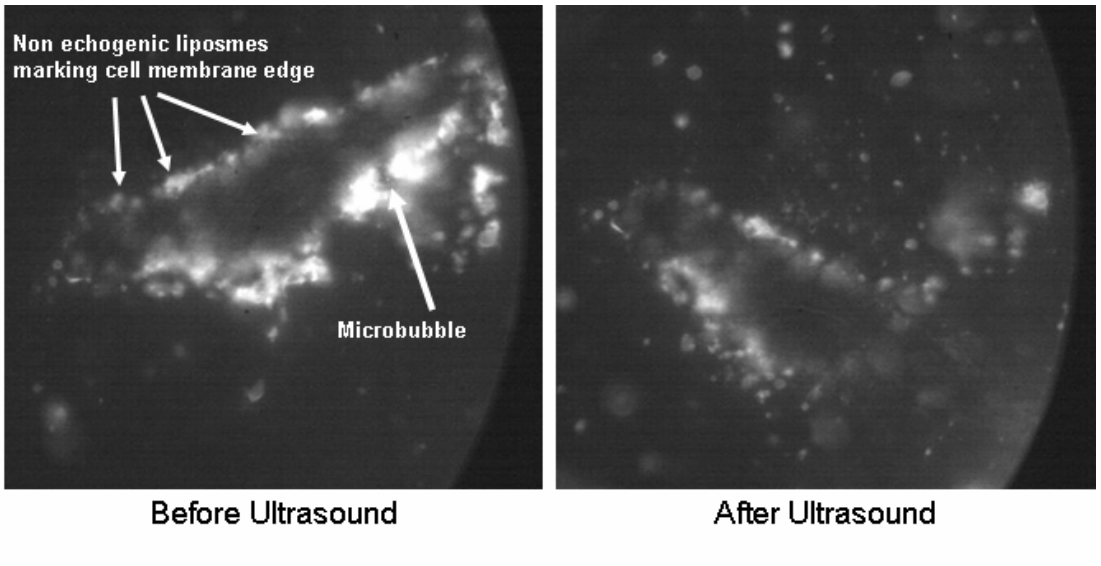

Figure 5.5 – Fluorescent image sequence of the interaction between a single microbubble and an adherent endothelial cell.
The cell is outlined by non-echogenic liposomes which have been biochemically targeted to integrin proteins present on the surface of the cell. The shockwave produced by the cavitation event provided enough energy to partially detach the cell from the glass and cause a 45 degree clockwise rotational translation as well as remove liposomes from the surface of nearly half the surface of the cell.

Documentation of Microstreaming and Fluid Flow around Microbubbles

The fluid motion effects of a microbubble exposed to a long duration pulse of ultrasound are shown in Figure 5.6. The microbubble is shown as the large dark circle in the center of the image in frame 1. It is surrounded by non-echogenic fluorescent liposomes which follow streamlines of fluid motion created around the oscillating microbubble when exposed to ultrasound. The particle shown by the arrow in frame 1 is tracked through frames 2-4 showing a circular flow pattern that drags particles along the edge of the bubble and sends them down towards the bottom of the frame away from the microbubble. These types of microstreaming interactions with cell surfaces are of great interest when considering ultrasound pulse sequence and vehicle design.

The region over which the microbubble microstreaming occurs can be much larger than the microbubble itself as shown in Figure 5.7. The arrow points to a single microbubble which is ensnared with focused ultrasound creating a flow pattern that has a diameter 6 times larger than the diameter of the microbubble itself. A large cluster of fluorescent lipids shown in the upper portion of frame 3 are pulled into the vortex motion of the fluid around the microbubble as seen in frame 4.

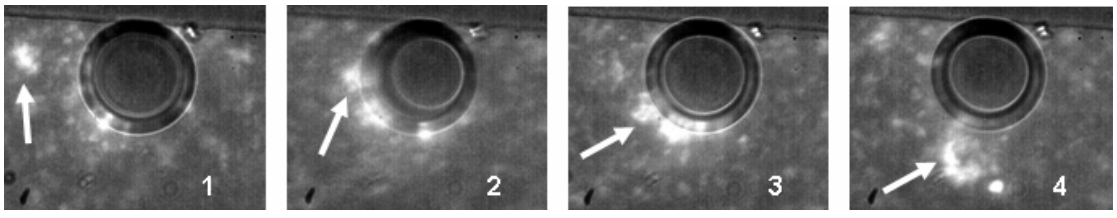

Figure 5.6 – Fluorescent image sequence of particles caught in streamlines of fluid motion created around the microbubble during resonation with ultrasound. The microbubble is shown as the dark circle in the middle of the frame. A single fluorescent particle is tracked by the white arrows from frame 1-4. The entire sequence is taken during the ensonation period of the ultrasound.

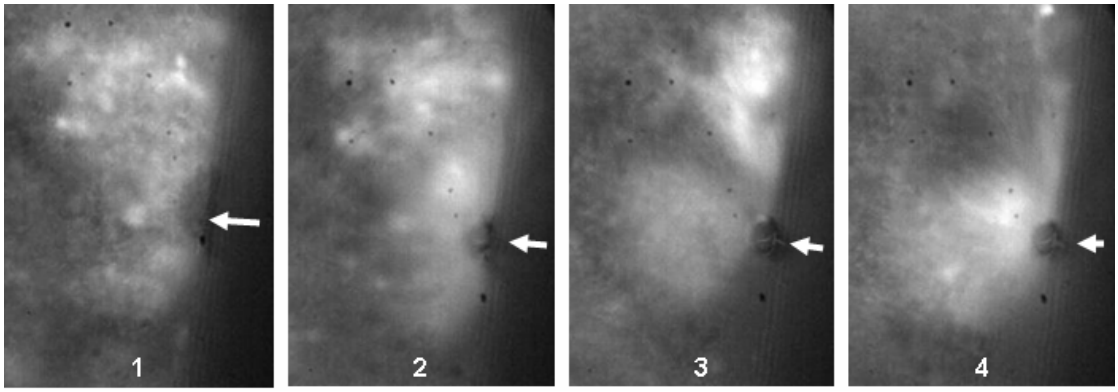

Figure 5.7 – Fluorescent image sequence showing microstreaming around a dark circular microbubble pointed out by the arrows in each frame.
Frame 1 shows the field of non-echogenic liposomes before ultrasound application. Frame 2 shows the microstreaming flow field starting at the beginning of ensonation. The diameter of the flow field is 6 times larger than the diameter of the microbubble itself and can pull in larger clusters of fluorescent liposomes as seen in frames 3 and 4.

Discussion

The instrument described here for the first time combines fluorescent imaging, focused ultrasound, and high speed videography to study interaction of an emerging class of echogenic drug delivery vehicles with adherent cell membranes. The documentation data shown here provides invaluable knowledge on the interaction between the vehicle and cells membranes allowing the properties of both the ultrasound pulse sequence and the vehicles themselves to be developed together to produce the desired properties. This system provides the ability to monitor the interaction of these vehicles with individual live cells in real-time providing essential information to tailor their properties for specific interactions with desired cell and tissue types.

Acknowledgments

The authors are grateful for the insightful discussions with Eugene Cho while designing this system. The study was supported by the NCI Grant No. 5U54CA119335-05, and by the UCSD Cancer Center Specialized Support Grant P30 CA23100.

The following people are co-authors of this chapter: Stuart Ibsen[1], Michael Benchimol[2], Sadik Esener[3]

[1]Department of Bioengineering, Moores Cancer Center, University of California San Diego, 3855 Health Sciences Dr. # 0815, La Jolla, CA 92093-0815, Phone (858) 534-9848, Fax: (858) 534-9830, Email: sibsen@ucsd.edu

[2]Department of Electrical & Computer Engineering, Moores Cancer Center, University of California San Diego, La Jolla, CA 92093 USA

[3]Department of Nanoengineering, Moores Cancer Center, University of California at San Diego, La Jolla, CA 92093 USA

Thesis Conclusions

This thesis demonstrates the feasibility of two novel drug delivery approaches which use external energy sources to highlight the tumor and achieve localized accumulation of active drug.

The first approach used 365 nm light to activate a doxorubicin prodrug. The successful synthesis of the photocleavable chemotherapy prodrug was demonstrated and the biological effects of this class of prodrug were documented for the first time. The DOX-PCB prodrug showed a 200 fold decrease in cytotoxicity as compared to the free DOX. When exposed to light at 365 nm it was shown that the DOX-PCB successfully converted into pure pharmacologically active DOX. The prodrug was shown to be resistant to liver microsome digestion. In-vivo pharmacological studies did not find any detectable amounts of DOX-PCB being converted after in vivo injection. The DOX-PCB was shown to have a circulation half life of 10 min in mice which is comparable to that of DOX at 20 min. The activation of the prodrug was also demonstrated in an in-vivo tumor model where the tumor exposed to the 365 nm light showed significantly higher DOX concentration than a control tumor in the same individual which did not receive a light dose.

Also demonstrated was the use of low intensity ultrasound to activate novel nested liposome drug delivery vehicles with incorporated microbubbles. The production of such liposome encapsulated microbubble structures (SHERPA) was demonstrated here for the first time. The interaction of these drug delivery vehicles

with ultrasound was documented using high speed fluorescence imaging. There were two main modes of ultrasound response. Exposure to high intensity ultrasound caused the microbubble to violently cavitate fragmenting the outer membrane. Exposure to lower intensity ultrasound resulted in a less violent popping of the outer membrane and a slow opening expansion. It was demonstrated that the activation could be localized to small regions within an agar tissue phantom by focusing of the ultrasound. Preliminary in-vitro testing showed that these SHERPA had little uptake by macrophages and good stability in blood of at least several hours. The SHERPA were loaded with water soluble free DOX. DOX-PCB could also be incorporated into the SHERPA using the same method, however demonstrating this directly was not possible due to the prohibitive cost of the DOX-PCB precursor molecules. The SHERPA should actually be able to retain the DOX-PCB for longer periods of time and at higher concentrations than the free DOX due to the DOX-PCB's lower membrane permeability.

A custom high speed camera system which combined fluorescent microscopy with focused ultrasound was also developed specifically to study the interaction of the microbubble with the SHERPA membrane as well as nearby cellular membranes. The shockwave produced by the microbubble bubble cavitation event was found to affect a radius of 12-40 μm across the membrane of HUVEC cells. This indicates that these cavitation events were highly localized and would only affect a few cells in the immediate vicinity of the microbubble itself.

Thesis Future Directions

Additional avenues of interest for the free DOX-PCB prodrug include exploring the possible effectiveness of the DOX-PCB prodrug against DOX resistant tumors. During a normal course of DOX treatment there is a slow die off of tumor cells as the DOX accumulates at sufficiently therapeutic levels over time. However, the slow accumulation of DOX can allow certain subpopulations of cancer cells within the shrinking tumor to develop resistance to the DOX due to over expression of cellular efflux pumps which actively pump out any DOX that passively diffuses in[125]. The DOX-PCB prodrug has demonstrated that the DOX portion is significantly inhibited due to its inability to intercalate DNA. It may be different enough to prevent the cellular efflux pumps from being able to attach to DOX as well. This would allow the DOX-PCB to build up to high levels within the cell and exposure to 365 nm light would cause a burst release of DOX within the cell. The shear amount of DOX may momentarily overwhelm the pumps allowing the remaining DOX to intercalate the DNA. A suddenly high concentration of DOX might also be created with the SHERPA through the sonoporation mechanism.

Additional in vivo testing with the DOX-PCB prodrug will also help understand the biodistribution of the activated DOX to determine how much actually leaves the tumor and is swept through the circulation system.

Additional avenues of interest for the SHERPA can be focused on studying their payload delivery abilities. The delivery on the cellular level through possible sonoporation facilitation will be determined. Also, effects on the internal

microbubble by different ultrasound pulse sequences can be used to design a pulse that gives maximum microbubble cavitation effect within a population of SHERPA with the least amount of tissue energy deposition.

The combination of both the DOX-PCB and the SHERPA can be studied as well to determine if the SHERPA cause a higher accumulation of the DOX-PCB than would otherwise occur with a systemic injection of free DOX-PCB. This can be very important to get the maximum amount of activated DOX within the tumor region without allowing toxic DOX accumulation in the liver or heart.

REFERENCES

1. Love R, Leventhal H, Easterling D, Nerenz D. Side Effects and Emotional Distress During Cancer Chemotherapy. Cancer 989;63(3):604-612.

2. Pawan K. Singal NI. Doxorubicin-Induced Cardiomyopathy. The New England Journal of Medicine 1998 September 24;339(13):900-905.

3. Olson RD MP. Doxorubicin cardiotoxicity: analysis of prevailing hypotheses. FASEB J 1990;4(13):3076-3086.

4. Giorgio Minotti PM, Emanuela Salvatorelli, Gaetano Cairo, Luca Gianni. Anthracyclines: Molecular Advances and Pharmacologic Developments in Antitumor Activity and Cardiotoxicity. Pharmacol Rev 2004;56:185–229.

5. Coldman A, Goldie J. Impact of dose-intense chemotherapy on the development of permanent drug resistance. Semin Oncol 1987;14(4 Suppl 4):29-33.

6. Shapiro C, Recht A. Side Effects of Adjuvant Treatment of Breast Cancer. N Engl J Med 2001;344(26):1997 - 2008.

7. Tator C, Wassenaar W. Intraneoplastic injection of methotrexate for experimental brain-tumor chemotherapy. J Neurosurg 1977;46(2):165-174.

8. Mairs R, Wideman C, Angerson W, Whateley T, Reza M, Reeves J, et al. Comparison of different methods of intracerebral administration of adioiododeoxyuridine for glioma therapy using a rat model. British Journal of Cancer 2000;82(1):74–80.

9. Bareford LM, Swaan PW. Endocytic mechanisms for targeted drug delivery. Advanced Drug Delivery Reviews 2007;59:748–758.

10. Fradet Y, Islam N, Boucher L, Parent-Vaugeois C, Tardif M. Polymorphic expression of a human superficial bladder tumor antigen defined by mouse monoclonal antibodies. Proc Natl Acad Sci 1987;84:7227-7231.

11. Park J, Hong K, Kirpotin D, Colbern G, Shalaby R, Baselga J, et al. Anti-HER2 Immunoliposomes: Enhanced Efficacy Attributable to Targeted Delivery. Clinical Cancer Research 2002;8:1172–1181.

12. Vaupel P, Kallinowski F, Okunieff P. Blood Flow, Oxygen and Nutrient Supply, and Metabolic Microenvironment of Human Tumors: A Review. Cancer Research 1989;49:6449-6465.

13. Gansauge S, Gansauge F, Yang Y, Muller J, Seufferlein T, Ramadani M, et al. Interleukin 1beta-converting Enzyme (Caspase-1) Is Overexpressed in Adenocarcinoma of the Pancreas. Cancer Research 1998;58:2703-2706.

14. Rooseboom M, Commandeur J, Vermeulen N. Enzyme-Catalyzed Activation of Anticancer Prodrugs. PHARMACOLOGICAL REVIEWS 2004;56(1):53-102.

15. Lavis L. Ester Bonds in Prodrugs. ACS CHEMICAL BIOLOGY 2008;3(4):203-206.

16. Gabizon AA. Pegylated Liposomal Doxorubicin: Metamorphosis of an Old Drug into a New Form of Chemotherapy. Cancer Investigation 2001;19(4):424-436.

17. Miele E, Spinelli GP, Miele E, Tomao F, Tomao S. Albumin-bound formulation of paclitaxel (Abraxane® ABI-007) in the treatment of breast cancer. International Journal of Nanomedicine 2009;4:99–105.

18. Moghimi SM, Hunter AC, Murray JC. Long-circulating and target-specific nanoparticles: theory to practice. Pharmacol Rev 2001;53:283-318.

19. Moghimi SM, Hunter AC, Murray JC. Long-circulating and target-specific nanoparticles: theory to practice. Pharmacol Rev 2001 Jun;53(2):283-318.

20. Bibby DC, Talmadge JE, Dalal MK, Kurz SG, Chytil KM, Barry SE, et al. Pharmacokinetics and biodistribution of RGD-targeted doxorubicin-loaded nanoparticles in tumor-bearing mice. International Journal of Pharmaceutics 2005;293:281–290.

21. Schiffelers RM, Koning GA, Hagen TLMt, Fens MHAM, Schraac AJ, Janssen APCA, et al. Anti-tumor efficacy of tumor vasculature-targeted liposomal doxorubicin. Journal of Controlled Release 2003;91:115–122.

22. Vlerken LEv, Vyas TK, Amiji MM. Poly(ethylene glycol)-modified Nanocarriers for Tumor-targeted and Intracellular Delivery. Pharmaceutical Research 2007;Expert Review.

23. Shenoy DB, Amiji MM. Poly(ethylene oxide)-modified poly(epsilon-caprolactone) nanoparticles for targeted delivery of tamoxifen in breast cancer. International Journal of Pharmaceutics 2005;293:261–270.

24. Scott RSCcaLJ. Dexrazoxane A Review of its Use for Cardioprotection During Anthracycline Chemotherapy. Drugs 2005;65(7):1005-1024.

25. Denny WA. Prodrug strategies in cancer therapy. Eur J Med Chem 2001;36:577-595.

26. Denny WA. Tumor-activated Prodrugs—A New Approach to Cancer Therapy. Cancer Investigation 2004;22(4):604-619.

27. Lutz F. Tietze MN, Thomas Mollers, Roland Fischer, Karl-Heinz Glusenkamp, Manfred F. Rajewsky, and Eckhard Jahde. Proton-mediated Liberation of Aldophosphamide from a Nontoxic Prodrug: A Strategy for Tumor-selective Activation of Cytocidal Drugs. Cancer Research 1989;49:4179-4184.

28. J.Martin Brown WRW. Exploiting Tumor Hypoxia in Cancer Treatment Nature Reviews Cancer 2004;4:437-447.

29. K. Breistol HRH, D.P. Berger, S.P. Langdon, H.H. Fiebig, and O. Fodstad. The Antitumour Activity of the Prodrug N-l-leucyl-doxorubicin and its Parent Compound Doxorubicin in Human Tumour Xenografts. European Journal of Cancer 1998;34(10):1602-1606.

30. Gopin A, Ebner S, Attali B, Shabat D. Enzymatic Activation of second-generation dendritic prodrugs: Conjugation of self-immolative dendrimers with PEG via click chemistry. Bioconjugate Chem 2006;17:1432-1440.

31. Shamis M, Lode HN, Shabat D. Bioactivation of self-immolative dendritic prodrugs by catalytic antibody 38C2. JACS 2004;126:1726-1731.

32. Barbara M. Mueller WAW, Ralph A. Reisfeldt. Antibody Conjugates with Morpholinodoxorubicin and Acid-Cleavable Linkers. Bioconjugate Chem 1990;1:325-330.

33. Dominic A. Scudiere RHS, Kenneth D. Paull, Anne Monks, Siobhan Tierney, Thomas H. Nofziger, Michael J. Currens, Donna Seniff, and Michael R. Boyd,. A distinct ‘‘side population’’ of cells with high drug efflux capacity in human tumor cells. PNAS 2004;101(39):14228-14233.

34. Yuta Shibamoto YT, Kazuhito Tanabe, Hiroshi Hatta, Sei-Ichi Nishimoto. In Vitro and In Vivo Evaluation of Novel Antitumor Prodrugs of 5-Fluoro-2 Deoxyuridine Activated by Hypoxic Irradiation. Int J Radiation Oncology Biol Phys 2004;58(2):397-402.

35. Noguchi M, Skwarczynski, Mariusz , Prakash, Halan , Hirota, Shun ,Kimura,Tooru , Hayashia,Yoshio, Kisoa, Yoshiaki Development of novel water-soluble photocleavable protective group and its application for design of photoresponsive paclitaxel prodrugs. Bioorganic & Medicinal Chemistry 2008;16:5389–5397.

36. Olga Greco GUD. Gene Directed Enzyme/Prodrug Therapy of Cancer: Historical Appraisal and Future Prospectives. Journal of Cellular Physiology 2001;187:22-36.

37. M. P. Napier SKS, C. J. Springer, K. D. Bagshawe, A. J. Green, J. Martin,, S. M. Stribbling NC, D. O'Malley, R. H. J. Begent. Antibody-directed Enzyme Prodrug Therapy: Efficacy and Mechanism of Action in Colorectal Carcinoma. Clinical Cancer Research 2000;6:765–772.

38. Mark W. Pandori DAH, Jerzy Olejnik, Edyta Krzymanska-Olejnik, Kenneth J. Rothschild, Abraham A. Palmer, Tamara J. Phillips, and Takeshi Sano. Photochemical Control of the Infectivity of Adenoviral Vectors Using a Novel Photocleavable Biotinylation Reagent. Chemistry and Biology 2002;9:567-573.

39. Amit B, Zehavi U, Patchornik A. Photosensitive Protecting Groups of Amino Sugars and Their Use in Glycoside Synthesis. 2-Nitrobenzyloxycarbonylamino and 6-Nitroveratryloxycarbonylamino derivatives. J Org Chem 1974;39:192-196.

40. J. Elisseeff KA, D. Sims, W.McIntosh, M. Randolph, and R. Langer. Transdermal photopolymerization for minimally invasive implantation. Proc Natl Acad Sci 1999;96:3104-3107.

41. Yuanlong Yang EJC, Jason A. Koutcher, R.R. Alfano. UV Reflectance Spectroscopy Probes DNA and Protein Changes in Human Breast Tissues. Journal of Clinical Laser Medicine & Surgery 2001;19(1):35-39.

42. Sutherland J, Griffin, K. Absorption Spectrum of DNA for Wavelengths Greater than 300 nm. Radiation Research 1981;86(3):399-410.

43. Elliot Botvinick, Berns M. Internet-Based Robotic Laser Scissors and Tweezers Microscopy. Microscopy Research and Technique 2005;68:65-74.

44. Alexander D. Lewis DHML, George E. Duran, C. Roland Wolf, and Branimir I. Sikic. Role of Cytochrome P-450 from the Human CYP3A Gene Family in the Potentiation of Morpholino Doxorubicin by Human Liver Microsomes. Cancer Research 1992;52:4379-4384.

45. Patchornik A, Amit B, Woodward RB. Photosensitive Protecting Groups. JACS 1970:6333-6335.

46. Olejnik J, Sonar, S., Krzymanska-Olejnik, E., Rothschild, K. Photocleavable biotin derivatives: A versatile approach for the isolation of biomolecules. Proc Natl Acad Sci USA 1995;92:7590-7594.

47. H. Schupp WKW, and W. Schnabel. Mechanistic Studies of the Photorearrangement of o-nitrobenzyl esters. Journal of Photochemistry 1987;36:85-97.

48. Gary J. Quigley AH-JW, Giovanni Ughetto, Gijs Van Der Marel, Jacques H. Van Boom, and Alexander Rich. Molecular structure of an anticancer drug-DNA complex: Daunomycin plus d(CpGpTpApCpG). Proc Nati Acad Sc USA 1980;77(12):7204-7208.

49. David L. Chin BLL, Branimir I. Sikic. Rapid determination of PEGylated liposomal doxorubicin and its major metabolite in human plasma by ultraviolet–visible high-performance liquid chromatography. Journal of Chromatography B 2002;779:259–269.

50. Shigeru Takanashi NRB. Adriamycin Metabolism in Man Evidence From Urinary Metabolites. Drug Metabolism and Disposition 1975;4(1):79 - 87.

51. Peters D. A Comparison of Mercury Arc Lamp and Laser Illumination for Flow Cytometers. The Journal of Histochemistry and Cytochemistry 1979;27(1):241-245.

52. D. B. Axworthy JMR, M. D. Hylarides, R. W. Mallett, L. J. Theodore, L. M. Gustavson, F.-M. Su, L. J. Hobson, P. L. Beaumier, and A. R. Fritzberg. Cure of human carcinoma xenografts by a single dose of pretargeted yttrium-90 with negligible toxicity. PNAS 2000;97(4):1802–1807.

53. Paul L. Weiden HBB. Pretargeted radioimmunotherapy (PRIT™) for treatment of non-Hodgkin's lymphoma (NHL). Critical Reviews in Oncology/Hematology 2001;40:37–51.

54. Loftsson T, Brewster ME. Pharmaceutical Applications of Cyclodextrins. 1. Drug Solubilization and Stabilization. Journal of Pharmaceutical Science 1996;85(10):1017-1025.

55. Johansen PB. Doxorubicin Pharmacokinetics after Intravenous and Intraperitoneal Administration in the Nude Mouse. Cancer Chemother Pharmacol 1981;5:267-270.

56. Gabizon A, Shmeeda H, Barenholz Y. Pharmacokinetics of pegylated liposomal Doxorubicin: review of animal and human studies. Clin Pharmacokinet 2003;42(5):419-436.

57. Cheong I, Huang X, Bettegowda C, Diaz LA, Jr., Kinzler KW, Zhou S, et al. A bacterial protein enhances the release and efficacy of liposomal cancer drugs. Science 2006 Nov 24;314(5803):1308-1311.

58. Karmali PP, Kotamraju VR, Kastantin M, Black M, Missirlis D, Tirrell M, et al. Targeting of albumin-embedded paclitaxel nanoparticles to tumors. Nanomedicine 2009 Mar;5(1):73-82.

59. Murphy EA, Majeti BK, Barnes LA, Makale M, Weis SM, Lutu-Fuga K, et al. Nanoparticle-mediated drug delivery to tumor vasculature suppresses metastasis. Proc Natl Acad Sci U S A 2008 Jul 8;105(27):9343-9348.

60. Allen T. Ligand-Targeted Therapeutics in Anticancer Therapy. Nature Reviews Cancer 2002;2:750-763.

61. Ulrich AS. Biophysical Aspects of Using Liposomes as Delivery Vehicles. Bioscience Reports 2002;22(2):129-150.

62. Park J, Hong K, Kirpotin D, Colbern G, Shalaby R, Baselga J, et al. Anti-HER2 Immunoliposomes: Enhanced Efficacy Attributable to Targeted Delivery. Clinical Cancer Research 2002;8:1172–1181.

63. Zanelli CI, DeMarta S, Hennige CW, Kadri MM. Beamforming for Therapy with High Intensity Focused Ultrasound (HIFU) Using Quantitative Schlieren. IEEE Ultrasonics Symposium 1993:1233-1238.

64. Wojcik G, Mould J, Lizzi F, Abboud N, Ostromogilsky M, Vaughan D. Nonlinear Modeling of Therapeutic Ultrasound. 1995 IEEE Ultrasonics Symposium Proceedings 1995:1617-1622.

65. Barnett S, Ter Haar G, Ziskin M, Rott HD, Duck F, Maeda K. International Recommendations and Guidelines for the Safe Use of Diagnostic Ultrasound in Medicine. Ultrasound in Medicine and Biology 2000;26(3):355-366.

66. Stride E, Saffari N. Microbubble ultrasound contrast agents: a review. Proc Instn Mech Engrs Part H: J Engineering in Medicine 2003;217:429-447.

67. de Jong N, Bouakaz A, Frinking P. Basic acoustic properties of microbubbles. Echocardiography 2002 Apr;19(3):229-240.

68. Von Bibra H, Voigt JU, Froman M, Bone D, Wranne B, Juhlin-Dannfeldt A. Interaction of Microbubbles with Ultrasound. Echocardiography 1999 Oct;16(7, Pt 2):733-741.

69. Katherine Ferrara RP, Mark Borden. Ultrasound Microbubble Contrast Agents: Fundamentals and Application to Gene and Drug Delivery. Annu Rev Biomed Eng 2007;9:415-447.

70. Gao Z, Kennedy AM, Christensen DA, Rapoport NY. Drug-loaded nano/microbubbles for combining ultrasonography and targeted chemotherapy. Ultrasonics 2007 Nov 19.

71. Sun Y, Zhao S, Dayton PA, Ferrara KW. Observation of contrast agent response to chirp insonation with a simultaneous optical-acoustical system. IEEE Trans Ultrason Ferroelectr Freq Control 2006 Jun;53(6):1130-1137.

72. Zhao YZ, Lu CT. [Recent advances in the applications of ultrasonic microbubbles as gene delivery systems]. Yao Xue Xue Bao 2007 Feb;42(2):127-131.

73. Willmann JK, Cheng Z, Davis C, Lutz AM, Schipper ML, Nielsen CH, et al. Targeted microbubbles for imaging tumor angiogenesis: assessment of whole-body biodistribution with dynamic micro-PET in mice. Radiology 2008 Oct;249(1):212-219.

74. Kheirolomoom A, Dayton PA, Lum AF, Little E, Paoli EE, Zheng H, et al. Acoustically-active microbubbles conjugated to liposomes: characterization of a proposed drug delivery vehicle. J Control Release 2007 Apr 23;118(3):275-284.

75. Klibanov A. Microbubble Contrast Agents Targeted Ultrasound Imaging and Ultrasound Assisted Drug-Delivery Applications. Investigative Radiology 2006;41(3):354-362.

76. Liu Y, Miyoshi H, Nakamura M. Encapsulated ultrasound microbubbles: Therapeutic application in drug/gene delivery. Journal of Controlled Release 2006;114:89–99.

77. Lentacker I, De Geest B, Vandenbroucke R, Peeters L, Demeester J, De Smedt S, et al. Ultrasound-Responsive Polymer-Coated Microbubbles That Bind and Protect DNA. Langmuir 2006;22:7273-7278.

78. Unger E, McCreery T, Sweitzer R, Caldwell V, Wu Y. Acoustically Active Lipospheres Containing Paclitaxel: A New Therapeutic Ultrasound Contrast Agent. Investigative Radiolog 1998;33(12):886-892.

79. Kheirolomoom A. D, P., Lum, A., Little, E., Paoli, E., Zheng, H., Ferrara, K. Acoustically-active microbubbles conjugated to liposomes: Characterization of a proposed drug delivery vehicle. Journal of Controlled Release 2007;118:275–284.

80. Huang S, MacDonald R. Acoustically active liposomes for drug encapsulation and ultrasound-triggered release. Biochemica et Biophysica Acta 2004;1665:134- 141.

81. Liu R, Wei X, Yao Y, Chai Q, Chen Y, Xu Y. The preparation and characterization of gas bubble containing liposomes. Proceedings of the 2005 IEEE Engineering in Medicine and Biology 27th Annual Conference Shanghai, China 2005.

82. Domazou A, Luisi P. Size Distribution of Spontaneously Formed Liposomes by the Alcohol Injection Method. Journal of Liposome Research 2002;12(3):205-220.

83. Hosaka Y, Semba T, Fukai K. Artificial Assembly of Envelope Particles of HVJ (Sendai Virus). Fusion Activity of Envelope Particles. J Gen Virol 1974;25:391-404.

84. Schutt E, Pelura T, Hopkins R. Osmotically-stabilized microbubble ultrasound contrast agents. Acad Radiol 1996;3:S188–S190.

85. Schutt E, Klein D, Mattrey R, Riess J. Injectable Microbubbles as Contrast Agents for Diagnostic Ultrasound Imaging: The Key Role of Perfluorochemicals. Angew Chem Int Ed 2003;42:3218 – 3235.

86. Borden MA, Pu G, Runner GJ, Longo ML. Surface phase behavior and microstructure of lipid/PEG-emulsifier monolayer-coated microbubbles. Colloids and Surfaces B: Biointerfaces 2004;35:209–223.

87. Singal PK, Iliskovic N. Doxorubicin-Induced Cardiomyopathy. The New England Journal of Medicine 1998 September 24;339(13):900-905.

88. Minotti G, Menna P, Salvatorelli E, Cairo G, Gianni L. Anthracyclines: Molecular Advances and Pharmacologic Developments in Antitumor Activity and Cardiotoxicity. Pharmacol Rev 2004;56:185–229.

89. Mayer LD, Bally MB, Cullis PR. Strategies for Optimizing Liposomal Doxorubicin. Journal of Liposome Research 1990;1(4):463-480.

90. Berger N, Sachse A, Bender J, Schubert R, Brandl M. Filter extrusion of liposomes using different devices: comparison of liposome size, encapsulation efficiency, and process characteristics. International Journal of Pharmaceutics 2001;223:55-68.

91. Young F. Cavitation London: Imperial College Press 1999.

92. Ohl C-D, Arora M, Ikink R, de Jong N, Versluis M, Delius M, et al. Sonoporation from Jetting Cavitation Bubbles. Biophysical Journal 2006;91:4285–4295.

93. Zarnitsyn V, Rostad C, Prausnitz M. Modeling Transmembrane Transport through Cell Membrane Wounds Created by Acoustic Cavitation. Biophysical Journal 2008;95(9):4124-4138.

94. Felgner PL, Gadek TR, Holm M, Roman R, Chan HW, Wenz M, et al. Lipofection: A highly efficient, lipid-mediated DNA-transfection procedure. Proc Nati Acad Sci 1987;84:7413-7417.

95. Cepko CL, Roberts BE, Mulligan RC. Constructions and applications of a highly transmissible murine retrovirus shuttle vector. Cell 1984;37:1053-1062.

96. Graessmann M, Graessmann A. Microinjection and Organelle Transplantation Techniques. London: Academic, 1986.

97. Soughayer JS, Krasieva T, Jacobson SC, Ramsey JM, Tromberg BJ, Allbritton NL. Characterization of Cellular Optoporation with Distance. Anal Chem 2000;72:1342-1347.

98. Weaver JC, Chizmadzhev YA. Theory of electroporation: A review. Bioelectrochemistry and Bioenergetics 1996;4:135-160

99. Koch S, Pohl P, Cobet U, Rainov NG. Ultrasound Enhancement of Liposome-Mediated Cell Transfection is Caused by Cavitation Effects. Ultrasound in Med & Biol 2000;26(5):897–903.

100. Bao S, Thrall BD, Miller DL. Transfection of a Reporter Plasmid Into Cultured Cells by Sonoporation in Vitro. Ultrasound in Med & Biol 1997;23(6):953-959.

101. Chin CT, Lance´e C, Borsboom J, Mastik F, Frijlink ME, Jong Nd. Brandaris 128: A digital 25 million frames per second camera with 128 highly sensitive frames. Review of Scientific Instruments 2003;74(12):5026-5034.

102. Ferrara RPK, Borden M. Ultrasound Microbubble Contrast Agents: Fundamentals and Application to Gene and Drug Delivery. Annu Rev Biomed Eng 2007;9:415-447.

103. Liu J, Lewis TN, Prausnitz MR. Non-Invasive Assessment and Control of Ultrasound-Mediated Membrane Permeabilization. Pharmaceutical Research 1998;15(6):918-924.

104. Sundaram J, Mellein BR, Mitragotri S. An Experimental and Theoretical Analysis of Ultrasound-Induced Permeabilization of Cell Membranes. Biophysical Journal 2003 84:3087–3101.

105. Zarnitsyn V, Rostad C, Prausnitz M. Modeling Transmembrane Transport through Cell Membrane Wounds Created by Acoustic Cavitation. Biophysical Journal 2008;95(9):4124-4138.

106. Okada K, Kudo N, Niwa K, Yamamoto K. A basic study on sonoporation with microbubbles exposed to pulsed ultrasound. J Med Ultrasonics 2005;32:3-11.

107. Miller MW, Miller DL, Brayman AA. A Review of In Vitro Bioeffects of Inertial Ultrasonic Cavitation from A Mechanistic Perspective. Ultrasound in Med & Biol 1996;22(9):1131-1154.

108. Karshafian R, Samac S, Banerjee M, Bevan P, Burns P. Ultrasound-Induced Uptake of Different Size Markers in Mammalian Cells. IEEE Ultrasonics Symposium 2005:13-16.

109. Gao Z, Kennedy AM, Christensen DA, Rapoport NY. Drug-loaded nano/microbubbles for combining ultrasonography and targeted chemotherapy. Ultrasonics 2007.

110. Trikha M, Zhou Z, Timar J, Raso E, Kennel M, Emmell E, et al. Multiple Roles for Platelet GPIIb/IIIa and v 3 Integrins in Tumor Growth, Angiogenesis, and Metastasis. Cancer Research 2002;62:2824–2833.

111. Rerat V, Dive G, Cordi AA, Tucker GC, Bareille R, Amedee J, et al. αvβ3 Integrin-Targeting Arg-Gly-Asp (RGD) Peptidomimetics Containing Oligoethylene Glycol (OEG) Spacer. J Med Chem 2009;52:7029–7043.

112. Nagel T, Resnick N, Atkinson WJ, C. Forbes Dewey J, Michael A. Gimbrone J. Shear Stress Selectively Upregulates Intercellular Adhesion Molecule-1 Expression in Cultured Human Vascular Endothelial Cells. J Clin Invest 1994;94:885-891.

113. Yamakoshi Y, Ozawa Y, Ida M, Masuda N. Effects of Bjerknes Forces on Gas-Filled Microbubble Trapping by Ultrasonic Waves. Jpn J Appl Phys 2001;40:3852-3855.

114. Miller DL. A Review of the Ultrasonic Bioeffects of Microsonation, Gas-Body Activation, and Related Cavitation-Like Phenomena. Ultrasound in Med & Biol 1987;13(8):443-470.

115. Kodama T, Tomita Y. Cavitation bubble behavior and bubble–shock wave interaction near a gelatin surface as a study of in vivo bubble dynamics. Appl Phys B 2000;70:139–149.

116. Gao AM, Kennedy DA, Christensen NY, Z. R. Drug-loaded nano/microbubbles for combining ultrasonography and targeted chemotherapy. Ultrasonics 2007;48(4):260-270.

117. Pitt WG, Husseini GA, Staples BJ. Ultrasonic drug delivery - a general review. Expert Opin Drug Delivery 2004;1(1):37-56.

118. Dayton PA, Allen JS, Ferrara KW. The magnitude of radiation force on ultrasound contrast agents. J Acoust Soc Am 2002;112(5):2183-2192.

119. Crum LA. Surface Oscillations and Jet Development in Pulsating Bubbles. Journal De Physique 1979;40(11):285-288.

120. Dayton PA, Chomas JE, Lum AFH, Allen JS, Lindner JR, Simon SI, et al. Optical and Acoustical Dynamics of Microbubble Contrast Agents inside Neutrophils. Biophysical Journa 2001;80:1547–1556.

121. Chomas JE, Dayton P, May D, Ferrara K. Threshold of fragmentation for ultrasonic contrast agents. Journal of Biomedical Optics 2001;6(2):141–150.

122. Wolfrum B, Mettin R, Kurz T, Lauterborn W. Observations of pressure-wave-excited contrast agent bubble in the vicinity of cells. Applied Physics Letters 2002;81(26):5060-5062.

123. Kudo N, Miyaoka T, Okada K, Yamamoto K. Study on Mechanism of Cell Damage Caused by Microbubbles Exposed to Ultrasound. IEEE Ultrasonics Symposium 2002:1383-1386.

124. Marmottant P, Hilgenfeldt S. Controlled vesicle deformation and lysis by single oscillating bubbles. Nature 2003;423:153-156.

125. Dean M, Fojo T, Bates S. Tumor Stem Cells and Drug Resistance. Nature Reviews 2005;5:275-284.